Stochastic many-particle systems with irreversible dynamics

Der Fakultät für Naturwissenschaften
der Universität Duisburg–Essen
(Campus Duisburg)

zur Erlangung des akademischen Grades eines

Doktors der Naturwissenschaften

eingereichte Dissertation von

Stephan M. Dammer

aus Duisburg-Rheinhausen

Referent: Prof. Dr. H. Hinrichsen
Koreferent: Prof. Dr. K. Usadel

Tag der Einreichung: 11. Juni 2004
Tag der mündlichen Prüfung: 30. November 2004

Abstract

In this thesis, several stochastic models are investigated, which are subjected to irreversible dynamics. Motivation for the presented work stems, on the one hand, from particular physical systems under consideration, which are modeled by the studied stochastic processes. Besides that, the models discussed in this thesis are, on the other hand, generally interesting from the point of view of statistical physics, since they describe systems far from thermodynamic equilibrium. Interesting properties to be encountered are, e.g., dynamical scaling behavior or continuous phase transitions.

The first issue to be addressed, is the investigation of irreversibly aggregating systems, where the main emphasis is laid on aggregation of monopolarly charged clusters suspended in a fluid. For this purpose, rate equations are analyzed and Brownian dynamics simulations are performed. It is shown that the system crosses over from power-law cluster growth to sub-logarithmic cluster growth. Asymptotically, the cluster size distribution evolves towards a universal scaling form, which implies a 'self-focussing' of the size distribution.

Another emphasis of this thesis is the investigation of nonequilibrium critical phenomena, in particular, the study of phase transitions into absorbing states (states that may be reached irreversibly). To this end, the continuous nonequilibrium phase transition of directed percolation, which serves as a paradigm for absorbing-state phase transitions, is analyzed by a novel approach. Despite the lack of a partition function for directed percolation, this novel approach follows the ideas of Yang-Lee theory of equilibrium statistical mechanics, by investigating the complex roots of the survival probability.

Stochastic models such as directed percolation mimic spreading processes, e.g., the spreading of an infectious disease. The effect of long-time memory, which is not included in directed percolation and which corresponds to immunization in epidemic spreading, is investigated through an appropriate model. This model includes dynamical percolation (perfect immunization) as a special case, as well as directed percolation (no immunization). The critical behavior of this model is studied by means of Monte Carlo simulations, in particular for weak immunization.

A further generalization is investigated, which allows spontaneous mutations and different species of spreading agents (pathogens). Restricting the analysis to perfect immunization and two spatial dimensions, it is shown by Monte Carlo simulations, that immunization leads to a crossover from dynamical to directed percolation. Other properties of this model are discussed in detail.

Zusammenfassung

Diese Arbeit untersucht verschiedene stochastische Modelle, die einer irreversiblen Dynamik unterliegen. Die Untersuchung solcher Modelle ist wichtig, da sich verschiedene natürliche oder experimentelle Systeme mit ihnen beschreiben lassen. Darüber hinaus sind die behandelten Modelle von grundsätzlichem Interesse für die statistische Physik, da sie Systeme beschreiben, die fern vom thermodynamischen Gleichgewicht sind. Interessante Eigenschaften, die behandelt werden, umfassen beispielsweise dynamisches Skalenverhalten und kontinuierliche Phasenübergänge.

Das erste behandelte Thema befasst sich mit irreversibler Aggregation, mit dem Schwerpunkt auf Aggregation gleichnamig geladener Cluster in einer Suspension. Zu diesem Zweck werden Ratengleichungen analysiert und Brownsche Dynamik Simulationen durchgeführt. Das System zeigt einen Übergang von algebraischem zu sub-logarithmischem Clusterwachstum. Asymptotisch nimmt die Größenverteilung der Cluster eine universelle Form an, was mit einem 'Selbstfokussieren' der Größenverteilung einhergeht.

Ein anderer Schwerpunkt dieser Arbeit ist die Untersuchung von kritischen Phänomenen im Nichtgleichgewicht, insbesondere von Phasenübergängen in absorbierende Zustände (Zustände die irreversibel erreicht werden können). So wird zum Beispiel der kontinuierliche Phasenübergang von gerichteter Perkolation, der ein Paradigma für diese Art von Phasenübergängen darstellt, mit einer neuen Methode untersucht. Obwohl es für gerichtete Perkolation keine Zustandssumme gibt, bedient sich diese neue Methode der Ideen der Yang-Lee Theorie aus der statistischen Physik des Gleichgewichts, indem die komplexen Nullstellen der Überlebenswahrscheinlichkeit untersucht werden.

Stochastische Modelle, wie solche für die gerichtete Perkolation, ahmen Ausbreitungsprozesse nach, etwa die Ausbreitung einer ansteckenden Krankheit. Langzeitgedächtniseffekte, die bei der gerichteten Perkolation nicht berücksichtigt sind und die Immunisierungseffekte bei epidemischer Ausbreitung beschreiben, werden mit Hilfe eines geeigneten Modells untersucht. Spezialfälle dieses Modells sind sowohl die dynamische Perkolation (perfekte Immunisierung) als auch die gerichtete Perkolation (keine Immunisierung). Das kritische Verhalten dieses Modells wird mit Monte Carlo Simulationen untersucht, insbesondere für schwache Immunisierung.

Darüber hinaus wird eine weitere Verallgemeinerung dieses Modells behandelt, die spontane Mutationen und verschiedene Typen von 'Krankheitserregern' erlaubt. Die Analyse beschränkt sich hier auf perfekte Immunisierung und zwei räumliche Dimensionen. Mit Monte Carlo Simulationen wird gezeigt, dass Mutationen einen Übergang von dynamischer zu gerichteter Perkolation bewirken. Weitere Eigenschaften dieses Modells werden im Detail diskutiert.

Contents

Abstract **3**

Zusammenfassung **5**

Contents **9**

List of Figures **12**

List of Tables **13**

1 Introduction **15**

2 Basic concepts and methods **21**
2.1 The master equation 21
2.1.1 Stationarity, detailed balance and the notion of nonequilibrium 24
2.2 Fokker-Planck and Langevin equations 26
2.2.1 The Fokker-Planck equation 26
2.2.2 The Langevin equation 28
2.3 Reaction-diffusion processes 30
2.4 Field theory and renormalization 31
2.5 Mean-field approximation 32
2.6 Computer simulations 33

3 Irreversible aggregation **35**
3.1 Single-species coagulation 35
3.1.1 Mean-field approximation 36
3.1.2 Taking fluctuations into account 36
3.2 Smoluchowski's coagulation equation 39
3.2.1 Brownian dynamics simulations of uncharged coagulating spheres 41
3.3 Self-focussing dynamics in monopolarly charged suspensions . 45

3.3.1 R_{ij} for monopolarly charged systems 46
3.3.2 Crossover 48
3.3.3 Asymptotic behavior 49
3.3.4 Details of the numerical integration algorithm 53
3.3.5 Brownian dynamics simulations of charged coagulating spheres 55
3.3.6 Summary and outlook 56

4 Introduction to the modeling of spreading processes 59
4.1 Critical behavior of absorbing-state phase transitions 61
4.1.1 Critical exponents and scaling theory 61
4.2 Directed percolation 66
4.2.1 Geometric model: Isotropic vs. directed bond percolation 66
4.2.2 Dynamical interpretation of directed percolation 69
4.2.3 Critical behavior of directed percolation 72
4.2.4 DP in 1+1 dimensions: Illustrations 75
4.2.5 Different realizations of DP 77
4.2.6 The DP conjecture 78
4.2.7 Nonintegrability 79
4.2.8 Experimental realizations 79
4.3 Summary 80

5 Yang-Lee zeros for nonequilibrium phase transitions 81
5.1 Yang-Lee zeros in equilibrium statistical mechanics 82
5.2 Yang-Lee zeros for directed percolation 85
5.2.1 Exact determination of the survival probability $P_{\mathrm{s}}(t)$. 86
5.2.2 Computational method 89
5.2.3 Critical points and 'Yang-Lee scenario' 91
5.2.4 Universal features 94
5.2.5 MC-Simulations 96
5.3 Analytical results for $P_{\mathrm{s}}(t)$ for DPb 97
5.3.1 Time-independent zero at p=2 97
5.3.2 Exact solution for p at the Golden Ratio 98
5.3.3 First coefficients of the polynomials $P_{\mathrm{s}}(t)$ in the limit $t\to\infty$ 100
5.4 Yang-Lee zeros in other nonequilibrium systems 101
5.5 Summary and outlook 103

6 Spreading in media with long-time memory **107**
6.1 Dynamical percolation and the general epidemic process . . . 109
6.2 Epidemic process with finite immunization (EPFI) 111
6.2.1 Monte Carlo simulations 113
6.2.2 Phenomenological properties 114
6.2.3 Scaling properties 118
6.2.4 Phase Diagrams 121
6.2.5 Temporal correlation length in the vicinity of the DP point 122
6.3 Summary and outlook 124

7 Epidemic spreading with immunization and mutations **127**
7.1 Simulation model 128
7.2 Phase diagram 129
7.3 Critical behavior along the phase transition line 132
7.3.1 Seed simulations 132
7.3.2 Full-lattice simulations 133
7.4 Critical behavior in the vicinity of the GEP point 136
7.4.1 Decay at the GEP point 137
7.4.2 λ-controled transition at the GEP point 137
7.4.3 Curvature of transition line at the GEP point 141
7.5 Summary and outlook 142

8 Conclusion **145**

Acknowledgments **147**

Appendix **149**

Bibliography **153**

Curriculum vitae **165**

Veröffentlichungen **167**

List of Figures

3.1 Brownian dynamics simulations of uncharged coagulating spheres 44
3.2 Criterion for the stability of suspensions of equally charged particles 46
3.3 Crossover from power-law to sub-logarithmic cluster growth . 49
3.4 Data collapse of the cluster size distribution in the asymptotic regime 50
3.5 Self-focussing of the relative width of the cluster size distribution 52
3.6 Sub-logarithmic cluster growth in the asymptotic regime . . . 53
3.7 Brownian dynamics simulations of monopolarly charged coagulating spheres 57

4.1 Isotropic versus directed bond percolation 67
4.2 Dynamical interpretation of directed bond percolation 69
4.3 Space-time plots of DP, starting from an active seed 76
4.4 Space-time plots of DP, starting from a fully occupied lattice . 77

5.1 Examples of clusters in directed bond and site percolation . . 87
5.2 All relevant configurations that contribute to $P_{\rm s}(2)$ 89
5.3 A configuration and one of its ancestors 90
5.4 Zeros of the survival probability $P_{\rm s}(t)$ in the complex plane . . 92
5.5 Zeros approaching the critical point 93
5.6 The distance from the critical point versus time 95
5.7 Example of different weights for $P_{\rm s}(t)$ and $R(t)$ 98
5.8 Decomposition of the configurational sum of non-surviving clusters into three subsets 100

6.1 Snapshot of a critical GEP-cluster 110
6.2 Phase diagram of the EPFI in 2+1 dimensions 112
6.3 Typical cluster of immune sites in 2+1 dimensions at the DP point 115
6.4 Number of primary infections versus time 116

6.5 Phase diagrams for the EPFI for $d = 3, 4, 5, 6$ 121
6.6 Data collapses for p=p_c and p_0=p_c−ϵ 123

7.1 Phase diagram of the spreading model with mutations in d=2 130
7.2 Snapshots of seed-simulations of the spreading model with mutations 131
7.3 $P_s(t)$ and $N(t)$ for different values of λ 134
7.4 $R^2(t)$ and $N_{sp}(t)$ for different values of λ 135
7.5 Data collapse of $\rho(t)$ for λ=0.5 136
7.6 Full-lattice simulations at the GEP point 138
7.7 Data collapse of ρ and ρ_{sp} 140
7.8 Double-logarithmic plot of the phase transition line $|\Delta_{p_0}(\lambda)|$ for $\lambda \ll 1$ 142

A.1 Sketch of an electrostatically supported coating process 150
A.2 Aggregation of 'wrong' partners 151

List of Tables

4.1 Estimates of p_c for directed bond percolation on a d-dimensional cubic lattice 70
4.2 Estimates of critical exponents for directed percolation 74

5.1 Bulirsch-Stoer extrapolants for the zeros approaching the critical point 91
5.2 Bulirsch-Stoer extrapolants of the exponent $1/\nu_{\parallel}$ 96

6.1 Numerical estimates for the GEP on a simple d-dimensional cubic lattice 111

Chapter 1

Introduction

This thesis investigates several stochastic models that are subjected to irreversible dynamics. Such models may be used to describe a large variety of different experimental situations or natural phenomena. Hence, they can improve the understanding of particular systems under consideration. In Chap. 3, for instance, irreversible aggregation is discussed, with a focus on monopolarly charged suspensions. That part of this thesis is mainly motivated by an experimental realization of a particle-coating process, which is outlined in further detail in the appendix. Irreversibility, i.e., irreversible aggregation, comes in this case from strong van der Waals forces. Suspended clusters may aggregate upon collision to form larger aggregates, whereas disintegration of aggregates into smaller ones does not take place. Another possible example can be found in Chap. 7, where the influence of mutations in a simple model for epidemic spreading is studied. Here, the state of an entirely healthy population may be reached irreversibly, because it is assumed that the spreading disease does not pop up spontaneously.

Besides their obvious relation to concrete natural phenomena, stochastic processes with irreversible dynamics are generally interesting from a fundamental point of view of statistical physics. The reason is that these models generically describe systems that are not at thermodynamic equilibrium, see Sec. 2.1.1. Though most systems in our environment are far from equilibrium, nonequilibrium statistical mechanics is, compared to the theoretical understanding of equilibrium systems, still at its beginning. Therefore, it is of basic interest to study different kinds of nonequilibrium models. The aim is to deepen the general insight into nonequilibrium behavior and to investigate, which theoretical concepts are appropriate for these systems. In this context, one typically investigates simplified models with a potentially wide range of approximate validity, rather than

detailed models for a particular situation. The present thesis contributes to this issue by investigating several nonequilibrium models. Interesting phenomena to be encountered are, e.g., dynamical scaling behavior or continuous phase transitions. Chaps. 4–7, for example, deal with simple models for the spreading of some nonconserved agent (e.g., a disease, as mentioned above). These models are especially interesting due to the fact that they exhibit continuous phase transitions from fluctuating active to non-fluctuating inactive (absorbing) states. Hence, in addition to their relevance for the understanding of natural spreading processes, these models are important 'workhorses' for general investigations on nonequilibrium critical phenomena. It turns out that the concepts of scale invariance and universality, well-known from equilibrium critical phenomena, apply in the nonequilibrium case as well. Thus, the classification of all possible transitions from fluctuating phases into absorbing states is currently one of the major goals of nonequilibrium statistical physics [1, 2].

Concerning the methodology, this thesis lays some emphasis on computational methods. Computer simulations and other numerical methods are very important for the whole research field in general, and for this thesis in particular. The reason is that many interesting models are unyielding to analytical treatment. Computational methods, in fruitful competition with other methods (e.g., renormalization group schemes [3] in the case of critical behavior) provide important insight into such intractable problems.

Since this thesis applies stochastic concepts to describe natural phenomena, I make some opening remarks about the use of probabilistic concepts in the natural science. Thereafter, the actual contents of this thesis is outlined.

Probabilistic concepts

The phenomena we may observe in our natural environment, are usually concerned with macroscopic objects and properties. However, macroscopic objects are composed of many microscopic constituents. This is easily illustrated by an everyday example: a sample of a simple gas. In spite of the fact that a vessel of gas contains an incredibly huge number of molecules (of order 10^{23}), its macroscopic behavior in thermodynamic equilibrium is entirely determined by only a few macroscopic variables. Namely, the volume, the pressure and the temperature [4, 5]. Moreover, these variables are not independent of each other, but related through an equation of state. How does the huge number of degrees of freedom in a

gas give rise to only a few relevant macroscopic observables? Or in general: How does macroscopic behavior of a system emerge from the microscopic properties of its constituents? In a somewhat more general sense, the term microscopic may refer to the scale of constituents that build up a much larger system, which defines the macroscopic scale. In this sense, to name an example, individuals may be viewed as microscopic objects, giving rise to a macroscopic epidemic spreading process in a society.

The derivation of macroscopic properties by an exact treatment of the microscopic constituents is simply impossible. In the case of a gas, for instance, this would require the solution of about 10^{23} coupled equations of motion. Already the treatment of the initial conditions is hopeless. Interestingly, even if such a solution was possible, one would have to compute some kind of average to obtain useful information from the solution.

It is remarkable that the theory of classical thermodynamics describes macroscopic behavior without even knowing about the microscopic world [5]. The laws that govern a simple gas, for instance, had been formulated long before it was accepted that a gas is composed of atoms or molecules. Hence, from a microscopic point of view, macroscopic statements can only be concerned with probabilities and averaged quantities. Furthermore, the measurement of macroscopic properties itself contains averaging, since it involves temporal and spatial scales that are large compared to microscopic scales. Therefore, *statistical physics* applies *probabilistic concepts* to derive macroscopic behavior given a microscopic model.

In statistical physics each microscopic configuration $\mathcal{C}$ is associated with the probability $P(\mathcal{C}, t)$ to find the system in configuration $\mathcal{C}$ at time t. Consider for example a system with fixed volume and particle number at thermal equilibrium with a heat bath. In this case the probability distribution is the stationary Boltzmann distribution $P_{\text{eq}}(\mathcal{C}) = Z^{-1} e^{-\beta \mathcal{H}(\mathcal{C})}$, where $\mathcal{H}(\mathcal{C})$ denotes the energy of the microscopic configuration $\mathcal{C}$ and $\beta = (k_{\text{B}} T)^{-1}$ with the temperature T and Boltzmann's constant k_{B}. Normalization is achieved by the factor Z^{-1}, with the partition function $Z = \sum_{\mathcal{C}} e^{-\beta \mathcal{H}(\mathcal{C})}$ [4]. It turns out that the partition function is a fundamental statistical quantity in its own right. It is simply related to the free energy of the system and thence through differentiation results in all other thermodynamic quantities. Therefore, the thermodynamic equilibrium properties are fully determined by the partition function. Hence, in equilibrium statistical physics there is a unified framework to derive macroscopic behavior from microscopic models by evaluating the partition function. Since for the majority of

models, this is a difficult task, powerful approximation techniques have been developed (see, e.g., Refs. [3, 6]). In this context, computer simulations are particulary useful [7]. It is important to note that equilibrium statistical physics does not describe dynamic aspects. It is irrelevant *how* the system evolves through different configurations as long as the relative frequencies of certain configurations are given according to the Boltzmann distribution. Nevertheless, as will be discussed in Sec. 2.1.1, dynamic processes may be used to generate the equilibrium ensemble.

In nature, however, most phenomena take place under *nonequilibrium* conditions (in fact, the author of this thesis is not at thermodynamic equilibrium). Possible examples are all kinds of non-stationary systems, which, of course, are not at equilibrium. The reverse is not true. Nonequilibrium systems may well exhibit stationary states. Important examples are driven diffusive systems, such as the asymmetric simple exclusion process (ASEP) [8–10]. The notion of nonequilibrium will be discussed in further detail in Sec. 2.1.1. For the moment, it shall be sufficient to associate nonequilibrium with some kind of flow (e.g., of energy or mass), which, in the statistical description, results in a probability flow between microscopic configurations.

Clearly, the theoretical description of nonequilibrium systems requires an explicit treatment of the underlying dynamics. However, in most cases the microscopic dynamics are very complicated or even unknown, usually due to the fact that the dynamics emerge from a large number of degrees of freedom (see below, the example of a Brownian particle). In this case, it is often appropriate to assume that the individual degrees of freedom behave randomly according to certain probabilistic rules. Thus, a large number of dynamical variables is modeled by an effective noise with certain postulated statistical properties. The modeling of microscopic dynamics by probabilistic concepts is done by *stochastic processes*. A paradigm for this kind of description is Brownian motion [11]. Think of a small but macroscopic particle suspended in a fluid. The particle is subjected to the influence of a huge number of fluid molecules which frequently 'kick' the particle. Instead of explicitely including the motion of the fluid molecules, one subsumes their influence in a random force acting on the particle.

In general, the theoretical description of nonequilibrium systems requires an explicit solution of a dynamical equation for the probability flow between microscopic configurations, e.g, the so-called *master equation* (or related equations, see Chap. 2). This is usually a difficult task and until now there

is no general approach to the solution of the master equation. Therefore, compared to the theoretical understanding of thermodynamic equilibrium, nonequilibrium statistical physics is still at its beginning.

Summarizing, probabilistic concepts may be used to derive macroscopic properties of a system from the behavior of its microscopic constituents. In equilibrium, this is done by evaluating the partition function, which encodes all statistically relevant information. In nonequilibrium statistical physics, there is no unified framework akin to that for thermodynamic equilibrium. The dynamics have to be included explicitely and corresponding dynamic equations for the probability distribution have to be solved. Modeling the dynamics of the microscopic constituents itself involves stochastic concepts. Usually, the dynamics emerge from many degrees of freedom that are treated as an effective stochastic noise with certain postulated statistical properties.

Outline of the thesis

Chap. 2 introduces selected concepts and methods of statistical mechanics and stochastic processes. The aim is to aquire a taste for the subject and to lay the basis for the work presented in the following chapters.

Irreversible aggregation is the topic of Chap. 3. An appropriate introduction is given by the discussion of known results for irreversible aggregation of uncharged particles. The main issue, however, is the investigation of irreversible aggregation of equally charged particles, which are suspended in a fluid. This is done by the analysis of rate equations and by Brownian dynamics simulations.

The stochastic modeling of spreading processes, which is the subject of the following chapters, is introduced in Chap. 4. These models exhibit continuous phase transitions between fluctuating active and absorbing states, that may be reached irreversibly. The scaling theory for phase transitions into absorbing states is summarized. Moreover, directed percolation is discussed in some detail, which serves as a paradigm for nonequilibrium phase transitions into absorbing states and is frequently encountered throughout the rest of the thesis.

An important theory that explains the appearance of nonanalyticities at phase transitions in equilibrium statistical mechanics is the Yang-Lee theory. It describes phase transitions in terms of the complex zeros of the partition

function. In spite of the lack of a partition function for directed percolation, the nonequilibrium phase transition of directed percolation is analyzed by a new approach in Chap. 5, following the ideas of Yang-Lee theory.

Directed percolation describes spreading in media without long-time memory. The aim of Chap. 6 is, to investigate the influence of memory in spreading processes. In the language of epidemic spreading, long-time memory accounts for the effect of immunization (or weakening). It is known that perfect immunization leads to the spreading behavior of dynamical percolation. In Chap. 6, a model with finite immunization is studied by means of Monte Carlo simulations.

A further generalization of epidemic spreading models is introduced in Chap. 7, by allowing spontaneous mutations, which overcome immunization. In contrast to the preceding chapters, this model includes different species of spreading pathogens. Restricting the analysis to perfect immunization and two spatial dimensions, the model is investigated by Monte Carlo simulations.

At the end of each chapter, conclusions summarize the main results of the particular studies, and provide possible perspectives for future activities in these fields. The thesis ends with further concluding remarks in Chap. 8.

Chapter 2

Basic concepts and methods

The aim of this chapter is to briefly introduce selected concepts and methods of statistical mechanics and stochastic processes. The intention is not to present a general or rigorous overview but rather to acquire a taste for the subject, and to sketch the theoretical context relevant for this thesis. For comprehensive treatments see, e.g., REFS. [4, 11–13] and the references given throughout this chapter. The topics addressed here, do not appear equally apparent in the following chapters. Nevertheless, all of them play a role at some point in this thesis, though some concepts are rather 'lurking in the background'.

2.1 The master equation

In statistical physics each microscopic configuration $\mathcal{C}$ is associated with the probability $P(\mathcal{C}, t)$ to find the system in configuration $\mathcal{C}$ at time t, given that it was in an initial configuration $\mathcal{C}_0$ at time t=0. Thus, $P(\mathcal{C}, t)$ is a *conditional* probability. The distribution $P(\mathcal{C}, t)$ contains complete information about the statistical properties of the system. As was mentioned above, in thermodynamic equilibrium $P(\mathcal{C}, t) = P_{\text{eq}}(\mathcal{C})$ is the stationary Gibbs ensemble and $P(\mathcal{C})$ is expressed in terms of the Hamiltonian $\mathcal{H}(\mathcal{C})$, see CHAP. 1. Often, models of statistical mechanics are defined on d-dimensional lattices, where the lattice represents the physical space. Hence, space is a discrete variable. Each lattice site i is associated with a local degree of freedom ('spin') s_i, where s_i usually assumes integer values. An example are reaction-diffusion

models, see SEC. 2.3, where s_i=1 represents a particle at site i and s_i=0 means that site i is empty. In this cases the configurations are countable, i.e, one has a discrete set of configurations $\{\mathcal{C}_\alpha\}$. A configuration $\mathcal{C}_\alpha$ is specified by the states of all s_i. The *expectation value* of an observable quantity A that depends on the microscopic configurations, is defined as

$$\langle A(t)\rangle = \sum_\alpha P(\mathcal{C}_\alpha, t) A(\mathcal{C}_\alpha) \ , \tag{2.1}$$

where $A(\mathcal{C}_\alpha)$ is the value of A in configuration $\mathcal{C}_\alpha$. Usually A is associated with a macroscopic quantity, e.g., the total energy of the system. Angular brackets $\langle\rangle$ denote the *ensemble average*. One may think of many different microscopic realizations of the same macroscopic physical system at time t, the ensemble. The relative frequencies of finding the microscopic systems in configuration $\mathcal{C}_\alpha$ is given by $P(\mathcal{C}_\alpha, t)$. Thus, in EQ. (2.1) A is averaged over all microscopic realizations which constitute the ensemble.

Similar reasonings apply for the case of a continuous configuration space as well. Then, the probability $P(\mathcal{C}_\alpha, t)$ has to be replaced by a probability density, and sums over $P(\mathcal{C}_\alpha, t)$ as in EQ. (2.1), are replaced by integrals over configuration space.

According to EQ. (2.1), the temporal evolution of macroscopic quantities is determined by the temporal evolution of the probability distribution $P(\mathcal{C}, t)$, which may be obtained from a so-called *master equation*. This is a linear differential equation for the probability flow in and out of microscopic configurations. Depending on whether the process evolves in continuous or discrete time one has to distinguish between *asynchronous* and *synchronous* dynamics.

Asynchronous dynamics – continuous time

The microscopic dynamics of a macroscopic system is usually to complicated to be treated by ab initio methods. Instead, one applies a stochastic description. In particular, *transition rates* $w(\mathcal{C}_\alpha, \mathcal{C}_\beta)$ are assigned for the spontaneous transition from configuration $\mathcal{C}_\alpha$ to configuration $\mathcal{C}_\beta$. Of course, the transition rates must reflect the actual dynamics of the physical system

under consideration [1]. The temporal change of $P(\mathcal{C},t)$ obeys the master equation of the form

$$\frac{\partial P(\mathcal{C}_\alpha,t)}{\partial t} = \underbrace{\sum_{\beta\neq\alpha} P(\mathcal{C}_\beta,t)w(\mathcal{C}_\beta,\mathcal{C}_\alpha)}_{\text{gain}} - \underbrace{P(\mathcal{C}_\alpha,t)\sum_{\beta\neq\alpha} w(\mathcal{C}_\alpha,\mathcal{C}_\beta)}_{\text{loss}} \ . \tag{2.2}$$

The probability distribution is normalized, i.e., $\sum_\alpha P(\mathcal{C}_\alpha,t)$=1, and the normalization is conserved by Eq. (2.2). The self-transition rate is given by

$$w(\mathcal{C}_\alpha,\mathcal{C}_\alpha) = -\sum_{\beta\neq\alpha} w(\mathcal{C}_\alpha,\mathcal{C}_\beta) \ . \tag{2.3}$$

Note that Eq. (2.2) has no memory in the sense that the time-derivative of $P(\mathcal{C},t)$ does only depend on the probability distribution at the actual time t and not on $P(\mathcal{C},t^*)$ at earlier times t^*<t. Processes that have no memory in this sense are called *Markov processes*.

It is often helpful to formulate the master equation in a vector space notation. Therefore, Eq. (2.2) can be written as

$$\frac{\partial}{\partial t}\,|P(t)\rangle = -\mathcal{L}\,|P(t)\rangle \ , \tag{2.4}$$

where $|P(t)\rangle$ is a vector whose components are given by the probabilities $P(\mathcal{C}_\alpha,t)$. Thus, the dimension of $|P(t)\rangle$ is the number of possible configurations. The matrix $\mathcal{L}$ is called *Liouville operator* or simply *transition matrix*. It is defined through its elements

$$[\mathcal{L}]_{\alpha\beta} = -w(\mathcal{C}_\beta,\mathcal{C}_\alpha) \ . \tag{2.5}$$

Given the initial condition $|P(t$=$0)\rangle$ the formal solution of the master equation reads

$$|P(t)\rangle = \exp(-\mathcal{L}t)|P(t$=$0)\rangle \ . \tag{2.6}$$

Thus, to solve the stochastic process the Liouville operator has to be diagonalized which is usually a difficult task. Note that each eigenvalue λ of $\mathcal{L}$ is associated with a 'mode' (eigenvector) of the system that relaxes with a time scale $\tau = 1/|\mathrm{Re}\lambda|$ with the real part $\mathrm{Re}\lambda$ of λ. Since stochastic processes are usually not invariant under time reversal, i.e., $w(\mathcal{C}_\alpha,\mathcal{C}_\beta) \neq w(\mathcal{C}_\beta,\mathcal{C}_\alpha)$, $\mathcal{L}$ is generally non-hermitean and thence it may have complex conjugate eigenvalues which are associated with oscillatory behavior.

[1] This is not necessary if one is solely interested in equilibrium properties. In this case unphysical dynamics may be chosen, as long as they enable a fast convergence towards equilibrium.

Synchronous dynamics – discrete time

If time elapses in discrete steps $t \to t+1$, instead of transition rates one assigns *transition probabilities* $p(\mathcal{C}_\alpha, \mathcal{C}_\beta) \in [0,1]$. In this case the master equation has the form

$$P(\mathcal{C}_\alpha, t+1) = P(\mathcal{C}_\alpha, t) + \underbrace{\sum_{\beta \neq \alpha} P(\mathcal{C}_\beta, t) p(\mathcal{C}_\beta, \mathcal{C})}_{\text{gain}} - \underbrace{P(\mathcal{C}_\alpha, t) \sum_{\beta \neq \alpha} p(\mathcal{C}_\alpha, \mathcal{C}_\beta)}_{\text{loss}} , \quad (2.7)$$

with $p(\mathcal{C}_\alpha, \mathcal{C}_\alpha) = -\sum_{\beta \neq \alpha} p(\mathcal{C}_\alpha, \mathcal{C}_\beta)$. In vector space notation Eq. (2.7) reads

$$|P(t+1)\rangle = \mathcal{T} |P(t)\rangle , \quad (2.8)$$

where the *transfer matrix* $\mathcal{T}$ depends on the probabilities $p(\mathcal{C}_\alpha, \mathcal{C}_\beta)$ in a similar way as $\mathcal{L}$ depends on the rates $w(\mathcal{C}_\alpha, \mathcal{C}_\beta)$ in Eq. (2.5). The formal solution of the master equation in discrete time is then given by $|P(t)\rangle = \mathcal{T}^t |P(t{=}0)\rangle$.

In Chaps. 5–7, lattice models are investigated that evolve according to synchronous dynamics, i.e., in discrete time steps. The formulation of the master equation as given above, does not appear explicitely in the following chapters. Nevertheless, the concept, to describe the behavior of a system by a dynamic equation for the probability flow between microscopic configurations, is fundamental for the whole field of nonequilibrium statistical physics in general, and thence for this thesis as well.

2.1.1 Stationarity, detailed balance and the notion of nonequilibrium

Often one is interested in the stationary solution of a stochastic process. A system is in a stationary state when its probability distribution does not change in time. Assume that this stationary state (steady state) is given by the limiting distribution

$$P_{\text{stat}}(\mathcal{C}) = \lim_{t \to \infty} P(\mathcal{C}, t) . \quad (2.9)$$

Here I shall assume that the process is *ergodic* in the sense that $P_{\text{stat}}(\mathcal{C})$ exists and is unique, independent of the initial distribution $P(\mathcal{C}, t{=}0)$. For a discussion of possible criterions for ergodicity see, e.g., Ref. [14]. An important property of ergodic processes is that the *ensemble average* Eq. (2.1) with respect to P_{stat} can be shown to equal to a *time average* over a single and infinitely long realization of the stochastic process [15]. This is in particular important from a computational point of view, since it allows to take

time averages in computer simulations of stochastic process. Note that the definition of ergodicity given above, which I will use in this chapter, is commonplace in the mathematical literature of stochastic processes. However, physicists also associate with ergodicity the exploration of the entire phase space in the steady state. According to Eq. (2.2) steady states fullfill (for continuous time) the *balance condition*

$$\sum_{\beta\neq\alpha} [P_{\rm stat}(\mathcal{C}_\beta)w(\mathcal{C}_\beta,\mathcal{C}_\alpha) - P_{\rm stat}(\mathcal{C}_\alpha)w(\mathcal{C}_\alpha,\mathcal{C}_\beta)] = 0 \ , \ \forall\alpha \ . \tag{2.10}$$

In order to find the steady state distribution of a stochastic process, one can try to make an appropriate ansatz. The balance condition Eq. (2.10) then results in certain conditions for the chosen ansatz. An example is the so-called method of matrix product states (see, e.g., Ref. [16]) where $P_{\rm stat}(\mathcal{C})$ is expressed as a product of matrices, and Eq. (2.10) then leads to relations between these matrices.

Detailed balance

A process is said to obey *detailed balance* when

$$P_{\rm stat}(\mathcal{C}_\beta)w(\mathcal{C}_\beta,\mathcal{C}_\alpha) = P_{\rm stat}(\mathcal{C}_\alpha)w(\mathcal{C}_\alpha,\mathcal{C}_\beta) \ , \ \forall\alpha,\beta \ , \tag{2.11}$$

i.e., each term in the summation in Eq. (2.10) is identical zero. Dynamics that satisfy Eq. (2.11) can be used to generate the equilibrium ensemble, e.g., for an Ising magnet. One may also study the relaxation towards equilibrium. Consider a system with Hamiltonian $\mathcal{H}(\mathcal{C})$ in contact with a heat bath. Then the steady state distribution is known to be the stationary Boltzmann distribution $P_{\rm stat}(\mathcal{C})$=$P_{\rm eq}(\mathcal{C})$=$Z^{-1}e^{-\beta\mathcal{H}(\mathcal{C})}$. Thus one can assign rates that fullfill detailed balance with respect to $P_{\rm eq}(\mathcal{C})$. Such a system will always evolve towards the equilibrium distribution, provided the process is ergodic. From a computational point of view, when sampling through configurational space, the relative frequency of encountering configuration $\mathcal{C}$ will eventually be given by $P_{\rm eq}(\mathcal{C})$.

The notion of nonequilibrium

One may argue that a system is not at thermodynamic equilibrium when its probability distribution is not given by the stationary Boltzmann distribution. This definition of nonequilibrium is convenient for systems with a well-defined Hamiltonian $\mathcal{H}$. However, stochastic processes are often not defined in terms of an energy function but rather in terms of the dynamics.

Hence, a definition of nonequilibrium using the transition rates is necessary. In this context detailed balance is of vital importance. It implies that there is no net flow of probability between two different configurations. Obviously, this is consistent with the intuitive idea of an equilibrium. Contrarily, the balance condition Eq. (2.10) only requires that that there is no *total* net flow of probability in and out of configurations. Nevertheless, a circulation of probability is still allowed which is at odds with the idea of an equilibrium. Therefore a pragmatic definition of nonequilibrium systems states that a system is not at equilibrium when its dynamics does not fullfill detailed balance. Note that irreversible dynamics generically imply a violation of detailed balance.

To conclude, in nonequilibrium systems there is always some kind of flow which results in a flow of probability between different configurations. Physically this flow may be connected to different mechanisms, such as transfer of heat or mass. This thesis deals with processes with underlying irreversible dynamics, and thus, with processes that violate detailed balance. Therefore, the thesis is concerned with nonequilibrium systems.

2.2 Fokker-Planck and Langevin equations

Instead of studying a stochastic process directly through its master equation one may rather wish to analyze approximate differential equations. In this section I introduce two approximate schemes: the *Fokker-Planck equation*, which may be viewed as a Taylor expanded version of the continuous master equation, and the *Langevin equation*, a stochastic differential equation which models the probabilistic nature of the dynamics by a fluctuating random term in the equations of motion.

2.2.1 The Fokker-Planck equation

Let us for simplicity first discuss a stochastic system with only one degree of freedom x. The configuration $\mathcal{C}$ is then simply given by the value of x, where now x may vary continously. Analogous to Eq. (2.2) the master equation for this case reads

$$\frac{\partial P(x,t)}{\partial t} = \int dx' P(x',t) w(x',x) - P(x,t) \int dx' w(x,x') \ . \tag{2.12}$$

A possible way to obtain the Fokker-Planck equation from Eq. (2.12) is via the so-called *Kramers-Moyal expansion* where one Taylor expands Eq. (2.12)

about x. If this expansion is truncated to second order, the result is the following equation,

$$\frac{\partial P(x,t)}{\partial t} = -\frac{\partial}{\partial x}\left[a(x)P(x,t)\right] + \frac{1}{2}\frac{\partial^2}{\partial x^2}\left[b(x)P(x,t)\right] \tag{2.13}$$

which is called Fokker-Planck equation. The functions $a(x)$ and $b(x)$ are determined from

$$a(x) = \int dx' w(x,x')(x'-x) \stackrel{\delta t\to 0}{\equiv} \frac{\langle \Delta x\rangle}{\delta t} , \tag{2.14}$$

$$b(x) = \int dx' w(x,x')(x'-x)^2 \stackrel{\delta t\to 0}{\equiv} \frac{\langle (\Delta x)^2\rangle}{\delta t} . \tag{2.15}$$

As an illustration, x may be interpreted as one coordinate of a charged particle diffusing in a highly viscous fluid (overdamped limit, see Sec. 3.2.1), subjected to an external electrostatic field. $a(x)$ describes the drift of the particle which in this case is proportional to the electrostatic force. With the well-known relation $\langle(\Delta x)^2\rangle{=}2D\delta t$ for Brownian motion and Eq. (2.15) follows that $b(x)$ in this example is independent of x and proportional to the diffusion constant.

Turning to systems with N degrees of freedom x_i ($i{=}1,\ldots,N$), the multivariate Fokker-Planck equation reads

$$\frac{\partial P(\mathbf{x},t)}{\partial t} = -\sum_{i=1}^{N}\frac{\partial}{\partial x_i}\left[a_i(\mathbf{x})P(\mathbf{x},t)\right] + \frac{1}{2}\sum_{i,j=1}^{N}\frac{\partial^2}{\partial x_i \partial x_j}\left[b_{ij}(\mathbf{x})P(\mathbf{x},t)\right] , \tag{2.16}$$

where $\mathbf{x}$ is the N-dimensional vector composed out of the x_i. Similar to Eqs. (2.14,2.15) one finds

$$a_i(\mathbf{x}) \stackrel{\delta t\to 0}{=} \frac{\langle \Delta x_i\rangle_{\mathbf{x}}}{\delta t} , \; b_{ij}(\mathbf{x}) = \frac{\langle \Delta x_i \Delta x_j\rangle_{\mathbf{x}}}{\delta t} . \tag{2.17}$$

The Fokker-Planck equation is an important tool for the investigation of systems with stochastic dynamics. An example for its application is reported in Chap. 3. There, one needs the so-called coagulation kernel to study irreversible aggregation of particles subjected to Brownian motion. The coagulation kernel basically determines how many particles with diffusion constant D and radius a collide per unit time, and it may be derived using an appropriate Fokker-Planck equation.

2.2.2 The Langevin equation

The investigation of *Langevin equations* is a very popular tool for modeling stochastic processes. Langevin equations are stochastic differential equations. The influence of the huge number of microscopic degrees of freedom is subsumed in an irregular fluctuating random term L in the equation of motion, where L is called *noise*. Hence, adding a noise term to a deterministic equation of motion one may study the influence of fluctuations on a system. Consider for simplicity again a system with one degree of freedom x. In this case the Langevin equation may have the form

$$\frac{dx}{dt} = f(x) + g(x)L(t) \ , \tag{2.18}$$

where $f(x)$ is the deterministic part and $g(x)L(t)$ accounts for fluctuations. Since the Langevin equation is set up by adding some noise to a well-known deterministic equation of motion, it is intuitively more appealing than a description using the Fokker-Planck or the master equation. The noise is often called *additive* if $g(x)$=const is simply a constant. Otherwise it is called *multiplicative*. Note that Eq. (2.18) describes a whole ensemble of trajectories in contrast to a single trajectory which is described by the corresponding deterministic equation. Therefore, to deal with Eq. (2.18) one needs information about the statistical properties of $L(t)$.

Usually one assumes that $L(t)$ is a *white Gaussian noise* which is defined through the following conditions.

1. $\langle L(t)\rangle$=0, since $L(t)$ describes the fluctuations about the mean behavior. Any drift may be absorbed in the deterministic part.

2. $\langle L(t)L(t')\rangle = \Gamma\delta(t-t')$, which means that the noise at different times is uncorrelated. For physical systems this can only be an idealization, since there will always be a finite (though maybe small) correlation time τ. However, if one is interested only in the physics on time scales large compared to τ, one may apply the delta-correlated noise.

3. $L(t)$ is Gaussian. This may be justified by the central limit theorem, since $L(t)$ is usually a sum over the influence of many microscopic degrees of freedom. An example is Brownian motion, where $L(t)$ is given by the sum over the momentum transfer from a huge number of fluid molecules to a suspended particle.

Then, knowing the statistical properties of $L(t)$, one may integrate Eq. (2.18) and perform ensemble averages to analyze the system under consideration.

I admit that there are further subtleties, which until now have been swept under the carpet. Eq. (2.18), with the rapidly fluctuating noise $L(t)$, is in a mathematical sense useless as it stands. One must specify how to integrate the right hand side of Eq. (2.18) since $L(t)$ is not an ordinary function. To this end I only note that there are two commonly used integration schemes for stochastic differential equations, namely the *Ito* stochastic integration and the *Stratonovich* stochastic integration. For additive noise both yield the same results while for multiplicative noise the results are different.

I also mention that the Langevin equation can be connected to the Fokker-Planck equation. It can be shown that a Langevin equation of the form Eq. (2.18) (with white Gaussian noise) for Stratonovich integration is equivalent to the Fokker-Planck equation

$$\begin{aligned} \frac{\partial P(x,t)}{\partial t} &= -\frac{\partial}{\partial x}\left[f(x)P(x,t) + \frac{\Gamma}{2}g(x)g'(x)P(x,t)\right] \\ &\quad + \frac{\Gamma}{2}\frac{\partial^2}{\partial x^2}\left[g^2(x)P(x,t)\right] \end{aligned} \tag{2.19}$$

where $g'(x)$ denotes the derivative of g with respect to x. Applying the Ito scheme for stochastic integration the corresponding Fokker-Planck equation reads

$$\begin{aligned} \frac{\partial P(x,t)}{\partial t} &= -\frac{\partial}{\partial x}\left[f(x)P(x,t)\right] \\ &\quad + \frac{\Gamma}{2}\frac{\partial^2}{\partial x^2}\left[g^2(x)P(x,t)\right] \ . \end{aligned} \tag{2.20}$$

In both cases, Eqs. (2.19,2.20), the connection can be made between $f(x)$ and $g(x)$ on the one hand and $a(x)$ and $b(x)$ in Eq. (2.13) on the other hand.

Generalizations to systems with many degrees of freedom are straight forward. Moreover, for spatially extended systems the noise will in general not only depend on time but on space as well, usually leading to the correlator $\langle L(\mathbf{x},t)L(\mathbf{x}',t')\rangle = \Gamma\delta^d(\mathbf{x}-\mathbf{x}')\delta(t-t')$, where d is the dimension of the spatial coordinate $\mathbf{x}$. For an introduction to the numerical treatment of Langevin equations I refer the reader to Ref. [17]. Langevin equations will be discussed in Chaps. 3, 4 and 6.

2.3 Reaction-diffusion processes

Many stochastic processes are formulated in the language of reaction-diffusion processes. Reaction-diffusion processes are models for chemical reactions, where the transport of the reactants is predominantly diffusive. Usually chemical reactions take place in an appropriate environment such as a solvent, a hosting gas or a catalytic surface. Furthermore, the reactions include complicated sequences of intermediate steps. In reaction-diffusion processes all these details are ignored. Instead, the reaction chain is modeled by simple stochastic rules and the configuration is entirely determined by the positions of the particles. If, for instance, A, B denote the reactants that diffuse with diffusion constant D, and react upon contact with rate λ to create a particle of species C, one may write

$$A + B \xrightarrow{\lambda} C \; . \tag{2.21}$$

If species C is subsequently not involved in any reactions, e.g., it is adsorbed on a catalytic surface, this process may also be modeled by

$$A + B \xrightarrow{\lambda} \emptyset \; . \tag{2.22}$$

Usually, the particle number in reaction-diffusion processes is not conserved. Apart from coagulation or annihilation one may incorporate other reactions, e.g., self-destruction ($A \to \emptyset$), transmutation ($A \to B$), offspring production ($A \to 2A$) and others.

Reaction-diffusion models are easily defined on a d-dimensional lattice. Consider a process that involves M different particle species A_k (k=1, ..., M), which are located on the lattice sites. If lattice site i is occupied by a particle of species A_k one assigns s_i=k. If there is no particle at site i one has s_i=0. The master equation for such a lattice model has been introduced in Sec. 2.1. The particles may diffuse where diffusion is modeled by stochastic hops from a lattice site to a neighboring site (according to some probability). Similarly, if particles arrive at the same lattice site, they may react according to some reaction scheme which can be translated into an update of the s_i. The problems studied in Chap. 3, as well as directed percolation, which is discussed in Chap. 4 and 5, are easily formulated as reaction-diffusion processes.

2.4 Field theory and renormalization

The formulation of the master equation in vector space notation, Eq. (2.4), is reminiscent of the Schrödinger equation in quantum mechanics. Moreover, it turns out that many lattice-based models are conveniently written in terms of creation and annihilation operators similar to the second-quantized description in quantum mechanics [18–20]. This makes it then possible to represent the master equation with path integrals which in turn may be analyzed by methods used in quantum field theory (see Ref. [20], for example). Hence, one may derive a *field-theoretic action* from a microscopic master equation. It was pointed out that, given such a field-theoretic action, it is possible to write down a Langevin equation for the process where the form of the noise is specified precisely by the microscopic master equation [21]. However, in Ref. [22] it was argued that the pivotal step in that approach is taking the continuum limit, and that a naive continuum limit may lead to untenable models. Therefore, many field-theories are based on purely mesoscopic Langevin equations.

A powerful tool to investigate the action of stochastic processes is field-theoretic *renormalization group analysis*, see for instance Ref. [23]. In general, the term renormalization refers to a loosely grouped framework of theoretical ideas that describe the scaling behavior of a system under coarse-graining of space and time [3]. Roughly speaking, it deals with the question how the parameters of the system have to be adjusted under coarse-graining of scales without changing the physical properties. This results in a so-called renormalization flow in parameter space, and fixed points of this flow are associated with the appearance of scaling behavior. Hence, the renormalization group approach applies to systems that exhibit scale invariance. Probably the most prominent examples are continuous phase transitions. Examples of simple mean-field renormalizations of Langevin equations can be found in Chaps. 3, 4 and 6. Besides that, there are no renormalization group or field-theoretic calculations in this thesis, and therefore these issues are not discussed in further detail. However, I note that field-theoretic treatments of critical phenomena are very important and particularly successful in coexistence and comparison with Monte Carlo simulations (see Sec. 2.6), which will be performed extensively in Chaps. 6 and 7. Both approaches are used to determine the critical properties of a system, and therefore they provide the possibility of mutual inspiration and inspection.

2.5 Mean-field approximation

In statistical physics one often encounters the following situation. The time derivative of a one-point quantity, e.g., the occupancy $\langle s_i \rangle$ of lattice site i in a reaction-diffusion process, depends on two-point quantities, e.g., $\langle s_i s_j \rangle$, where $\langle\rangle$ denotes the ensemble average. However, two-point quantities in turn depend on three-point quantities and this procedure may be repeated leading to an *infinite* set of equations. A possible method to deal with this situation is to approximate the two-point function by the product of two one point function, i.e.,

$$\langle s_i s_j \rangle \to \langle s_i \rangle \langle s_j \rangle \ . \tag{2.23}$$

This approximation is denoted as *mean-field approximation* (MF) and it clearly neglects fluctuations and correlations of a random variable. MF may be viewed as the limit of infinitely many dimensions. Roughly speaking, in this case all particles are nearest neighbors and correlations and fluctuations are 'washed out'. Mean-field approximation is not only very useful to make qualitative predictions of the behavior of a system. It yields correct results for the asymptotic behavior in large spatial dimensions. In particular, for dimensions $d{>}d_{\rm c}$ mean-field approximation is appropriate whereas for $d{<}d_{\rm c}$ fluctuations and correlations are relevant which invalidates MF. $d_{\rm c}$ is denoted as *upper critical dimension* and the behavior of a system at $d_{\rm c}$ is usually that predicted by MF subjected to *logarithmic corrections*. Possible methods to determine the upper critical dimension are, e.g., renormalization group analysis or computer simulations in varying spatial dimensions.

In reaction-diffusion processes, mean-field approximation is often realized by the so-called *law of mass action* which assumes that the probability of a reaction between two species is proportional to the product of the densities of the species. This assumption is justified when the system is well-mixed so that fluctuations and correlations are irrelevant.

An example where MF is encountered in this thesis, can be found in Chap. 3. Rate equations for irreversible aggregation are analyzed, which apply the law of mass action. Furthermore, it is shown by computer simulations, that the upper critical dimension for the studied systems is smaller than $d{=}3$.

2.6 Computer simulations

Computer simulations play a major role in this thesis. Here I make some general remarks while further details are given in the corresponding chapters. I restrict myself to computer simulations of stochastic processes. A discussion about the general role of computer simulations in the natural science can, e.g., be found in REF. [24].

It is a matter of fact that many interesting stochastic models are unyielding to analytical treatment. In this cases much can be learned from computer simulations. Intuitively this is a very appealing approach since one actually *realizes* the stochastic process on a computer. This means that one basically performs a tour through configuration space according to the prescribed rates. Doing so for many realizations of randomness, one may approximately generate the statistical ensemble, and averaging over the different realizations renders information about statistical properties. Since such simulations involve the use of random numbers (more precisely, pseudo random numbers) they are usually called *Monte Carlo simulations* (MC) [7]. Depending on whether the systems evolves according to asynchronous or synchronous dynamics (see SEC. 2.1), one applies random sequential updates or parallel updates, respectively.

Simulations provide qualitative as well as quantitative results and they are essential for a comparison with other approaches. Thus, they can be used to verify or disprove scenarios predicted by other methods. Moreover, often computer simulations provide the missing hint that is needed to work out an appropriate theory.

The main idea in random sequential updates is only briefly sketched in the following, since the MC simulations that are reported in this thesis, apply parallel updates. In random sequential updates, a possible event is chosen, e.g., a hop of a particle from lattice site i to lattice site j. The event is realized according to the assigned rate. The time increment Δt that is associated with the event is inverse proportional to the sum over the rates for all possible events. For reaction-diffusion models, $1/\Delta t$ is therefore usually proportional to the number of particles. Hence, in the limit of large systems this methods describes the temporal evolution in continuous time $\Delta t \to 0$. In contrast to random sequential updates, in parallel updates the whole system is updated in parallel in each discrete time step $t \to t+1$, according to the given transition probabilities. In CHAPS. 6 and 7, MC simulations for spreading processes are performed, which evolve in discrete time. Further details are presented in that chapters.

Which update scheme is chosen should depend on the particular situation under consideration. In most cases both schemes lead to the same results. One might argue that random sequential updates appear to be more realistic compared to parallel updates. However, both schemes are simplified models for more complicated physical systems and thus it is misleading to consider the one or the other to be more 'realistic'. In MC simulations, the generation of random numbers often consumes most of the computer time. Since random sequential updates usually require more random numbers than parallel updates (selection of random events) they are in many cases less efficient. Furthermore, models with parallel updates are easier implemented as parallelized programs, since different processors only communicate after an update of the whole system. In contrast to that, for random sequential updates the processors usually have to exchange information after each single event, which leads to more communication between the processors and thus slows down the computation.

In Chap. 3, so-called Brownian dynamics simulations for particles suspended in a liquid are carried out. In these simulations, one integrates the deterministic equations of motion of the particles, and adds a stochastic contribution, which models the Brownian motion. Thus, one basically simulates the corresponding Langevin equations. Further details are given in that chapter.

Chapter 3

Irreversible aggregation

In many fields of science irreversible aggregation (or coagulation, agglomeration, clustering) phenomena are important. Examples include aerosol coalescence, polymerization, gelation, or planetesimal accumulation (see, e.g., Refs. [25–30] and references therein) as well as the dynamics of laser-induced excitons [31, 32]. This chapter deals with stochastic models for irreversibly aggregating systems. The main issue is the investigation of monopolarly charged suspensions, where strong van der Waals forces lead to irreversible aggregation upon contact of the suspended particles, see Sec. 3.3. However, in the first section I will briefly discuss single-species coagulation. The aim is to introduce a crude model which nevertheless exhibits interesting behavior and provides a convenient approach to irreversibly aggregating systems. Sec. 3.2 introduces Smoluchowski's coagulation equation, a mean-field equation for multi-species aggregation, which has been extensively used to study aggregation of uncharged particles. In Sec. 3.3 the coagulation equation is applied to study monopolarly charged systems. The results are supported by Brownian dynamics simulations. In Sec. 3.3.6 a summary of the main results is given, together with a perspective of possible future investigations.

3.1 Single-species coagulation

One of the crudest models for irreversible aggregation is the single-species coagulation of particles denoted as A, where it is assumed that particles diffuse independently of each other with diffusion constant D. The reaction

$$A + A \longrightarrow A \,, \tag{3.1}$$

where two particles react irreversibly upon contact to form a single particle, may be interpreted as a simple reaction-diffusion model for chemically

reacting species. Interestingly, this reaction shows the same behavior as single-species annihilation $A + A \to \emptyset$. This can be shown by the existence of a similarity transformation between the master equations of the two reactions [33, 34], by field-theoretic methods [35] or by the method of interparticle distribution functions (IPDF) [30]. In the following I will first analyze this model on a simple mean-field level, before I discuss the influence of fluctuations and correlations.

3.1.1 Mean-field approximation

Assume that particles coagulate if their distance equals $2a$. Thus, a is an effective radius of the particles. Assume further that the system is well-mixed, i.e., the number density of particles $n(\mathbf{x}, t)$ at time t and position $\mathbf{x}$ is the same everywhere. $n(\mathbf{x}, t)$ is a coarse-grained density, averaged over volumes large compared to a and small compared to the system. Since coagulation is a two particle process, one may immediately write down the naive rate equation

$$\frac{dn(t)}{dt} = -rn^2(t) \ , \tag{3.2}$$

where r is a rate constant that depends on D and the effective radius a. For example, in three spatial dimensions r may be calculated by solving an appropriate Fokker-Planck equation (see Sec. 2.2.1) in the presence of an absorbing sphere [27] leading to $r{=}8\pi aD$. Eq. (3.2) applies the *law of mass action* and thereby neglects spatial inhomogeneities and fluctuations as well as correlations between the reacting particles. Note that on a mean-field level *single-species annihilation* obeys $dn/dt{=}-2rn^2$, since in this case *two* particles disappear in a reaction instead of just one as for single-species coagulation. This shows already that for $d{>}d_c$ the two processes show the same behavior. The solution of Eq. (3.2) with the initial condition $n(t{=}0){=}n_0$ is given by

$$n(t) = \frac{1}{rt + 1/n_0} \overset{t\to\infty}{\sim} \frac{1}{rt} \ . \tag{3.3}$$

Eq. (3.3) implies that asymptotically $n_1{=}n(t_1)$ and $n_2{=}n(t_2)$ with $t_2{=}bt_1$ are simply related by a change of scales $n_2{=}b^{-1}n_1$. Hence, this is a very simple example of a process that is *scale invariant* under the transformation $t{\to}bt$ and $n{\to}b^{-1}n$, at least under mean-field assumptions.

3.1.2 Taking fluctuations into account

It turns out that the density decay $n(t){\sim}t^{-1}$ is asymptotically correct for spatial dimensions $d{>}d_c{=}2$ [35], whereas fluctuations and correlations

are *relevant* below d_c in the sense that they change the entire temporal evolution of the process. For $d{=}d_c$ fluctuations and correlations are said to be *marginal*, leading to *logarithmic corrections* (see below). The fact that the upper critical dimension is $d_c{=}2$ may be seen from the following [36]. The random walk executed by the particles is *recurrent* in $d{\leq}2$, which means that the probability of the walk passing through any given point approaches one (see, e.g., REF. [37]). Thus, each particle 'sweeps out' a region with linear size proportional to the diffusion length $l_D{=}\sqrt{2Dt}$. In this region, probably all pairs will have coagulated to a single particle and therefore the particles are strongly *anti-correlated*. Hence, one expects that the volume per particle is of order $l_D^d{=}(2Dt)^{d/2}$, leading to a density decay $n(t){\sim}(2Dt)^{-d/2}$. For $d{>}2$ the random walk loses its recurrent property, which makes the anti-correlations irrelevant and results in an asymptotic density decay according to EQ. (3.3).

The claim that the upper critical dimension is $d_c{=}2$ is supported by a simple *mean-field renormalization* of the corresponding Langevin equation [2], see SEC. 2.4 and SEC. 2.2.2. On heuristic grounds one may derive the Langevin equation for single-species coagulation by taking into account the space dependence of $n(\mathbf{x},t)$ and adding Gaussian noise and a diffusion term to EQ. (3.2). This leads to

$$\frac{\partial n}{\partial t} = -rn^2 + D\nabla^2 n + nL \ , \tag{3.4}$$

$$\langle L(\mathbf{x},t)\rangle{=}0 \ , \ \langle L(\mathbf{x},t)L(\mathbf{x}',t')\rangle = \Gamma\delta^d(\mathbf{x}-\mathbf{x}')\delta(t-t') \ . \tag{3.5}$$

The assumption that the noise is proportional to n may be made plausible as follows. Of course, when there are no particles, the noise must vanish, hence one has multiplicative noise. Then the ideas is that only pairs of particles contribute to the noise since single particles inside a volume element cannot change the density. Applying the mean-field assumption, the number of pairs is proportional to n^2 and the noise originates therefore from n^2 contributions. The *central limit theorem* states that the probability distribution for the noise in this case is Gaussian with a variance proportional to n^2, which leads to a noise amplitude proportional to n. Note that this reasoning ignores additional contributions to the noise, e.g., due to higher powers of n or diffusion. Now one assumes that the process is invariant under the scaling transformation

$$\mathbf{x} \to b\mathbf{x} \ \ , \ \ t \to b^z t \ \ , \ \ n \to b^\chi n \ , \tag{3.6}$$

where $b{>}1$ is a dilatation, z is the so-called *dynamic exponent* that relates the scaling of space and time, and χ governs the scaling properties of the

density. The scaling transformation EQ. (3.6) corresponds to 'coarse-graining the view of the process'. Simple power-counting yields that invariance of EQS. (3.4,3.5) under rescaling, EQ. (3.6), implies z= 2 and χ=−2. Then the noise scales as

$$nL \to b^{1-d/2} nL \ . \tag{3.7}$$

One argues that according to EQ. (3.7) for d>2 the noise decreases under successive rescaling. Therefore the noise is irrelevant on large scales, which leads to mean field behavior. For d<2 the noise amplitude increases under successive rescaling, thus fluctuations are relevant, invalidating the mean-field assumptions. For d=2 the noise stays finite, i.e., it is marginal which usually leads to logarithmic corrections.

One has to keep in mind that the above presented arguments are based on heuristic considerations and therefore have to be supplemented by an analysis with other methods. This can, for example, be done by a field-theoretic treatment [35] that confirms the above described behavior, leading indeed to a density decay according to

$$n(t) \sim \begin{cases} t^{d/2} & \text{for } d < 2 \\ t^{-1} \ln t & \text{for } d = 2 \\ t^{-1} & \text{for } d > 2 \ . \end{cases} \tag{3.8}$$

For most irreversibly aggregating systems the spatial dimension is d=3. Then, for systems that can be modeled by the reaction $A+A \to A$, a simple rate equation approach provides correct results for the asymptotic behavior. Moreover, the critical dimension of single-species coagulation is basically determined by the critical dimension of Brownian motion d_c=2 (recurrent). This suggests that also for more complicated reactions a mean-field analysis yields correct results in the physically most relevant case d=3. Remarkably, even the influence of fluctuations and correlations, leading to $n(t) \sim t^{-1/2}$ in one spatial dimension, has been verified experimentally by analyzing the kinetics of laser-induced excitons on tetramethylammonium manganese trichloride (TMMC) [31, 32]. In that system, laser-induced electronic excitations of Mn^{2+} ions may be interpreted as quasi-particles, called excitons. Their motion is diffusive due to exciton-phonon lattice distortions and one dimensional since the Mn^{2+} ions are arranged in chains. When two excitons meet, the corresponding ion is first excited to twice the exciton energy and then relaxes back to a single exciton state by emission of phonons. Hence, this system

may be modeled by the reaction $A+A\rightarrow A$, where A denotes an exciton. The density n of excitons was measured indirectly via the luminescence intensity which is proportional to n, confirming experimentally the decay $n(t)\sim t^{-1/2}$.

3.2 Smoluchowski's coagulation equation

The above discussed model did not take into account that the properties of the particles may change in a reaction. Usually particles grow when they coagulate, leading to altered diffusion constants or reaction rates. A widely used method to investigate such systems on a mean-field level is to study *Smoluchowski's coagulation equation*. To this end, extensive analytical and numerical studies have been carried out for uncharged systems [26, 38]. In this section I summarize the main results. Coagulation in charged systems will be discussed in the next section.

Assume that the masses of the particles (or clusters) are integral multiples of a minimum mass m^*. The coagulation equation reads

$$\frac{dn_i(t)}{dt} = \frac{1}{2}\sum_{j+k=i} R_{jk} n_j(t) n_k(t) - n_i(t) \sum_{j=1}^{\infty} R_{ij} n_j(t) \ , \tag{3.9}$$

where $n_i(t)$ denotes the number density at time t of clusters of mass $m_i{=}im^*$ and radius $a_i{=}i^\alpha a^*$. $1/\alpha$ is the fractal dimension of the aggregates. If they are spherical (e.g., coagulating droplets) one has $\alpha{=}1/3$. More generally one may assume that $1{>}\alpha{>}1/3$ for fluffier aggregates. The most relevant initial conditions are monodisperse, i.e., $n_1(t{=}0){=}$const and $n_i(t{=}0){=}0$ for $i{>}1$. For simplicity I assume $n_1(t{=}0){=}1$. Particles with index 1 are called *primary particles*. R_{ij} is the rate coefficient, also called coagulation kernel, for mergers between clusters with indices i and j. Analogous to Eq. (3.2), the coagulation equation, Eq. (3.9), neglects spatial fluctuations and correlations between the positions of the reacting clusters. In Sec. 3.2.1 I demonstrate, that a Brownian dynamics simulation of aggregating spheres (where the properties of the spheres change in an aggregation event) in three dimensions is in accordance with the corresponding mean field description.

One may wonder that the contribution to dn_i/dt from reactions where both particles have index i is $-R_{ii}n_in_i$ and *not* $-2R_{ii}n_in_i$, though in this reaction *two* particles with index i coagulate. Contrarily, in a reaction that corresponds to $-R_{ij}n_in_j$ with $i{\neq}j$, only one particle with index i coagulates (and one with index j). The reason may be illustrated as follows. Assume

that $n_i{=}n_j$ with $i{\neq}j$. The number of possible pairs of particles, both with index i, is asymptotically half the number of possible pairs of particles with indices i and j. Hence, the apparent factor 2 due to the annihilation of two particles for reactions between particles with the same index drops out.

The particular physical system under consideration determines the choice of the rate coefficients R_{ij}. Consider, for instance, a suspension where clusters of mass m_i diffuse with diffusion constant D_i. Aggregation with a cluster of mass m_j occurs when the distance between the clusters equals $a_i{+}a_j$. As was already mentioned in SEC. 3.1.1, for this situation R_{ij} can be calculated by solving the Fokker-Planck equation in the presence of an absorbing sphere [25, 27] leading to $R_{ij}{=}4\pi(a_i + a_j)(D_i + D_j){\equiv}r_{ij}$. If Einstein's formula applies, one can insert $D_i{=}k_\mathrm{B}T/6\pi\eta a_i$, with the temperature T and the viscosity η of the carrying fluid and Boltzmann's constant k_B. This leads to

$$r_{ij} = \frac{2k_\mathrm{B}T}{3\eta}(i^\alpha + j^\alpha)(i^{-\alpha} + j^{-\alpha}) \ . \tag{3.10}$$

Note that these rates are homogenous functions of degree $\lambda{=}0$, which means that

$$r_{bi\,bj} = b^\lambda r_{ij} \ , \tag{3.11}$$

with the dilatation b.

In general, for most *uncharged* coagulating systems discussed in the literature, the coagulation kernels are homogeneous functions of degree λ where λ is not restricted to $\lambda{=}0$ [26]. Coagulation of spherical particles in the kinetic gas regime leads, for example, to $\lambda{=}1/6$ [25]. Besides λ the R_{ij} are usually characterized by another exponent μ. According to

$$R_{ij} \sim \begin{cases} i^\lambda & \text{for } i \sim j \\ i^\mu j^\nu & \text{for } i \ll j \text{ with } \mu + \nu = \lambda \end{cases} \tag{3.12}$$

the exponent λ determines mergers of particles of comparable mass. Contrarily, mergers of particles with much heavier particles are specified by the exponent μ. Since the number of reactive sites on a particle cannot increase faster than its mass, one usually imposes the physical restrictions $\lambda{\leq}2$ and $\nu{\leq}1$. For Brownian coagulation obeying EQ. (3.10) one has $\lambda{=}0$ and $\mu{=}{-}\alpha$.

The coagulation equation, EQ. (3.9), can be solved exactly only for a few simple coagulation coefficients and monodisperse initial conditions. However, these results and extensive analytical (e.g., based on self-similarity assumptions) as well as numerical studies [26, 38] led to the conclusion that the most

important parameter is the degree of homogeneity λ. Depending on its value, the coagulation equation shows two types of qualitatively different solutions. **(i)** For $\lambda \leq 1$ the cluster size distribution decays exponentially for large sizes at all times. In the scaling limit the solutions are self-similar and (for $\lambda<1$) have the form

$$n_i(t) = s(t)^{-2}\phi\left[i/s(t)\right] \text{ with } s(t) \sim t^{\frac{1}{1-\lambda}} \tag{3.13}$$

and a scaling function ϕ that depends on the details of the underlying coagulation kernels. The average size $s(t)$ is a measure for the average number of primary particles per cluster. A possible definition is $s=M_1/M_0$ with the moments defined as $M_l=\sum_i i^l n_i$. M_1 is proportional to the constant total mass of the system and M_0 to the total number of particles at time t. The fact that s^{-2} precedes the scaling function in Eq. (3.13) comes from the conservation of the total mass, i.e., $\sum_i i n_i$=const. In coagulation experiments on aerosols and emulsions, it has indeed been observed that after a transient period the cluster size distribution approaches a scaling form (see Ref. [26] and references therein). If $\lambda=1$ and $\mu=0$ the solution also obeys Eq. (3.13) but with $s(t) \sim e^t$. For $\lambda=1$ and $\mu>0$ a slightly different self-similar solution has been derived with $(\ln s(t))^2=a+bt$ and constants a and b [39]. **(ii)** For $2\geq\lambda>1$ the cluster size distribution develops a power-law tail in finite time $\tilde{t}$ at large sizes that violates mass conservation. This is sometimes called *runaway growth* and the physical interpretation of this is the occurrence of a *gelation transition*. In this case a self-similar solution is only valid for $t<\tilde{t}$ with the average size s diverging at $\tilde{t}$ as

$$s(t) \sim (\tilde{t}-t)^{-1/\delta} \text{ with } \delta = \frac{1}{2}(\lambda - 1)\ . \tag{3.14}$$

3.2.1 Brownian dynamics simulations of uncharged coagulating spheres

The aim of this section is to provide numerical evidence that fluctuations and correlations, which are neglected in Smoluchowski's coagulation equation, are irrelevant in (uncharged) three dimensional systems, in the sense that they do not change the behavior predicted by Eq. (3.9). Therefore, I perform Brownian dynamics simulations of coagulating spheres and compare the results with predictions based on the analysis of Eq. (3.9). In particular, the time dependence of $s(t)$ for four different choices of R_{ij}, will be investigated and compared to Eq. (3.13). Note that to my knowledge, there is no similar comparison between Brownian dynamics simulations and Smoluchowski theory in the literature.

I simulate irreversibly aggregating spherical particles in a suspension. According to EQ. (3.10), in this case the coagulation kernel in the Smoluchowski equation obeys $R_{ij}\sim(D_i+D_j)\,(a_i+a_j)$. The initial configuration is a system of N randomly distributed spheres (primary particles) in a cubic simulation box with periodic boundary conditions. The particles initially have the same radius a and diffusion constant $D=C/a$ with a constant C. The positional shift $\Delta\mathbf{r}_p(t)=\mathbf{r}_p(t+\Delta t)-\mathbf{r}_p(t)$ of particle p within a time step Δt is given by

$$\Delta\mathbf{r}_p(t) = \xi_p(\Delta t)\ , \tag{3.15}$$

where ξ_p is the displacement caused by Brownian motion. The time step was chosen such that the displacement was smaller than a few percent of the radius of the particles. The justification of EQ. (3.15) is based on a separation of time scales. The particles are subjected to frequent 'kicks' by the fluid molecules of the surrounding liquid. Hence, on time scales larger than the velocity correlation time $\tau=m/(6\pi\eta a)$ (m and a are mass and radius of a spherical particle) the particles do not move ballistically but randomly. τ has to be compared with the typical time particles need to diffuse on average a distance of their own diameter $t_{\text{diff}}=12\pi\eta a^3/(k_{\text{B}}T)$. As was argued in REF. [40], under typical experimental conditions τ is always much smaller than t_{diff}, even if one considers particles as small as 1nm. Therefore it is justified to neglect inertia effects and to apply the so-called *overdamped limit* in EQ. (3.15). Note that the overdamped limit was also applied in the derivation of EQ. (3.10).

Each cartesian coordinate $\xi_{p,\gamma}$ ($\gamma=1,2,3$) of the displacement ξ_p caused by Brownian motion was drawn from a Gaussian distribution of random numbers with the probability distribution

$$P(\xi_{p,\gamma}) = \frac{1}{\sqrt{2\pi\sigma^2}} e^{-\frac{\xi_{p,\gamma}^2}{2\sigma^2}}\ , \quad \text{with} \quad \sigma = \sqrt{2D_p\Delta t}\ . \tag{3.16}$$

where D_p is the diffusion constant of particle p. As long as the particles do not collide, the positions of the particles are updated as $\mathbf{r}_p(t+\Delta t)=\mathbf{r}_i(t)+\Delta\mathbf{r}_p(t)$. During the simulation, all particles remain spherical. In general, when two particles l and m with radii a_l and a_m are separated by a distance $d<a_l+a_m$, they coagulate to form a new spherical particle. The position of the new particle is given by the center of mass of the colliding particles. The further details of this coalescence process, i.e., how the properties of the new particle, such as the diffusion constant, depend on the particles l and m, will be discussed in the following. Four different cases are studied. Each of these cases realizes coalescence events in the simulation in a different way and each

way is associated with a particular form of the coagulation kernel R_{ij} in the Smoluchowski equation. Let index p denote the new particle which is formed upon collision of particles l and m.

Case A) The diffusion constant D_p is given by $D_p{=}C/a_p$ with the new radius $a_p{=}\left(a_l^3{+}a_m^3\right)^{1/3}$. This is ordinary Brownian coagulation which corresponds to the coagulation kernel r_{ij} in EQ. (3.10) with $\alpha{=}1/3$. In particular, for this case the degree of homogeneity is $\lambda{=}0$. Therefore, the mean-field equation predicts an increase of the average size $s(t)$ proportional to t.

Case B) The radius and the diffusion constant is not altered in a coalescence event, i.e, particle p has radius a and diffusion constant D. This results in a constant coagulation kernel $R_{ij}{=}$const with $\lambda{=}0$ as above, leading to $s(t){\sim}t$ as well.

Case C) The radius increases as $a_p{=}\left(a_l^3{+}a_m^3\right)^{1/3}$ but D_p is kept constant, $D_p{=}D$. This corresponds to $R_{ij}{\sim}(i^{1/3}{+}j^{1/3})$, i.e., $\lambda{=}1/3$ and $s(t){\sim}t^{3/2}$.

Case D) The radius is kept constant, $a_p{=}a$, but the diffusion constant decreases as if the particles would grow. During the simulation I keep track of how many primary particles the particle p is composed of. Let n denote the number of primary particles in particle p. The diffusion constant is then given by $D_p{=}C/(n^{1/3}a)$. This case is associated with the coagulation kernel $R_{ij}{\sim}(i^{-1/3}{+}j^{-1/3})$, yielding $\lambda{=}{-}1/3$ and therefore $s(t){\sim}t^{3/4}$.

FIG. 3.1 presents data for the average size $s(t)$ for the cases A) to D) in comparison with the predictions of Smoluchowski's coagulation equation [41]. The average size $s(t)$ was chosen as the number N of initial particles (primary particles) divided by the number of particles at time t. The dashed lines show the asymptotic power-law behavior which is predicted by the mean-field approximation for the different cases, as discussed above. The transients are not shown, see below. It can be observed that for all cases asymptotically the simulation exhibits the behavior predicted by Smoluchowski's coagulation equation. This strongly supports the claim that the mean-field approximation is appropriate for irreversible coagulation of uncharged particles in $d{=}3$.

In the following I make some technical remarks concerning the algorithmic implementation. To avoid an N^2-algorithm (for the update of collisions) the simulation box was divided into cells such that only collisions between

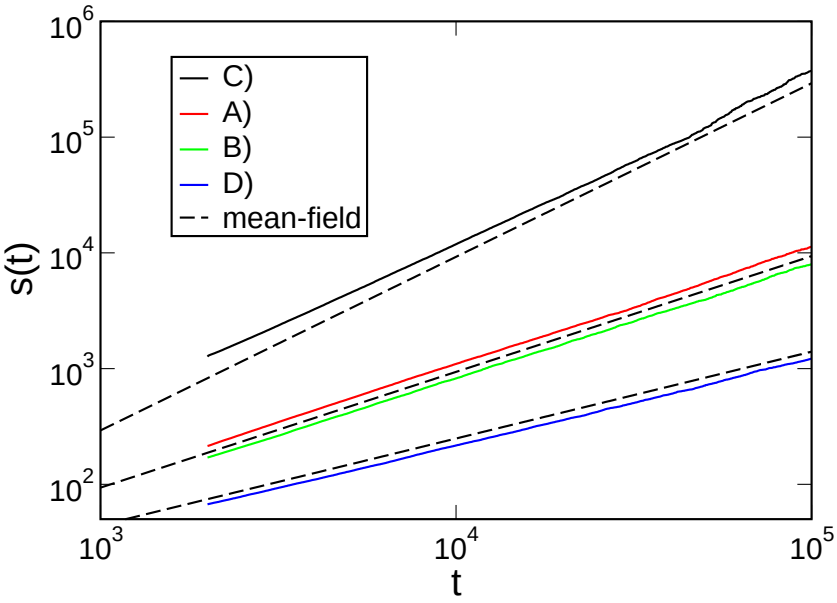

FIGURE 3.1: *Data from Brownian dynamics simulations for the cases A) to D) in comparison with the predictions of Smoluchowski's coagulation equation.*

particles within the same or neighboring cells had to be checked [42]. The simulation was started with initially N=8·10^4 primary particles in a cubic simulation box of length L. The volume fraction was ν=0.003. The simulation was carried out once (for each of the discussed cases) until a certain time t=$\hat{t}$. Then it was stopped and the configuration of the particles was stored. The stored configuration was duplicated 8 times and the duplicates were placed in 8 cubic cells of length L within a larger cubic simulation box of length $2L$. This larger system was then taken as initial configuration for successive simulations. The data in FIG. 3.1 was obtained by averaging over several runs which started at t=$\hat{t}$ with the larger system as initial configuration. By this method, spending a lot of computer time in simulating the transients was avoided, and the data correspond to an initial number of 8·8·10^4=640000 primary particles. An exception is D) where the process is slower than in the other cases, since the diffusion constant decreases but the radius is kept constant. In this case the configuration obtained from the first run at t=$\hat{t}$ was take as initial system, without duplicating the configuration and increasing the size of the simulation box.

3.3 Self-focussing dynamics in monopolarly charged suspensions

In spite of the fact that charges are present in a lot of aggregating systems, much less is known for irreversibly aggregating systems of charged particles. In this section the influence of charges on the aggregation process is investigated [28]. In contrast to previous work which studied aggregation in bipolar charged systems [43], here the aggregation dynamics of equally charged particles is investigated with the focus on suspensions. A practical example is given in REF. [40], where monopolarly charged clusters are suspended in liquid nitrogen. The clusters collide due to Brownian motion, and strong van der Waals forces lead to irreversible aggregation (Brownian coagulation). Further information about the work reported in REF. [40], which initiated the present study, are given in the appendix. However, the results derived in this section are valid for more general systems, as well. Asymptotically neither the solvent nor the diffusion properties are important, as long as particles may have high kinetic energy, albeit as rare events, and charges accumulate in the aggregation process.

Usually a suspension is regarded as stable with respect to the aggregation of equally charged particles, if the particle diameter d_p is small compared to the *Bjerrum length* $l_\mathrm{B}{=}q^2/4\pi\epsilon_0\epsilon_\mathrm{r}k_\mathrm{B}T$, where q is the charge of the particles, T and ϵ_r are the temperature and the relative dielectric constant of the carrying fluid, k_B is Boltzmann's constant and ϵ_0 is the dielectric constant of vacuum. The reason is that in this case the energy barrier for bringing two particles into contact, so that the distance between the charges is of order d_p, is larger than the thermal energy. A simple sketch of this energy argument is presented in FIG. 3.2.

Let me consider the case, where a suspension is initially unstable (as was the case in REF. [40]), which means that initially aggregation events are frequent. I am going to show that charge accumulation eventually leads to a crossover from fast (power-law) cluster growth to slow (sub-logarithmic) aggregation after a characteristic time t_c at a characteristic cluster size (or mass) s_c. Above t_c, the Bjerrum length becomes larger than the aggregate diameter, so that one would regard the suspension as stable for later times. However, the cluster size distribution keeps evolving slowly and approaches a *universal* self-similar form which is independent of *any* parameter included in the theory. A particular important consequence of this is that the relative width of the cluster size distribution σ_r starts decreasing at t_c and asymptotically reaches

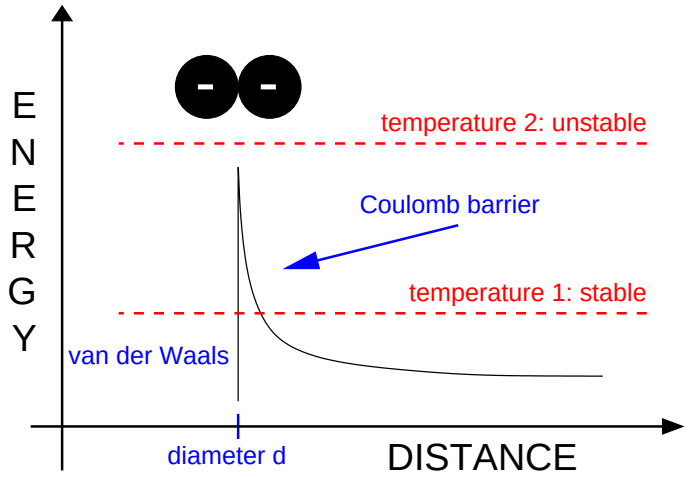

FIGURE 3.2: *Sketch of the comparison between the Coulomb barrier and the thermal energy. This leads to a criterion for the stability of suspensions of equally charged particles, which may be expressed in terms of the so-called Bjerrum length, see text. In this sketch strong van der Waals forces lead to irreversible aggregation upon contact of the particles.*

a universal value $\sigma_r^\infty \approx 0.2017$. In this sense, the cluster size distribution becomes narrower, and I refer to this effect as charge-induced *self-focussing*. For Brownian coagulation the value $\sigma_r^\infty \approx 0.2017$ must be compared to $\sigma_r \approx 1$ for the uncharged case. The conjecture seems plausible that σ_r^∞ is a lower bound for the asymptotic value of σ_r for all physical systems with irreversible aggregation.

3.3.1 R_{ij} for monopolarly charged systems

In the following, I investigate Smoluchowski's coagulation equation for monopolarly charged clusters and monodisperse initial conditions, i.e., in the beginning all particles have the same mass m^* and radius a^* and carry the same charge q^*. As mass and charge of aggregates are proportional to each other in this case, one index i is sufficient in the coagulation equation which then is given by EQ. (3.9). The index i specifies the mass, the radius *and* the charge. Hence, $n_i(t)$ denotes the number density at time t of clusters of mass $m_i = im^*$, charge $q_i = iq^*$ and radius $a_i = i^\alpha a^*$. For non-monodisperse initial conditions, two indices are required to specify mass and charge of the clusters separately.

How do the rate coefficients R_{ij} depend on the charges? A derivation similar to the uncharged case leads to the coagulation kernel for Brownian coagulation of *charged* clusters [27]

$$\begin{aligned} R_{ij} &= W_{ij} r_{ij} \ , \\ W_{ij} &= \kappa_{ij} / \left[\exp(\kappa_{ij}) - 1\right] \ , \\ \kappa_{ij} &= q_i q_j / \left[4\pi\epsilon_0\epsilon_\mathrm{r}(a_i + a_j) k_\mathrm{B} T\right] \ , \end{aligned} \tag{3.17}$$

where r_{ij} is the coagulation kernel for uncharged clusters, Eq. (3.10). It was assumed that at contact of the clusters the charges are separated by a distance $a_i{+}a_j$. κ_{ij} is the Coulomb energy at contact of the clusters divided by $k_\mathrm{B}T$. Comparison with the Bjerrum length leads to $\kappa_{ij}{=}l_\mathrm{B}/d_\mathrm{p}$, provided that all particles are equal and have diameter d_p.

A similar result was obtained for the collision frequency f between equally charged particles in a granular gas [44], which is a quantity analogous to the coagulation kernel. In this case $f{\sim}f_0 \exp(-\frac{E_q}{T_G})$ where f_0 is the collision frequency for uncharged particles, E_q is the energy barrier to be overcome to let two particles collide and T_G is the so-called granular temperature, which is a measure for the mean square fluctuations of the grain velocities.
Led by these observations, I investigate rate coefficients according to

$$R_{ij} = (i^\alpha + j^\alpha)(i^{-\alpha} + j^{-\alpha}) \, \frac{\kappa_{ij}}{\exp(\kappa_{ij}) - 1} \tag{3.18}$$

$$\text{or} \quad R_{ij} = (ij)^{\lambda/2} \, \exp(-\kappa_{ij}) \tag{3.19}$$

$$\text{with} \quad \kappa_{ij} = \frac{k^2 ij}{(i^\alpha + j^\alpha)} \ . \tag{3.20}$$

κ_{ij} is proportional to the Coulomb energy at contact of the clusters divided by a temperature-like variable. Eq. (3.18) is the dimensionless coagulation kernel for Brownian coagulation of charged clusters, Eq. (3.17), with $k^2{=}q^{*2}/(4\pi\epsilon_0\epsilon_\mathrm{r}a^* k_\mathrm{B}T)$ and $2k_\mathrm{B}T/3\eta{=}1$. For $\kappa_{ij}{\approx}0$, Eq. (3.18) corresponds to a degree of homogeneity $\lambda{=}0$, see Eq. (3.11), as was pointed out in Sec. 3.2. To investigate the influence of $\lambda{\neq}0$, I use the general rate coefficient Eq. (3.19). In the following, the behavior of Eq. (3.9) is studied, for rate coefficients that obey Eqs. (3.18,3.19,3.20). Note that the rates depend on three parameters, namely, λ, k, α.

3.3.2 Crossover

Let the system initially be unstable ($k^2 \ll 1$), which means that in the beginning the exponential terms in EQS. (3.18,3.19) are close to unity. The system basically behaves as if it was uncharged. This changes as soon as values of $\kappa_{ij} \approx 1$ become important so that the exponential terms must be taken into account. Then, further aggregation is exponentially suppressed and cluster growth becomes very slow. This happens when the average cluster size s approaches a characteristic value s_c given by $\kappa_{s_c s_c} \approx 1$. Note that even systems, which in the uncharged case exhibit runaway growth, i.e. $1 < \lambda \leq 2$, eventually cross over to slow aggregation. According to EQ. (3.13) the crossover time t_c is given by $s_c \sim t_c^{1/(1-\lambda)}$ for $\lambda < 1$, leading to

$$s_c \approx k^{-\frac{2}{2-\alpha}} \ , \ t_c \approx k^{-\frac{2-2\lambda}{2-\alpha}} \, t^* \ \text{ for } \lambda < 1 \ , \tag{3.21}$$

where t^* is the appropriate time unit. Though similar arguments may be applied for t_c and $\lambda \geq 1$, I do not discuss this case here.

The rate equations (3.9) were solved numerically for various choices of the coagulation kernels R_{ij} and different values of k. Details of the numerical procedure are given in SEC. 3.3.4. FIG. 3.3 shows data for Brownian coagulation of charged spheres (EQ. (3.18) with $\alpha = 1/3$). The average size $s(t)$ was calculated as $s = M_1/M_0$ with the moments defined as $M_l = \sum_i i^l n_i$. M_1 is proportional to the constant total mass of the system and was chosen equal 1. s_c and t_c were determined according to EQ. (3.21). FIG. 3.3 clearly shows the crossover from fast power-law cluster growth to slow aggregation. Moreover, EQ. (3.21) is confirmed by the data collapse. In addition, I checked rate coefficients obeying EQ. (3.19) with different values of λ and α and found in all cases agreement with EQ. (3.21), as well.

Comparison of the dimensionless rate (3.18) with EQ. (3.10) shows that the time unit is $t^* = \frac{3\eta}{\tilde{n} 2 k_B T}$, where $\tilde{n}$ is the initial number density of primary particles. As an example, I compute the physical time scale t^* for possible realistic parameters. With $\eta = 10^{-4}$Pa s, $T = 300$K, $a^* = 1\mu$m and volume fraction $\nu = 10^{-3}$ ($\tilde{n} \approx 2 \cdot 10^5 \text{mm}^{-3}$) one obtains $t^* \approx 150$s. Assuming $\epsilon_r \approx 1$, charging with a single elementary charge on each primary particle corresponds to a value $k \approx 0.2$. For these parameters one finds with the dimensionless results of FIG. 3.3 that the crossover to slow aggregation occurs within hours.

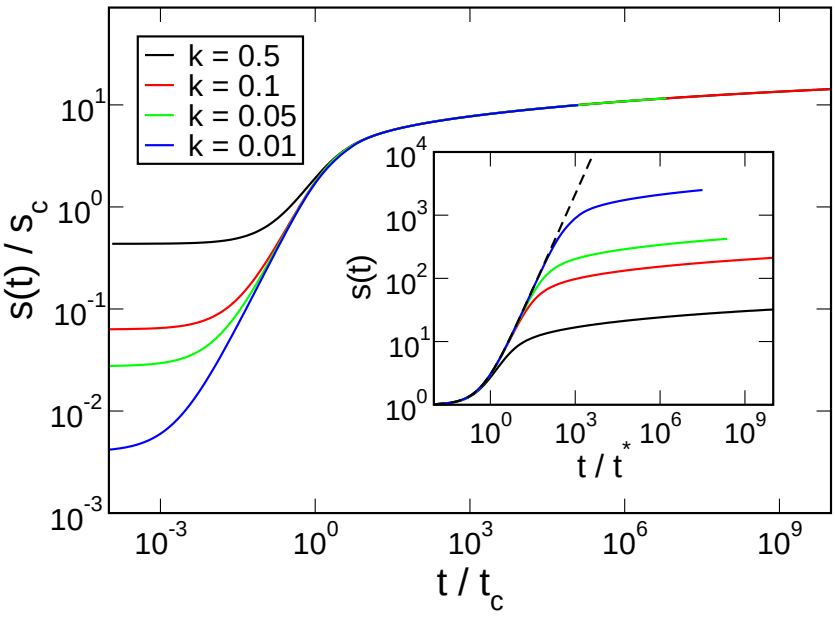

FIGURE 3.3: *The average size $s(t)$ scaled with s_c vs. time t scaled with t_c for different values of k. The data collapse shows that in all cases the crossover to slow cluster growth happens at t=t_c and s=s_c. The inset shows the original data, and the dashed line is the behavior for an uncharged system (k=0). Note that during the integration the time step could be increased, since the rates for mergers become small in the stable regime. Thus, t/t^* is larger than the number of time steps, see* SEC. *3.3.4.*

3.3.3 Asymptotic behavior

In the unstable regime the system behaves basically as in the uncharged case and the cluster size distribution is approximately given by EQ. (3.13). FIG. 3.4 displays a double logarithmic plot of the scaled size distribution in the *stable* regime for three different times and two different choices of the rate coefficients. The coagulation kernel for the red dashed lines obeys EQ. (3.18) with k=0.1 and α=1/3 (Brownian coagulation of charged spheres). Solid black lines correspond to EQ. (3.19) with k=0.05, α=0 and λ=−2. The inset shows these data unscaled (t_1<t_2<t_3). The parameter α=0 corresponds to the limiting case, where the Coulomb repulsion of large clusters becomes independent of the cluster radius. For comparison, the dot-dashed line shows a decay proportional x^{-2}. The labels a, b, $\phi(a)$ and $\phi(b)$ mark analytical expressions for the asymptotic edges of the distribution and the corresponding heights, which will be derived in the following.

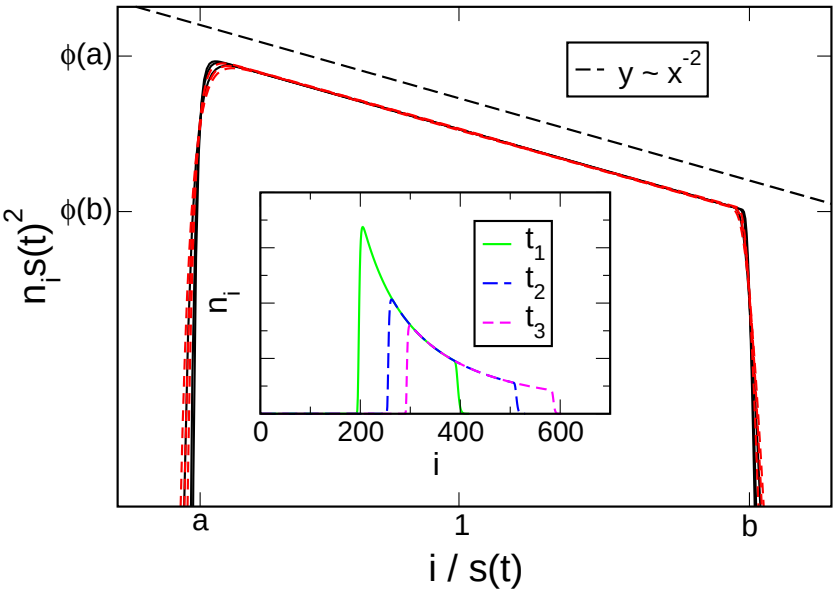

FIGURE 3.4: *Double logarithmic plot of the scaled cluster size distribution for different times and choices of the coagulation kernels. The inset shows original data.*

It can be seen that for monopolarly charged systems the cluster size distribution asymptotically converges to a self-similar solution analogous to EQ. (3.13). Furthermore, FIG. 3.4 strongly supports the claim that $\phi(x)$ is independent of the details of the underlying coagulation kernel. The data suggest that the scaling function $\phi(x)$ decays as $\phi(x) \sim x^{-2}$ between sharp edges and is zero outside. As can be observed in the inset of FIG. 3.4, a consequence of this is that n_i is independent of the average size s between the edges of the size distribution. Based on the numerical data I assume

$$\phi(x) \;=\; \begin{cases} \phi_0\, x^{-2} & \text{for } x \in [a,b] \\ 0 & \text{for } x \notin [a,b]\ . \end{cases} \tag{3.22}$$

Applying EQ. (3.22) one finds

$$M_0 = \frac{\phi_0}{s}\left[\frac{1}{a} - \frac{1}{b}\right] \quad \text{and} \quad M_1 = 1 = \phi_0 \ln\left(\frac{b}{a}\right)\ . \tag{3.23}$$

These expressions for the moments together with $s = M_1/M_0$ lead to

$$\ln\left(\frac{b}{a}\right) = \frac{1}{a} - \frac{1}{b}\ . \tag{3.24}$$

The characteristic feature of the coagulation rates for monopolarly charged systems is that (in the stable regime) coagulation is exponentially suppressed with increasing cluster sizes. This feature does not depend on λ, k, and α or whether one applies Eq. (3.18) or Eq. (3.19). The exponential suppression causes the rates for coagulation of clusters located at the left edge of the size distribution to be much larger than rates for any other coagulation events. Thus, clusters at the left edge with index $i\in[as, as+\Delta i]$ coagulate, and mass conservation requires that this leads to an increase of the number of clusters with $i\in[2as, 2as+2\Delta i]$. Hence, one expects that asymptotically $b=2a$. Between the left and the right edge of the size distribution, n_i is essentially not changed. The scaling function Eq. (3.22) is the only possibility to guarantee such a behavior. Inserting $b=2a$ into Eqs. (3.24,3.23) leads to

$$a = \frac{1}{2\ln 2} \quad , \quad b = \frac{1}{\ln 2} \quad , \quad \phi_0 = \frac{1}{\ln 2} \tag{3.25}$$

in good agreement with the numerical data, Fig. 3.4.

A particular important consequence of the universal form Eqs. (3.22,3.25) is that the relative width of the cluster size distribution

$$\sigma_{\rm r} = \sqrt{\frac{M_2 M_0}{M_1^2} - 1} \tag{3.26}$$

approaches a universal value $\sigma_{\rm r}^{\infty}$ with

$$\sigma_{\rm r} \;\longrightarrow\; \sigma_{\rm r}^{\infty} = \sqrt{\frac{1}{2[\ln 2]^2} - 1} \approx 0.2017 \; . \tag{3.27}$$

Fig.3.5 shows numerical data for $\sigma_{\rm r}$ with $\lambda=(0,-2,-4)$ for monopolarly charged particles (solid lines) in comparison to the corresponding uncharged cases (red lines). $\sigma_{\rm r}^{\infty}$ is considerably smaller than the relative width for any physical system I found in the literature. An example are the data for $\lambda=0$ in Fig. 3.5, which were obtained for Brownian coagulation of spheres. As can be observed, in the uncharged case the relative width approaches a value close to one. This must be compared to $\sigma_{\rm r} \approx 0.2017$ for the charged case.

For an initially narrow cluster size distribution like the one we chose, the relative width first grows similar to the uncharged situation until the crossover time $t_{\rm c}$, when it starts decreasing again, induced by the exponential suppression of further aggregation. I refer to this as *self-focussing*. The example discussed above, with $t^*\approx$150s, shows that this self-focussing effect

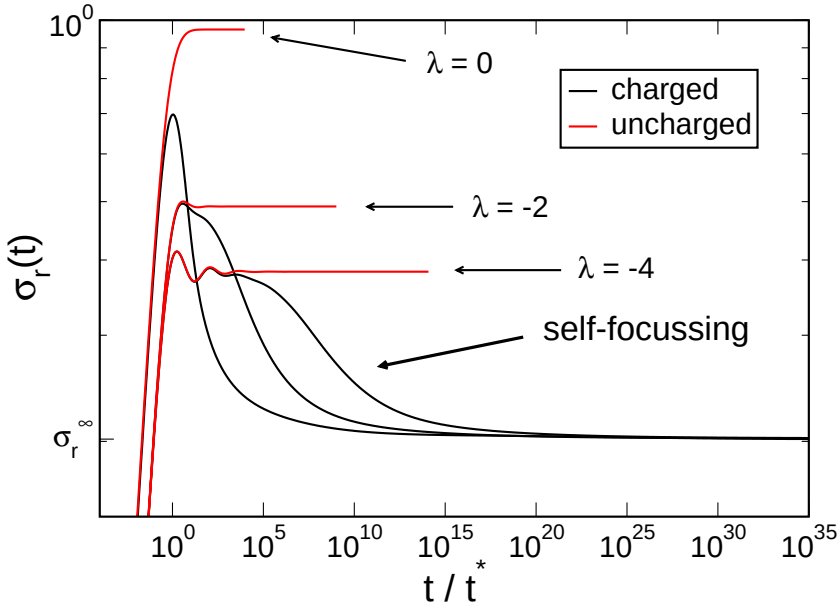

FIGURE 3.5: *Relative width σ_r of the cluster size distribution for monopolarly charged and corresponding uncharged systems. $k = (0.5, 0.1, 0.05)$ for $\lambda = (0, -2, -4)$.*

can occur within an experimentally accessible time. Furthermore, the analysis suggests that σ_r^∞ in EQ. (3.27) is a lower bound for the asymptotic value of σ_r for physical irreversibly aggregating systems.

In the following, it is specified what kind of time dependence the average size s exhibits in the stable regime. For this purpose the time derivative $\frac{d}{dt}M_0 = \sum_i \frac{d}{dt}n_i(t)$ is calculated. According to the previous results, in the stable regime $\frac{d}{dt}M_0$ reduces to a transfer from the left edge of the size distribution ($i \approx as$) to the right edge ($i \approx 2as$). This behavior together with EQ. (3.22) leads to

$$\frac{d}{dt}M_0 = -\frac{1}{2}\,R_{as\,as}\,\frac{\phi_0^2}{(as)^4}\ . \tag{3.28}$$

In the stable regime the coagulation kernels asymptotically obey $R_{y,y} \sim \exp(-k^2 y^{2-\alpha})$. Using $s = M_1/M_0$ one arrives at

$$\frac{ds(t)}{dt} \sim \frac{1}{s(t)^2}\,e^{-Ks(t)^{2-\alpha}} \text{ with } K = k^2 a^{2-\alpha}\ . \tag{3.29}$$

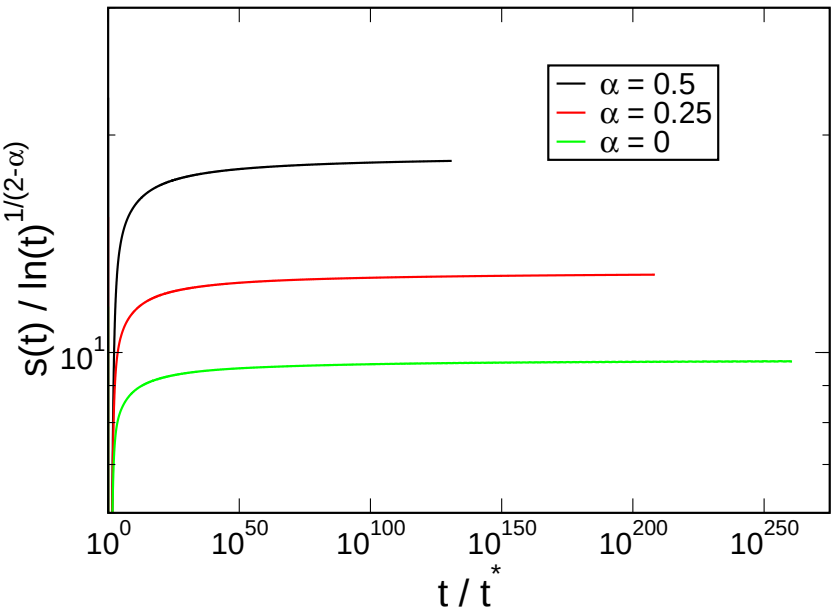

FIGURE 3.6: *$s(t)$ times $[\ln(t)]^{-\frac{1}{2-\alpha}}$ for different values of α.*

This results in the time interval $t_2 - t_1 \approx I(s_2) - I(s_1)$, in which the average cluster size increases from s_1 to s_2, with

$$I(y) = \int_1^y dx\, x^2 \exp(Kx^{2-\alpha}) \ . \tag{3.30}$$

Application of $I(y) \approx y^\gamma \exp(Ky^{2-\alpha})$ for large $y \gg 1$, with the exponent γ depending on α, leads to $s(t) \sim [\ln t - \gamma \ln s(t)]^{\frac{1}{2-\alpha}}$. Thus, asymptotically the average size obeys

$$s(t) \sim (\ln t)^{\frac{1}{2-\alpha}} \ . \tag{3.31}$$

A similar long-time behavior was observed in REFS. [44–46]. FIG. 3.6 shows numerical data for R_{ij} obeying EQ. (3.19) with λ=0, k=0.2 and different values of α, in accordance with the predicted asymptotic behavior in EQ. (3.31).

3.3.4 Details of the numerical integration algorithm

In this section I describe how the coagulation equation has been solved numerically. For this purpose it is convenient to write it down again:

$$\frac{dn_i}{dt} = \underbrace{-\, n_i \sum_{j=1}^{\infty} R_{ij} n_j}_{A} + \underbrace{\frac{1}{2} \sum_{j+k=i} R_{jk} n_j n_k}_{B} \ . \tag{3.32}$$

I introduced cutoffs for the sums in Eq. (3.32). This is justified by the fact that contributions from indices larger than a certain maximum index have no influence on the process since the cluster size distribution falls off exponentially at large sizes. Even without an explicit introduction of the cutoffs, they would implicitly be present due to the limited precision of floating point numbers on a computer. The sum A in Eq. (3.32) involved only indices $i \leq i_{\max}$. To ensure that Eq. (3.32), subjected to cutoffs, nevertheless conserves the total mass, i.e., $M_1 = \sum_i i n_i = \text{const}$, sum B involved indices $i \leq 2i_{\max}$. Hence, the equation

$$\frac{dn_i}{dt} = -n_i \sum_{j=1}^{i_{\max}} R_{ij} n_j + \frac{1}{2} \sum_{\substack{j+k=i \\ j+k \leq 2i_{\max}}} R_{jk} n_j n_k \tag{3.33}$$

was solved numerically, the maximum index growing in time $i_{\max} = i_{\max}(t)$. Roughly speaking, $i_{\max}$ was determined such that the corresponding density $n_{i_{\max}}$ was much smaller than typical densities n_i. More precisely, at a time t the number density $n_{\mathrm{MAX}}(t)$ with the largest value was determined. Note that $n_{\mathrm{MAX}} \neq n_{i_{\max}}$. The maximum index was then determined according to

$$\begin{aligned} n_{\mathrm{MAX}}(t) &= \mathsf{max}\{\, n_i(t) \,|\, i \,\} \\ i_{\max}(t + dt) &= \mathsf{max}\{\, i \,|\, n_i(t) > \epsilon n_{\mathrm{MAX}}(t) \} \end{aligned}$$

with a small number ϵ and the time increment dt used in the numerical integration. Due to the fact that $n_i = 0 \,\forall\, i > 2i_{\max}$ the range of possible indices is limited, $1 \leq i \leq 2i_{\max}(t)$. The parameter ϵ was usually of order 10^{-5}. I also performed numerical integrations with smaller values of ϵ without getting any difference in the results. The numerical integration was carried out using a standard second-order Runge-Kutta algorithm [47].

The time step dt used in the numerical integration was variable and increased in time since at late times the coagulation rates become very small due to the exponential suppression of aggregation events. In particular, the amount that a density n_i decreases within one time step due to interaction with n_j is determined by $R_{ij} n_i n_j dt$, where $R_{ij} \ll 1$ at late times for all involved indices i and j. This allows an appropriate increase of dt during the integration. However, one has to ensure that the relative decrease of n_i, namely $(R_{ij} n_j dt)$, is small for all i and j. During the integrations carried out, the relative decrease was smaller than 10^{-4} at late times. Additionally, it has also been checked that the total mass was conserved during the whole integration.

3.3.5 Brownian dynamics simulations of charged coagulating spheres

Similar to SEC. 3.2.1 the aim of this section is to show that even in the presence of charges Smoluchowski's rate equations are appropriate for spatial dimension d=3. Therefore, Brownian dynamics simulations of charged coagulating spheres are performed. It is shown that the crossover predicted by EQ. (3.21) can be observed in the simulations as well, with the correct dependence of s_c and t_c on the charges carried by the primary particles.

As was discussed in SEC. 3.2.1, the dynamics of the particles is modeled in the *overdamped limit*. The influence of electrostatic forces, Stokes friction and Brownian motion is included. The positional shift $\Delta\mathbf{r}_p(t)$ of particle p within a time step Δt is given by

$$\Delta\mathbf{r}_p(t) = \mu_s \mathbf{F}_p(t)\Delta t + \xi_p(\Delta t) \ , \tag{3.34}$$

with the total electrostatic force $\mathbf{F}_p(t)$ acting on particle p at time t, the mobility μ_p and the displacement ξ_p caused by Brownian motion, which obeys EQ. (3.16). The total electrostatic force is calculated as

$$\mathbf{F}_p(t) = \frac{q_p}{4\pi\epsilon_0\epsilon_\mathrm{r}} \sum_{k\neq p} q_k \frac{\mathbf{r}_p(t) - \mathbf{r}_k(t)}{|\mathbf{r}_p(t) - \mathbf{r}_k(t)|^3} \ , \tag{3.35}$$

with the charge q_p located in the center of particle p. The sum in EQ. (3.35) runs over all particles in the simulation box where periodic boundary conditions according to the minimum image method [42] are applied. The diffusion constant and the mobility were obtained from Einstein's relation, leading to

$$D_p = \frac{k_\mathrm{B}T}{6\pi\eta a_p} \quad , \quad \mu_p = \frac{D_p}{k_\mathrm{B}T} = \frac{1}{6\pi\eta a_p} \ , \tag{3.36}$$

where a_p is the radius of particle p.

Coalescence events are treated as in case A) of SEC. 3.2.1. Let index p denote the new particle that is formed upon collision of particles l and m. The new radius a_p is given by $a_p = (a_l^3 + a_m^3)^{1/3}$. Charges are located in the centers of the particles and the charge accumulates in a collision, $q_p = q_l + q_m$. The initial configuration is a monodisperse system, where all particles have the same radius a and charge q. According to the analysis of the coagulation equation, s initially increases algebraically as $s(t) \sim t$ until

the system eventually crosses over to slow coagulation at a characteristic time t_c and particle size s_c. EQ. (3.21) predicts that t_c and s_c scale as $q^{-6/5}$ when the charge of the primary particles is varied and the other parameters are kept constant. Of course, q must be small enough so that it has no distinct influence on the coagulation process for early times.

Due to the long-ranged Coulomb forces, simulating charged particles results in an N^2-algorithm, since each particle interacts with all the other particles. A possible way to speed up the computation is to apply approximate hierarchical algorithms, such as that of Barnes and Hut [48]. However, I chose a different way. As the primary charge q is small, for early times the influence of charges on the process may be neglected. Thus, the system is simulated until a certain time $\hat{t}<t_c$, *ignoring* the charges. The configuration at time $\hat{t}$ is stored and taken as initial configuration of successive simulations, where then, for times $t>\hat{t}$, the influence of the charges is included.

FIG. 3.7 shows data which was obtained from Brownian dynamics simulations of monopolarly charged spheres for three different values of q. The initial configuration consisted of N=160000 particles in a cubic box such that the volume fraction was ν=0.0031. The transient, i.e., data for times smaller than $\hat{t}$, where the charges were ignored, is not shown.

Qualitatively, the expected crossover from power-law growth to slow coagulation is immediately observed in the inset of FIG. 3.7. Even for the largest value of q, the average size s initially increases as $s(t)\sim t$, which justifies the neglect of the charges for early times ($t<\hat{t}$). $s(t)$ was determined as in SEC. 3.2.1. More important is the quantitative agreement between the simulation results and the mean-field analysis, which is expressed by the data collapse in FIG. 3.7. Hence, as in the uncharged case, the data support the claim that Smoluchowski's coagulation equation yields asymptotically correct results for irreversible coagulation in three dimensional systems of charged particles as well.

3.3.6 Summary and outlook

The issue of SEC. 3.3 was to investigate the dynamics of irreversibly aggregating systems of monopolarly charged particles. In the first place, this work was motivated by a study of monopolarly charged suspensions, as outlined in the appendix. However, the results derived in this section are valid for more general systems, as well. The reason is that asymptotically

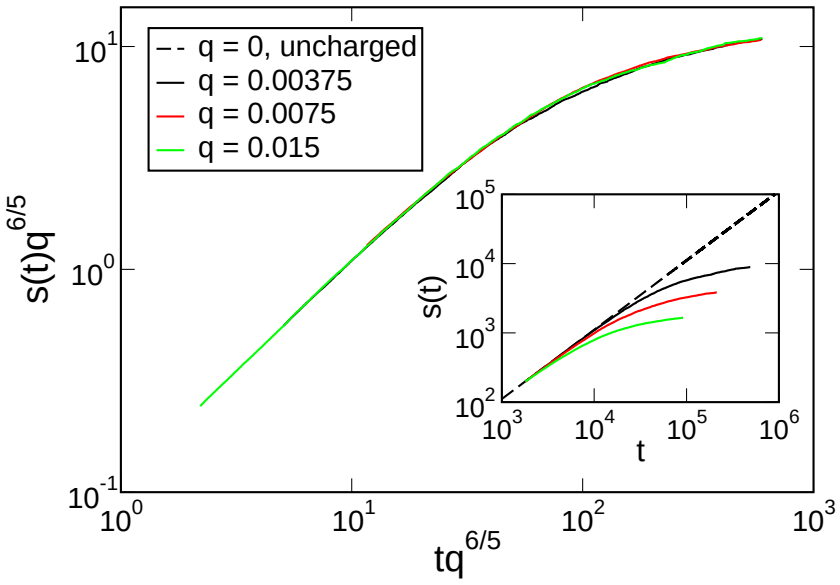

FIGURE 3.7: *$s(t)$ scaled with $q^{6/5}\sim s_c^{-1}$ and t scaled with $q^{6/5}\sim t_c^{-1}$. The data was obtained from Brownian dynamics simulations of monopolarly charged spheres. The inset shows the original data. The transients, i.e. $t<\hat{t}$ (see text), is not shown. The dotted line in the inset shows the asymptotic behavior of an uncharged system, $s(t)\sim t$. The charges q are measured in arbitrary units.*

neither the solvent nor the diffusion properties are important, as long as particles may have high kinetic energy, albeit as rare events, and charges accumulate in the aggregation process.

In order to investigate the aggregation process, the Smoluchowski equation for irreversible aggregation of equally charged particles was studied. Accumulation of charges during the aggregation process leads to a crossover from power-law to sub-logarithmic cluster growth, at a characteristic time and cluster size. For larger times the suspension is usually called stable, although aggregation still proceeds slowly. In this regime the size distribution evolves towards a *universal* scaling form, independent of *any* parameter included in the theory. As a consequence, the relative width falls off to a universal value $\sigma_r^\infty\approx 0.2017$ that is considerably smaller than in the uncharged case. It seems that σ_r^∞ is a lower bound for the asymptotic relative width for all physical systems with irreversible aggregation. The validity of Smoluchowski's coagulation equation for spatial dimension d=3 was supported by Brownian dynamics simulations for the charged and the uncharged case.

The most intriguing perspective for future studies is the experimental verification of the predictions made in this section. In particular, the appearance of the crossover from fast to slow aggregation and the experimental investigation of the self-focussing effect. Another important point is to study how the charges influence the structure of the aggregates and how the charges are located on these aggregates. Moreover, the rate equation approach applied above neglects long-ranged hydrodynamic interactions [40]. These interactions shall not change the asymptotic behavior for monopolarly charged systems but may have an influence on the early time behavior or on systems without charges. The study of such questions is important for the further understanding of aggregation in suspensions and challenging since long-ranged hydrodynamic interactions have to be included appropriately in the theory and simulations.

Chapter 4

Introduction to the modeling of spreading processes

Spreading phenomena are ubiquitous in nature. They occur in a vast variety of different situations such as epidemic spreading [49–52], the growth of mushrooms in 'fairy rings' [53], forest fires [54], transport in random media [55], and even catalytic reactions [56] or flowing sand [57]. The following chapters (Chaps. 5–7) investigate stochastic models for spreading processes. Therefore, the present chapter gives an introduction to the stochastic modeling of spreading phenomena. In general, the following behavior shall be encountered. If the spreading agent (also denoted as activity) finds hostile conditions, the spreading process terminates after a finite time and the process can spread only across a finite part of the system. For spreading agents that are not spontaneously created, the inactive state cannot be left unless activity is imported from outside the system. Contrarily, if the spreading agent finds suitable conditions, there is a chance that it spreads over the entire system for arbitrary long times.

The detailed underlying mechanisms in realistic spreading processes are usually unknown or very complicated. Therefore, one investigates simplified stochastic models with a potentially wide range of approximate validity rather than detailed models for certain phenomena. In this way one can study generic properties of spreading phenomena. The common feature of the models discussed in this and the following chapters, is the existence of one or more non-fluctuating so-called *absorbing states*. This notion describes a configuration of the system which can be reached by the dynamics *irreversibly*, i.e., once the system enters an absorbing state, in cannot leave it and is trapped forever. As a simple illustration one may think of a forest fire. The fire propagates from tree to tree with a certain probability,

depending on the environmental conditions. If the fire eventually ceases, the forest stays in the inactive state since no spontaneous ignition takes place. In reality, of course, the forest will not be trapped forever in the absorbing state. However, in order to leave it, fire must be imported from outside.

Depending on the model parameters, the stochastic process either reaches a non-fluctuating absorbing state with certainty (inactive phase), or there is a chance that it remains active in a fluctuating state in perpetuity (active phase). In the inactive phase only absorbing states are stationary, whereas in the active phase there is an additional active steady state. These two regimes of extinction and survival are typically separated by a *continuous nonequilibrium phase transition*, usually denoted as absorbing-state phase transition. Such transitions are in many respects similar to continuous phase transitions at thermodynamic equilibrium. In particular, it is possible to apply the concepts of *scale invariance* and *universality*. Close to the transition, the microscopic constituents behave collectively over large scales, though the underlying dynamics are short-ranged. Major interest stems from the fact that this type of critical behavior does not depend on the details of the underlying model, i.e., it is universal. This allows to categorize absorbing-state phase transitions into distinct universality classes. The classification of all possible transitions from fluctuating phases into absorbing states is currently one of the major goals of nonequilibrium statistical physics [1, 2]. Hence, beside their obvious relation to natural spreading phenomena, the models discussed in the following provide an ideal ground for performing fundamental studies on nonequilibrium critical phenomena.

In Sec. 4.1, I give a general overview of the critical behavior of absorbing-state phase transitions and the corresponding scaling theory. A brief summary of absorbing-state universality classes is presented at the end of this section. By far the most prominent universality class of absorbing-state phase transitions is that of *directed percolation* (DP). The scaling behavior of DP serves as a paradigm for nonequilibrium critical behavior and will be frequently encountered throughout this thesis. Therefore, DP and its critical behavior is discussed in some detail in Sec. 4.2. Sec. 4.3 summarizes the main results. In conclusion, the aim of this chapter is to establish the foundation for the investigations carried out in Chaps. 5–7.

4.1 Critical behavior of absorbing-state phase transitions

Close to the transition between survival and extinction of activity, models with absorbing states typically show universal behavior similar to that observed in equilibrium critical phenomena. The hallmark of equilibrium phase transitions is the appearance of nonanalyticities of certain thermodynamic quantities (see CHAP. 5). In the case of continuous phase transitions this leads to a continously vanishing order parameter when approaching the critical point. For an Ising magnet, for instance, without external magnetic field the magnetization m increases close to the transition as $|T_\mathrm{c} - T|^\beta$, where T and T_c denote the temperature and its critical value, respectively, and β is a *universal critical exponent*. Moreover, the correlation length diverges algebraically and other quantities of interest (e.g., the susceptibility) show (typically) power-law behavior, as well. Hence, a continuous phase transition at thermodynamic equilibrium is characterized by a set of so-called critical exponents. As a consequence, close to the transition the system is invariant under certain scaling transformations. Remarkably, the values of the critical exponents do not depend on the details of the underlying model. This led to the well-established *universality hypothesis* which states that the critical behavior of a system in thermodynamic equilibrium does only depend on the spatial dimension and the symmetry of the order parameter [58, 59] (in the case of short-range interactions). Thus, it is possible to categorize a great variety of models into distinct *universality classes*. Universality is one of most impressive features of continuous phase transitions. The foundation for its further theoretical understanding is led by Wilsons renormalization group (WG) approach [60, 61].

It turns out that a very similar picture applies for absorbing-state phase transitions. In particular, the concepts of scale invariance and universality proves to be suitable as well. The aim of this section is to give a general overview of the critical behavior of absorbing-state phase transitions and the corresponding scaling theory.

4.1.1 Critical exponents and scaling theory

Consider a stochastic model that is defined on a d-dimensional lattice with N lattice sites. Let me first deal with the case of an infinite system. One may think of a reaction-diffusion model (see SEC. 2.3) where each lattice site i at time t is associated with a state $s_i(t)$=0 or $s_i(t)$=1, i.e., vacancy or occu-

pation with a single particle. The dynamics are controled by a parameter p. Assume that the model exhibits an absorbing-state phase transition at the critical control parameter $p{=}p_\mathrm{c}$. The order parameter is usually the stationary density of active sites

$$\rho^\mathrm{stat} = \lim_{t\to\infty} \rho(t) = \lim_{t\to\infty} \lim_{N\to\infty} \frac{1}{N} \sum_i \langle s_i(t) \rangle \,, \tag{4.1}$$

where $\langle\rangle$ denotes the ensemble average. Note that the order of the limits is decisive, since a *finite* system will reach the absorbing state with certainty, though this might need a rare fluctuation. Starting from a fully occupied lattice, $\rho(t{=}0){=}1$, in the active phase the density decays until it saturates at the stationary value ρ^stat. Approaching the phase transition in the active phase, close to the transition the stationary density decreases algebraically as

$$\rho^\mathrm{stat} \sim |p - p_\mathrm{c}|^\beta \equiv |\Delta_p|^\beta \,, \tag{4.2}$$

with the critical exponent β. Another suitable order parameter besides ρ^stat is the ultimate survival probability $P^\infty{=}\lim_{t\to\infty} P_\mathrm{s}(t)$. The survival probability $P_\mathrm{s}(t)$ is the probability that the stochastic process, originating from a single active site at time $t{=}0$ (called active seed), has *not* entered the absorbing state up to time t, i.e., it remains active until t or even longer. P^∞ vanishes in the inactive phase, since then the process terminates with certainty. Contrarily, $P^\infty{>}0$ in the active phase and increases as

$$P^\infty \sim |p - p_\mathrm{c}|^{\beta'} \,, \tag{4.3}$$

with the exponent β'. As will be argued in Sec. 4.2.3, for directed percolation $\beta{=}\beta'$, due to a time reversal symmetry.

Furthermore, spreading processes are characterized by *two independent* correlation lengths. Apart from a spatial correlation length $\nu_\perp$ ('perpendicular to time') there is an additional temporal correlation length $\nu_\parallel$ ('parallel to time'). Since space and time are different in character, these two correlation lengths are independent. Near criticality they diverge as

$$\xi_\perp \sim |p - p_\mathrm{c}|^{-\nu_\perp} \quad , \quad \xi_\parallel \sim |p - p_\mathrm{c}|^{-\nu_\parallel} \quad , \tag{4.4}$$

with independent critical exponents $\nu_\perp$ and $\nu_\parallel$. In the scaling regime, these two correlation lengths can be related according to $\xi_\parallel{\sim}\xi_\perp^z$, where $z{=}\nu_\parallel/\nu_\perp$ is the so-called dynamic exponent. The physical meaning of these lengths may be illustrated by the equal-time spatial correlation function $C_\mathrm{s}(j)$ and

the temporal correlation function $C_{\rm t}(\tau)$, both taken in the steady state. Assuming translational invariance one obtains

$$\begin{aligned} C_{\rm s}(j) &= \langle s_0(0)s_j(0)\rangle - \langle s_0(0)\rangle^2 \sim \exp(-j/\xi_\perp) \ , \\ C_{\rm t}(\tau) &= \langle s_0(0)s_0(\tau)\rangle - \langle s_0(0)\rangle^2 \sim \exp(-\tau/\xi_\parallel) \ . \end{aligned}$$

Here, for convenience it was assumed that the distance between site 0 and site j equals j (which is only valid for d=1). However, the correlation lengths are not only present in the active phase but also in the inactive phase. Further illustrations of the physical meaning are provided in Sec. 4.2.3.

In general, absorbing-state phase transitions are characterized by *four* independent critical exponents such as $(\beta, \beta', \nu_\perp, \nu_\parallel)$, together with appropriate universal scaling functions that will be discussed below. Note that at the upper critical dimension (see Sec. 2.5) the scaling behavior is modified by logarithmic corrections.

According to the scaling behavior described by Eqs. (4.2,4.3,4.4) the process is invariant under the scaling transformation [2]

$$\begin{aligned} x \ \to \ x' = bx \ , \quad t \ \to \ t' = b^z t \ , \quad \Delta_p \ \to \ \Delta_p' = b^{-1/\nu_\perp}\Delta_p \ , \\ \rho \ \to \ \rho' = b^{-\beta/\nu_\perp}\rho \ , \quad P_{\rm s} \ \to \ P_{\rm s}' = b^{-\beta'/\nu_\perp}P_{\rm s} \ , \end{aligned} \tag{4.5}$$

where x and t denote length and time, respectively, and b is a dilatation. Universal scaling functions depend only on scale-invariant quantities such as t/x^z, $\Delta_p\, t^{1/\nu_\parallel}$ and $\Delta_p\, x^{1/\nu_\perp}$.

Besides the time-independent quantities $\rho^{\rm stat}$ and P^∞ there are interesting time-dependent scaling properties, as for instance, the density of active sites $\rho(t)$ starting from a fully occupied lattice and the survival probability $P_{\rm s}(t)$ starting from a single active seed. Following the usual scaling concept of equilibrium statistical mechanics, sufficiently close to the phase transition both quantities are expected to scale as [62, 63]

$$\rho(t) \simeq t^{-\alpha}\phi(\Delta_p\, t^{1/\nu_\parallel}) \quad , \quad P_{\rm s}(t) \simeq t^{-\delta}\psi(\Delta\, t^{1/\nu_\parallel}) \ , \tag{4.6}$$

where α and δ are critical exponents and ϕ and ψ are *universal scaling functions*, i.e., they are independent (apart from rescaling) of the specific realization of the stochastic process. For small arguments, ϕ and ψ both tend to a

constant, whereas for large positive arguments they scale in a way that the time dependence drops out, and for large negative arguments they approach zero:

$$\phi(\zeta) \sim \begin{cases} \text{const} & \text{for } \zeta \to 0 \\ \zeta^{\alpha\nu_\parallel} & \text{for } \zeta \to +\infty \\ 0 & \text{for } \zeta \to -\infty \end{cases} \quad , \quad \psi(\zeta) \sim \begin{cases} \text{const} & \text{for } \zeta \to 0 \\ \zeta^{\delta\nu_\parallel} & \text{for } \zeta \to +\infty \\ 0 & \text{for } \zeta \to -\infty \; . \end{cases} \tag{4.7}$$

Hence, in the active phase ρ and P_s reach stationary values $\rho(\infty)\sim\Delta_p^{\alpha\nu_\parallel}$ and $P_\mathrm{s}(\infty)\sim\Delta_p^{\delta\nu_\parallel}$. Comparison with Eqs. (4.2) and (4.3) leads to

$$\alpha = \beta/\nu_\parallel \quad , \quad \delta = \beta'/\nu_\parallel \; . \tag{4.8}$$

Eqs. (4.6,4.7) imply that the survival probability $P_\mathrm{s}(t)$ for $|\Delta_p|\ll 1$ initially decays according to a power law, $P_\mathrm{s}(t)\sim t^{-\delta}$, until the time $\xi_\parallel\sim|\Delta_p|^{-\nu_\parallel}$ is reached. From there on $P_\mathrm{s}(t)$ either saturates ($\Delta_p>0$) or it decays exponentially ($\Delta_p<0$). In the inactive phase($\Delta_p<0$), the length $\xi_\perp$ determines the maximal spatial extension of the process (see Sec. 4.2.3). An analogous scenario is valid for the behavior of the density $\rho(t)$.

Starting from a single active seed at the origin $s_0(0)=1$, an important quantity is the *pair connectedness function* $c(x,t)$. This is the probability that a site, separated by a distance x from the origin, is active at time t. According to Ref. [62] it should obey

$$c(x,t) \sim t^{\theta-d/z}\, \Phi(x/t^{1/z}, \Delta_p\, t^{1/\nu_\parallel}) \; , \tag{4.9}$$

with an appropriate universal scaling function Φ and the *critical initial slip exponent* θ that governs the increase in time of the number of active sites in the cluster (see below). From Eqs (4.6,4.7,4.9) follows [2] that at criticality ($\Delta_p=0$) the survival probability $P_\mathrm{s}(t)$, the number of active sites $N(t)$ (averaged over all runs) and the mean square displacement from the origin $R^2(t)$ (averaged over surviving runs) behave algebraically according to [62, 64]

$$P_\mathrm{s}(t) \sim t^{-\delta} \quad , \quad N(t) \sim t^{\theta} \quad , \quad R^2(t) \sim t^{2/z} \; . \tag{4.10}$$

In addition, from the properties of the autocorrelation function $c(0,t)$ one may derive the so-called *generalized hyperscaling relation* [65] for phase transitions into absorbing states

$$\theta - \frac{d}{z} = -\frac{\beta+\beta'}{\nu_\parallel} \; . \tag{4.11}$$

Note that the hyperscaling relation fails *above* the upper critical dimension, which is related to the fact that in sufficiently high dimensions the spreading region becomes very sparse and diffuses away.

Until now I have summarized the scaling properties in infinite systems. Recall that a *finite* system will reach the absorbing state with certainty (though this might take very long). For finite systems, the behavior is also governed by the ratio $\xi_\perp^d/N$. This is due to the fact that the spatial correlation length $\xi_\perp$ must be compared to the lateral size $L{=}N^{1/d}$ of the system. Hence, universal scaling functions also depend on the scale-invariant quantity $t^{d/z}/N$, and the scaling functions ϕ, ψ and Φ must be generalized to take this into account.

There are, of course, other interesting quantities that are associated with certain critical exponents (e.g., the mean cluster size in the inactive phase, or the fluctuations of the order parameter). However, these exponents are typically related to those introduced above via scaling relations. Moreover, further generalizations are possible, as by the introduction of external fields (conjugate fields to the order parameter, e.g., spontaneous particle creation), which also gives rise to a susceptibility [66–68].

Absorbing-state universality classes

The by far most important universality class of absorbing-state phase transitions is that of directed percolation, which will be discussed in the next section. It is believed that critical behavior different from DP may emerge when the conditions of the so-called *DP conjecture* (see Sec. 4.2.6) are violated. Examples include the dynamical percolation class (DyP) (see Sec. 6.1), the parity conserving class (PC) (see, e.g.,Ref. [69]), processes with particle conservation [70, 71] or the Voter model class [72]. I also mention that there is a lively debate about the critical behavior of the so-called PCPD (see, e.g., Refs. [73, 74]). For a more detailed discussion of different absorbing-state universality classes I refer the interested reader to Refs. [2, 73].

4.2 Directed percolation

The generic universality class for phase transitions into absorbing states is that of directed percolation (DP). Directed percolation is recognized as a paradigm for critical behavior far from equilibrium. In fact, it has been argued that, in the field of nonequilibrium critical phenomena, DP might play a similar role as the Ising model in equilibrium statistical physics [75]. Note that until now there is no exact solution for any model that belongs to the DP universality class. Moreover, there are further indications that DP is a *nonintegrable* process. Since DP has such a distinguished role in the field of absorbing-state phase transitions and since it will frequently be encountered in the following, this section deals with directed percolation and its critical behavior in some detail.

4.2.1 Geometric model: Isotropic vs. directed bond percolation

Although directed percolation is a generic model for dynamical spreading processes, it was originally introduced as a geometric model for the connectivity in random media [76]. To this end it is an anisotropic variant of isotropic percolation (to which a comprehensive review is presented in Ref. [77]). Consider a porous medium, for instance a rock, with pores that are connected by channels. Water may penetrate into the rock through these channels which have varying permeability. In such a context an important question is, how deep water penetrates into the rock when injected at a certain pore.

In *isotropic percolation* water penetrates isotropically in all spatial directions. One of the simplest models for this situation is *bond percolation* on a D-dimensional simple (tilted) cubic lattice, see left panel of Fig. 4.1. In this model the sites of the lattice represent the pores of the medium and the bonds represent the channels. It is assumed that the states of the channels are uncorrelated. The bonds are permeable (or open, active) with probability p and blocked (or closed, inactive) otherwise, i.e., with probability $q=1-p$. The value of p is the same for every bond in the lattice, thus, there is no quenched randomness. There are numerous alternative models, e.g, site percolation where the sites are blocked or open, instead of the bonds, or models with a different underlying lattice structure. They all show the same critical behavior. A *cluster* is the set of sites that are connected by a contiguous set of open bonds. Percolation theory is concerned with the statistical properties of such cluster, in particular, with

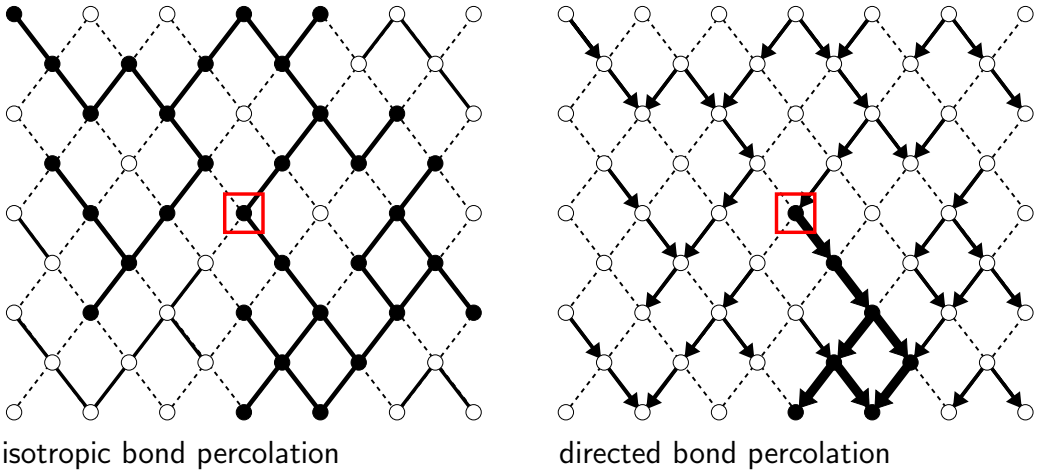

FIGURE 4.1: *Isotropic versus directed bond percolation on a tilted square lattice. Solid (dashed) lines denote permeable (blocked) bonds. The marked site is the origin. Filled circles represent pores that are reached from the origin. The states of the bonds are equal in both panels.*

the question whether a macroscopic cluster emerges. Solid lines in FIG. 4.1 denote permeable bonds whereas dashed lines represent blocked bonds. The thick solid lines in the left part of FIG. 4.1 show the bonds of the isotropic bond percolation cluster that contains the origin (marked site). Filled circles denote the sites of that cluster. If water was injected into the origin, it would reach all sites of the cluster. For small probability p of channels being permeable, clusters are small and injected water can fill only small volumes of the medium. In contrast, if p is sufficiently large, macroscopic clusters emerge and water penetrates over distances comparable to the size of the system. These two regimes are separated by a continuous phase transition at a critical value $p{=}p_c$. This transition is not an absorbing-state phase transition. However, *dynamical percolation* (DyP), a dynamic procedure to grow isotropic percolation cluster (see Sec 6.1), exhibits an absorbing-state phase transition with a universality class different from DP. Due to a duality symmetry, for isotropic bond percolation on a square lattice $p_c{=}1/2$ [77]. Numerical estimates for p_c in $D{>}2$ can be found in TAB. 6.1.

Directed percolation was introduced in 1957 by Broadbent and Hammersley [76] as an anisotropic variant of isotropic percolation. As illustrated by the arrows in the right part of FIG. 4.1, in directed percolation there is a preferred direction. Propagation is only possible along this specific direction. Using the picture of water penetrating into a rock, one may think of the

influence of a strong gravitational field, which forces the water to move downwards through the open channels. As for isotropic bond percolation, the bonds are open with probability p and closed otherwise. A directed bond percolation cluster generated by the origin, is the set of sites connected to the origin by a directed path of open bonds. Water (or, in general, activity) would propagate in the preferred direction along this cluster when injected into the origin. The thick solid lines in FIG. 4.1 show the bonds of the cluster generated by the origin. Filled circles represent active (wetted) sites, i.e., the sites of the cluster generated by the origin. Note that the state of the bonds in the left and right part of FIG. 4.1 are equal. Obviously the directed percolation cluster is a subset of the corresponding isotropic percolation cluster. Similar to isotropic percolation, there are two regimes. For small values of p the propagation depths is small whereas for large values of p infinite propagation is possible (in an infinite system). At a critical value $p{=}p_c$ these regimes are separated by a continuous phase transition. In contrast to isotropic bond percolation, the value of p_c is not exactly known. Currently the best estimate for p_c for directed bond percolation on a square lattice is obtained from series expansions, leading to $p_c{=}0.644700185(5)$ [78]. Numerical estimates for p_c in $D{>}2$ can be found in TAB. 4.1.

Besides the similarities between isotropic and directed percolation, their critical behavior is very different. The critical properties of isotropic percolation are the same in all spatial directions (apart from lattice effects, which are usually irrelevant on large scales). This implies that the long-range correlations, that emerge at the phase transition, are invariant under rotation. Hence, there is a single correlation length. Contrarily, the anisotropy of DP is reflected by anisotropic scaling behavior, i.e., in this case there are two independent correlation lengths. Moreover, the critical exponents for isotropic bond percolation for $D{=}2$ are known exactly and turn out to be rational numbers (see SEC. 6.1). Directed percolation, however, has not yet been solved exactly for $D{>}1$ [1]. The numerical estimates suggest that p_c and the critical exponents are given by irrational numbers rather than by simple rational numbers. This might indicate that directed percolation is a nonintegrable process.

[1] The case $D{=}1$ is trivial for isotropic and directed percolation, since all bonds must be open ($p_c{=}1$) to generate an infinite cluster.

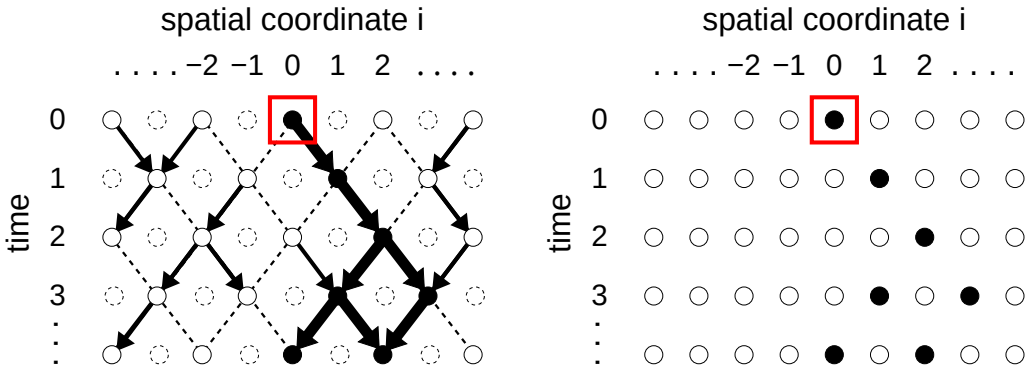

FIGURE 4.2: *Directed bond percolation as a time-dependent stochastic process. Explanations are in the text.*

4.2.2 Dynamical interpretation of directed percolation

In the following it will be shown, how directed bond percolation results in a *dynamical process* by interpreting the preferred direction as time. In the present thesis, I will adopt this interpretation of a time-dependent stochastic process. However, the geometrical interpretation of directed paths is fully equivalent.

FIG. 4.2 illustrates how directed bond percolation can be regarded as a dynamical process. The left panel shows the directed bond percolation cluster (generated by the origin,) of FIG. 4.1 in the geometrical picture. The dashed circles are instructive for the interpretation as a dynamical process but they do not alter the behavior as they have no connections to other sites. One may interpret the preferred direction as a discrete time variable and the remaining axis as a spatial coordinate on a lattice. Hence, in the dynamical interpretation, the spatial lattice has dimension $d{=}D{-}1$ where D is the dimensionality in the geometrical interpretation. Therefore, in the time-dependent picture, one usually refers to a process in $d{+}1$ dimensions, where the additional dimension is time. The right panel of FIG. 4.2 shows how the geometric directed bond percolation cluster on the D-dimensional lattice gives rise to a time-dependent spreading process on a d-dimensional lattice. An illustrative interpretation is to regard the lattice sites i as individuals. Activity is an infectious disease. At a given time t, individuals can be in two possible states. They are either healthy (or inactive, empty), $s_i(t){=}0$, or infected (or active, occupied), $s_i(t){=}1$. Injected activity (infection) at the origin means $s_0(0){=}1$. Within one time step, an infected individual can transmit the disease to its

d	p_c	d	p_c
1	0.644700185(5) [78]	5	0.1016796(5) [81]
2	0.287338(3) [80]	6	0.0841997(14) [81]
3	0.1774970(5) [81]	7	0.07195(5) [81]
4	0.1288557(5) [81]		

TABLE 4.1: *Estimates of p_c for directed bond percolation on a d-dimensional cubic lattice.*

nearest neighbors with probability p, while it recovers from its disease with certainty. Therefore, when starting from an active seed, an infected site at time t is healthy with certainty at time $t+1$. The dashed circles in the left part of FIG. 4.2 represent such sites that are inactive with certainty and therefore have no connections to other sites. The right permeable bond that originates at the origin (left part of FIG. 4.2) results in an infection of the neighboring individual at site $i=1$ at time $t=1$. Similarly the whole directed graph on the D-dimensional lattice can be translated into subsequent infections and recovery of the individuals on the d-dimensional lattice. Note that in the dynamical interpretation the spreading agent, the disease in the example, is not conserved. To generate this time-dependent stochastic process in $d=1$, one can apply the following update rules (parallel dynamics). For each pair of bonds between the sites $i\pm1$ at time t and i at time $t+1$ two random number $r_i^{\pm}\in(0,1)$ are generated. A bond is considered to be open (with probability p) if $r_i^{\pm}<p$. For an infection to occur, it is sufficient that one of the two bonds is open. This leads to

$$s_i(t+1) = \begin{cases} 1 & \text{for } s_{i-1}(t) = 1 \text{ and } r_i^- < p \ , \\ 1 & \text{for } s_{i+1}(t) = 1 \text{ and } r_i^+ < p \ , \\ 0 & \text{otherwise} \ . \end{cases} \tag{4.12}$$

This process does not include any long-time memory effects in the sense that the configuration at a given time does only depend on the s_i in the previous time step, i.e., it is a Markov process. As always for dynamical systems, one has to specify the initial conditions. Common initial states are the fully occupied lattice, random initial conditions, and a single infected site at the origin. The influence of correlated initial conditions on DP has been studied in REF. [79].

Update schemes similar to Eq. (4.12) are easily formulated for higher spatial dimensions. In Tab. 4.1 current estimates of p_c for directed bond percolation on a d-dimensional cubic lattice are summarized (each site as $2d$ neighbors). The values for $d>2$ were obtained during the studies that are reported in Chap. 6.

In the dynamical interpretation of directed bond percolation, the absorbing state is reached when at a given time all lattice sites are healthy. Since activity is not created spontaneously but may only propagate from one time step to the next, the inactive lattice cannot be left. In the geometrical interpretation this happens when there are no directed paths of open bonds from the initial configuration to a certain depths. As discussed above, in the geometrical picture there is a continuous phase transition at p_c between finite and infinite propagation of activity in the preferred spatial direction. In the dynamical interpretation this corresponds to an absorbing-state phase transition at p_c, for which the scaling theory of Sec 4.1.1 is valid.

Another dynamical interpretation that is often used in the field of absorbing-state phase transitions, is that of a reaction-diffusion process (see Sec. 2.3). Associating an occupied site with a particle A and an empty site with a vacancy $\emptyset$, directed percolation corresponds to the reaction-diffusion scheme

$$\begin{array}{ll} \text{self-destruction:} & A \to \emptyset \ , \\ \text{diffusion:} & \emptyset + A \to A + \emptyset \ , \\ \text{offspring production:} & A \to 2A \ , \\ \text{coagulation:} & 2A \to A \ . \end{array} \tag{4.13}$$

This reaction-diffusion scheme emerges from directed bond percolation on a square lattice (D=2) as follows. A single activated site may recover without infecting its neighbors (self-destruction). It may also infect one of its nearest neighbors (diffusion) or both (offspring production). It is also possible that a site is infected simultaneously by two active neighbors, resulting in one active site (coagulation). The directed bond percolation cluster in Fig. 4.2, expressed in terms of this reaction-diffusion, scheme corresponds to diffusion, diffusion, offspring production, offspring production+diffusion+coagulation. Coagulation shows that DP is a 'fermionic' model with an exclusion principle that allows (for a given time) only a single particle at a site. In the language of reaction-diffusion processes the absorbing state is reached when there are no particles left. The existence of the absorbing state in DP arises from the fact, that no spontaneous particle creation takes place.

4.2.3 Critical behavior of directed percolation

Directed percolation obeys the general scaling theory presented in SEC. 4.1.1. In this section, the critical behavior of DP is discussed in further detail.

Time reversal symmetry of directed percolation

As already mentioned in SEC. 4.1.1, due to a time reversal symmetry, the exponents β for the stationary density, see EQ. (4.2), and β' for the ultimate survival probability, see EQ. (4.3), are equal in the case of directed percolation. Applying EQ. (4.8), one obtains that therefore also the exponents α for the density decay and δ for the decay of the survival probability, see EQ. (4.6), are equal,

$$\beta = \beta' \quad , \qquad \alpha = \delta \ . \tag{4.14}$$

Inserting this into the generalized hyperscaling relation, EQ. (4.11), one arrives at the well-known hyperscaling relation for DP

$$\theta = d/z - 2\delta = \frac{d\nu_\perp - 2\beta}{\nu_\parallel} \ . \tag{4.15}$$

An exact proof for the equality of β and β' is given in REF. [62]. To understand the underlying principle, one can consider a reversed directed bond percolation process, i.e., reverse the direction of the arrows in the right part of FIG. 4.1. The reversed process follows *exactly* the same probabilistic rules as the original process. Two sites that are connected by a path of permeable bonds in the original process, are also connected in the reversed process. Assume that one has a large D-dimensional lattice similar to FIG. 4.1, whose bonds are inactive or active according to the probability p. Starting the process with a *fully occupied* row at t=0, one ends up with a certain density $\rho(t^*)$ of active sites at row t=t^*. Consider now a reversed process (which would propagate upwards in FIG. 4.1), starting with a *single* active seed i at row t=t^*. As was pointed out above, if site i at t=t^* was active in the original process (starting from the fully occupied lattice), then the reversed spreading process starting with the single active seed i at t=t^*, will also be active at row t=0, i.e., after t^* time steps. Alike, when site i was inactive at t=t^* in the original process, then the reversed spreading starting from i will not survive t^* time steps. To measure the survival probability, one could take each site of the row at t=t^* as an active seed in a reversed process. The relative frequency of process that do survive or do not survive t^* time steps then tends to the value of the survival probability $P_\mathrm{s}(t^*)$. However, the relative frequency of surviving and non-surviving runs is exactly given by the density $\rho(t^*)$ of the original process starting from a fully occupied lattice. For directed bond percolation this leads to the *exact* relation $\rho(t)$=$P_\mathrm{s}(t)$, and hence, taking the limit $t\to\infty$, β=β'.

Critical behavior above d_c, mean-field regime

If the spatial dimension is larger than the upper critical dimension d_c (see Sec. 2.5), the scaling behavior of directed percolation is correctly described by a mean-field approximation. Let $\phi(\mathbf{x},t)$ denote the coarse-grained density of active sites at position $\mathbf{x}$ and time t. The reaction-diffusion scheme Eq. (4.13) leads to the Langevin equation [3, 82]

$$\frac{\partial\phi}{\partial t} = \lambda\phi - \kappa\phi^2 + D\nabla^2\phi + \sqrt{\phi}\,L\ , \tag{4.16}$$

$$\langle L(\mathbf{x},t)\rangle{=}0\ ,\ \langle L(\mathbf{x},t)\,L(\mathbf{x}',t')\rangle{=}\Gamma\delta^d(\mathbf{x}{-}\mathbf{x}')\delta(t{-}t')\ . \tag{4.17}$$

Offspring production ($A\to 2A$) and spontaneous self-destruction ($A\to\emptyset$) is modeled by $\lambda\phi$ where λ is determined by the difference of the corresponding rates. $\kappa\phi^2$ accounts for pair annihilation with rate κ and $D\nabla^2\phi$ for diffusion with the diffusion constant D. Here, the assumption that the noise is proportional to $\sqrt{\phi}$ may be made plausible as in Sec. 3.1.2, while for DP (in contrast to the process $A{+}A{\to}A$) single active sites contribute to the noise. Additional contributions are either irrelevant under renormalization group transformations or absorbed by a redefinition of the parameters λ, κ and D in Eq. (4.16) (see, e.g., Ref. [3]). More detailed discussions of the Langevin equation Eq. (4.16) may, for instance, be found in Refs. [3, 82]. Neglecting the noise one arrives at the mean-field equation for DP.

Near criticality, the process is invariant under the scaling transformations Eq. (4.5). Applying Eq. (4.5) to Eq. (4.16) and neglecting the influence of the noise (mean-field renormalization, similar to Sec. 3.1.2) simple power counting yields that the Langevin equation is invariant for

$$\delta = 1\ ,\quad z = 2\ ,\quad \nu_\perp = \frac{1}{2}\ , \tag{4.18}$$

which are the mean-field critical exponents for DP. The scaling of the noise implies that Eq. (4.16) is only invariant for

$$d = d_c = 4\ , \tag{4.19}$$

with the upper critical dimension for DP $d_c{=}4$ (see, e.g., Ref. [3]). For $d{>}d_c$ the noise decreases under rescaling. Thus, in this case the noise is irrelevant on large scales and the mean-field approximation provides correct results concerning the scaling behavior, i.e., the exponents assume their

exponent	d=1 [78]	d=2 [80, 89]	d=3 [81, 90]	d=4−ϵ [88]	d=4
β	0.27646(8)	0.584(4)	0.81(1)	$1-\epsilon/6-0.01128\epsilon^2$	1^*
$\nu_\parallel$	1.733847(6)	1.295(6)	1.105(5)	$1+\epsilon/12+0.02238\epsilon^2$	1^*
$\nu_\perp$	1.096854(4)	0.734(4)	0.581(5)	$1/2+\epsilon/16+0.02110\epsilon^2$	$1/2^*$
z	1.580745(10)	1.766(2)	1.897(5)	$2-\epsilon/12-0.02921\epsilon^2$	2^*
δ	0.159464(6)	0.4505(10)	0.737(5)	$1-\epsilon/4-0.01283\epsilon^2$	1^*
θ	0.313686(8)	0.2295(10)	0.107(5)	$\epsilon/12-0.03751\epsilon^2$	0^*

TABLE 4.2: *Estimates of critical exponents for directed percolation. For d=4, * denotes that the mean-field behavior is subjected to logarithmic corrections.*

mean-field values EQ. (4.18). For $d<d_c$ the noise increases under rescaling. Hence, the noise becomes relevant on large scales which invalidates the mean-field approximation. For $d=d_c$, the mean-field behavior is subjected to logarithmic corrections [67, 83].

Field theory

Field-theoretic calculations may be used to go beyond the mean-field approximation by an expansion in terms of $\epsilon=d_c-d$. Moreover, field-theoretic treatments provide further insights into the origins of universality. Interestingly, the field-theory for DP was originally developed and studied in a different field of physics, namely the physics of hadronic interactions at high energies. In this context the properties of the so-called *Reggeon field theory* were investigated (for a review see REF. [84]). Only later it was realized that Reggeon field theory is the appropriate field theory for directed percolation [85–87].

Critical behavior below d_c

For spatial dimension $d>d_c=4$ the critical exponents assume their mean-field values EQ. (4.18). Below d_c, the critical behavior may be investigated by different methods such as field-theoretic expansions in $\epsilon=d_c-d$ [88], Monte Carlo simulations [80, 81, 89] or series expansions [78]. TAB. 4.2 lists current estimates for critical exponents for directed percolation, where the values for z, δ and θ in d=3 were obtained during the investigations that are reported in CHAP. 6.

4.2.4 DP in 1+1 dimensions: Illustrations

In order to get a clearer idea of directed percolation processes, FIGS. 4.3 and 4.4 show space-time plots of MC-simulations of directed percolation in one spatial dimension. Additionally, the figures provide illustrative interpretations of the correlation lengths $\xi_\parallel$ and $\xi_\perp$, respectively. The plots were generated for processes that obey the update scheme of EQ. (4.12).

Note that a black dot in the figures does *not* represent a single active site at a certain time. In order to display sufficiently large times and spatial extensions of the clusters, each dot denotes a block of 8 neighboring sites at 32 successive time steps. This block is active (black) when at least one of the 8 sites was active at least once within the 32 time steps. The figures show 5760 sites and 28800 time steps. Furthermore, be aware that each panel in FIGS. 4.3 and 4.4 provides only a single realization of randomness. However, when analyzing a DP process, e.g., by measuring the survival probability $P_\mathrm{s}(t)$, one is concerned with averages over many independent realizations. This should be kept in mind when interpreting the figures and especially the sketched scales $\xi_\perp$ and $\xi_\parallel$.

Starting from an active seed

FIG. 4.3 shows space-time plots of simulations for different values of $\Delta_p{=}p{-}p_\mathrm{c}$. The initial condition is a single active seed. The value of Δ_p decreases from panel *a*) to panel *e*), with $\Delta_p{=}0$ for critical DP in panel *c*). Obviously the visual appearance differs drastically between the active phase ($\Delta_p{>}0$) in panels *a*) and *b*), and the inactive phase ($\Delta_p{<}0$) in panels *d*) and *e*). In the active phase, the space-time plots show spreading within a certain 'light cone'. The slope of this spreading cone is determined by the ratio $\xi_\perp/\xi_\parallel$, see also REF. [91]. The reason is that for times larger than the correlation time, the spatial extension of the process grows linearly in time, with the velocity given by $\xi_\perp/\xi_\parallel$. In the inactive phase, $\xi_\parallel$ plays the role of a characteristic decay time. Processes that survive longer than $\xi_\parallel$ are exponentially suppressed. The maximal spatial extension of active clusters (in the inactive phase) is determined by $\xi_\perp$. At the transition, $\xi_\parallel$ and $\xi_\perp$ diverge, which leads to fractal distributions of active spots in space-time plots.

Starting from a fully occupied lattice

FIG. 4.4 shows space-time plots with a fully occupied lattice as initial condition. The value of Δ_p decreases from panel *a*) to panel *e*). Again, the visual appearance changes drastically when Δ_p is decreased from the

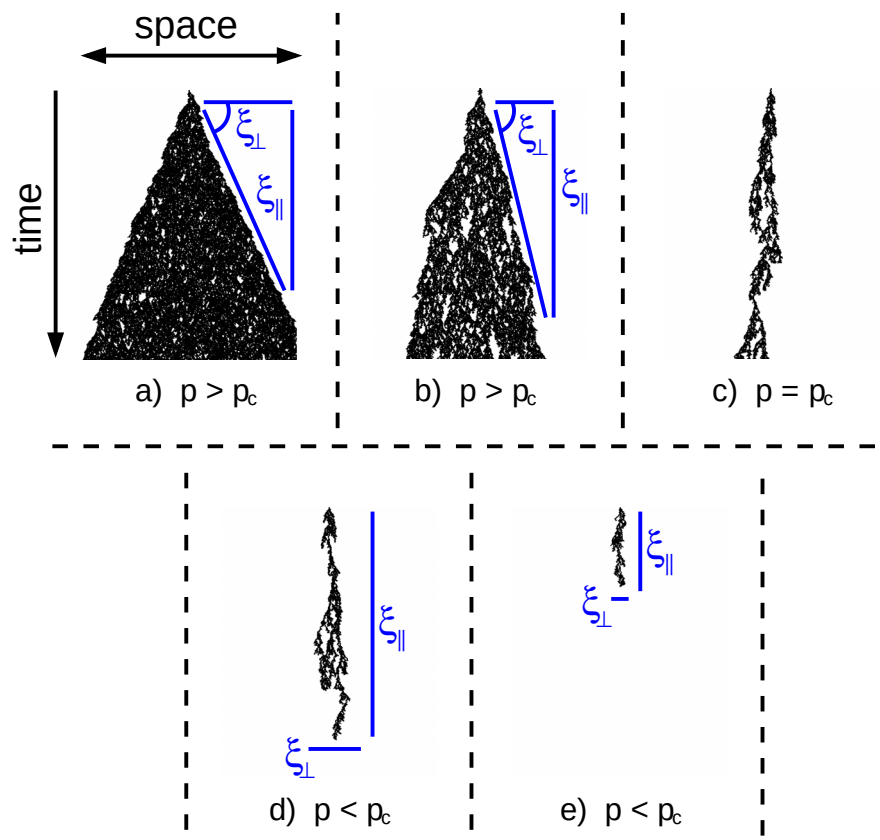

FIGURE 4.3: *Space-time plots of MC-simulations of DP in* 1+1 *dimensions. The initial configuration is a single active seed. A dot denotes a block of sites (see text). Further explanations of the illustrations of* $\xi_\perp$ *and* $\xi_\parallel$ *are in the text.*

active to the inactive phase. In the active phase, the process creates a stationary density of active sites. Nevertheless, the space-time plots show *inactive* voids up to a characteristic size. The maximal temporal and spatial extension of these inactive voids is given by $\xi_\parallel$ and $\xi_\perp$, respectively. In the inactive phase, $\xi_\parallel$ determines the decay time. Initially the density decays according to a power law, see EQ. (4.6), until the time scale $\xi_\parallel$ is reached from where on it decays exponentially. At criticality the correlation lengths diverge which results in active spots separated by ever growing inactive voids.

It is straight forward to generalize the above discussed illustrations of DP and the correlation lengths, respectively, to higher dimensions.

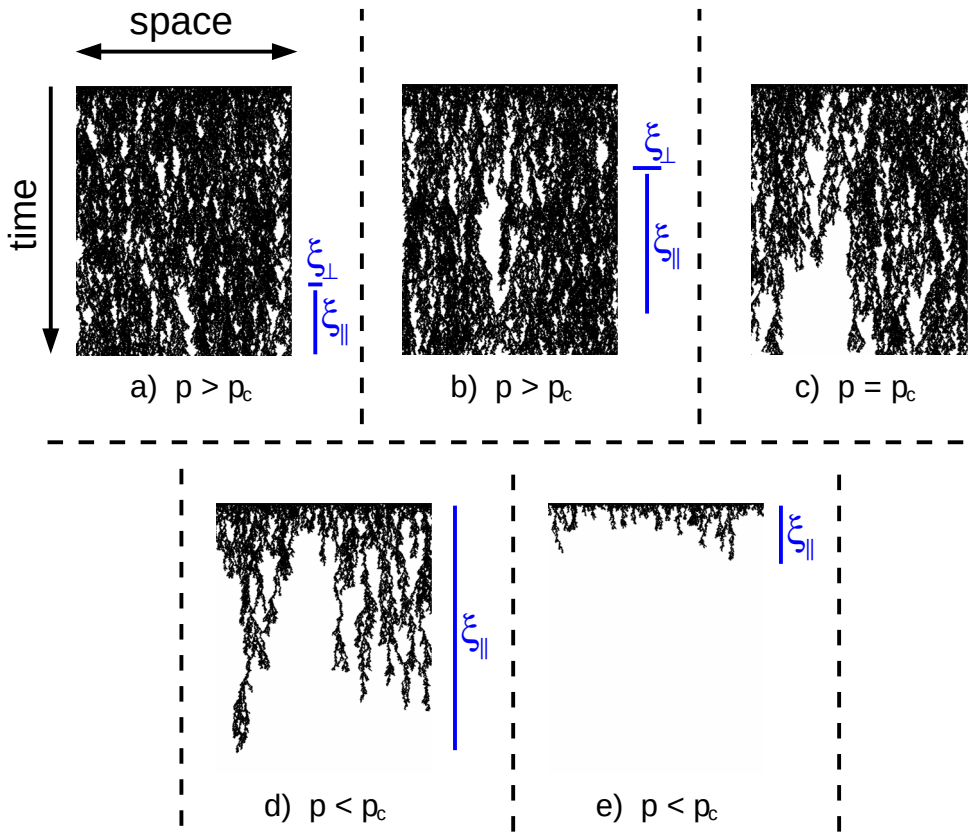

FIGURE 4.4: *Space-time plots of MC-simulations of DP in* 1+1 *dimensions. The initial configuration is a fully occupied lattice. A dot denotes a block of sites (see text). Further explanations of the illustrations of* $\xi_\perp$ *and* $\xi_\parallel$ *are in the text.*

4.2.5 Different realizations of DP

Major interest in DP stems from the fact that directed percolation is an extremely robust universality class with respect to the underlying microscopic dynamic rules. This means that a large variety of different models, designed to describe rather unrelated phenomena (such as catalytic reactions [56] or epidemic spreading [52, 92]), exhibit the same critical behavior of directed percolation. Thus, directed bond percolation is only a possible, and very simple, representative of the directed percolation universality class. The fact that DP is so commonly encountered in systems with absorbing states culminates in the so-called DP conjecture, see SEC. 4.2.6.

In the following I mention some models belonging to the DP universality class. Other simple realizations of DP use different underlying lattice structures, e.g., honeycomb instead of simple cubic lattices [93]. It is also possible to choose the sites of the lattice to be active or blocked, respectively (resulting in directed site percolation, see CHAP. 5), instead of the bonds. In contrast to directed bond percolation there are important lattice models for DP that apply asynchronous dynamics (i.e., continuous time, see SEC. 2.1). An example is the so-called contact process (CP) [92] which was introduced as a model for epidemic spreading without immunization. Even models including many different species [52] or models with infinitely many absorbing states [66] may exhibit DP critical behavior. Nonuniversal properties, such as the critical control parameter p_c, differ between different models. The critical exponents and universal scaling functions (apart from nonuniversal metric factors [67]), and hence the long-range correlations, are unaltered.

4.2.6 The DP conjecture

The robustness of the DP universality class, see SEC. (4.2.5), led Janssen and Grassberger to the so-called 'DP-conjecture' [82, 94]. This conjecture states that a process which fulfills the following conditions belongs to the directed percolation universality class:

1. The process exhibits a continuous phase transition from an active fluctuating state into a *unique* nonfluctuating absorbing state.
2. The phase transition is characterized by a *positive single-component* order parameter.
3. The process involves exclusively *short-range* interactions.
4. There are no *'additional special feature'*, such as additional symmetries, long-time memory or quenched randomness.

Until now there is no rigorous proof of the 'DP-conjecture' but it is highly supported by extensive numerical studies. All models that are known to exhibit critical behavior different from DP, violate at least one of the above stated conditions, see end of SEC. 4.1. Hence, one may argue that in the field of absorbing-state phase transitions the 'DP-conjecture' plays a similar role as the universality hypothesis in equilibrium critical phenomena. It is important to note that the conditions of the 'DP-conjecture' are sufficient but not necessary. There are, for instance, models with infinitely many absorbing states that belong to the DP universality class [66]. Another example is the model discussed in CHAP. 7, which involves long-time memory effects and 'mutations' and was shown to exhibit DP critical behavior, as well [52].

4.2.7 Nonintegrability

It has not been possible to solve models of the directed percolation universality class exactly, even in one spatial dimension d=1. Moreover, there are further indications that DP a nonintegrable process.

Usually for integrable models, such as the asymmetric simple exclusion process (ASEP) [8–10], the critical exponents are found to be rational numbers. The critical exponents of DP for d=1 have been determined very accurately (see TAB. 4.2). The most precise estimates do not suggest that the DP exponents are given by 'reasonable' rational numbers but rather by *irrational* numbers. This is usually viewed as an indication for the nonintegrability of directed percolation.

Another indication for the nonsolvability of DP comes from exact solutions of the contact process for small system sizes. In REF. [14] the real parts of the eigenvalues of the transition matrix for the contact process are plotted for small system sizes. One can observe a 'spiders-web' of crossing eigenvalues which is reminiscent of bifurcations of the logistic map, well known in chaos theory. In REF. [14] it was argued that this observation suggests that the contact process cannot be solved exactly.

I want to mention an observation which might serve as another indication of the nonintegrability of DP. In the spirit of Yang-Lee theory, in CHAP. 5 the zeros of the survival probability $P_{\mathrm{s}}(t)$ for directed percolation are investigated for small systems (up to t=15). For solvable models partition function zeros are usually found to lie on well-defined curves. Contrarily, as is discussed in CHAP. 5, the zeros of the survival probability show a more complicated and rather irregular distribution, i.e., they approach the critical point on *many* trajectories. This may be a further fingerprint of the nonintegrability of DP.

4.2.8 Experimental realizations

In spite of the intriguing robustness of DP with respect to the microscopic dynamic rules of stochastic models (see SEC. 4.2.5), the directed percolation phase transition still awaits a convincing experimental verification. This is in fact a major problem in the field of nonequilibrium phase transitions as Grassberger emphasized in a summary of open problems [95]:

> *" ... there is still no experiment where the critical behavior of DP was seen. This is a very strange situation in view of the vast and successive theoretical efforts made to understand it. Designing and performing such an experiment has thus top priority in my list of open problems." .*

Though this statement was made in 1995, it has not lost its topicality. Over the years, a variety of possible experimental realizations has been suggested, ranging from catalytic reactions [56] over flowing sand [57] to spatiotemporal intermittency in magnetic fluids [96]. For a detailed discussion I refer to Ref. [75]. Among the mentioned examples, there are experiments where the estimated exponents are in rough agreement with the predictions of DP. Nevertheless, until now there is still no clear experimental evidence for the DP transition.

It is important to note that it is rather easy to observe nonequilibrium phase transitions between active and absorbing states in experiments or our natural environment on a *qualitative level*. The problem is to verify the universal critical behavior of directed percolation in experiments on a *quantitative level*, i.e., to verify the critical exponents. The lack of experimental evidence may come from the fact that certain assumptions, which are inherent in DP models, are difficult to realize in nature [75]. In nature it is, for instance, difficult to realize a perfectly nonfluctuating absorbing state. Though fluctuations may be strongly suppressed, this effect might be strong enough to 'soften' the phase transition, by this destroying the pure critical behavior of DP. A second possible reason is the influence of *quenched disorder*. It can be shown that spatially and temporally quenched disorder affect the critical behavior of DP whereas spatio-temporally quenched disorder is an irrelevant perturbation, see Ref. [75] and references therein. In models for epidemic spreading, for instance, spatially quenched disorder results in a susceptibility to infections that varies between individuals. Summarizing, it remains an experimental challenge to verify the DP transition quantitatively.

4.3 Summary

The aim of the present chapter was to introduce important concepts, used in the stochastic modeling of spreading phenomena. It was pointed out that models, exhibiting a continuous phase transition between fluctuating active and non-fluctuating inactive states, are appropriate to mimic various spreading processes. Additionally, such models are particularly interesting from the point of view of statistical physics, since they show nonequilibrium critical behavior. Similar to the case of continuous equilibrium phase transitions, the concepts of scale invariance and universality apply in the nonequilibrium case as well. The classification of all possible transitions from fluctuating phases into absorbing states is currently a major goal of nonequilibrium statistical physics. The general scaling theory of phase transitions into absorbing states was summarized. Moreover, directed percolation was discussed, as a paradigm of phase transitions into absorbing states.

Chapter 5

Yang-Lee zeros for nonequilibrium phase transitions

When dealing with nonequilibrium systems, one cannot utilize such a well-established theoretical framework as it is known in equilibrium statistical mechanics. Therefore it is interesting to investigate which concepts of equilibrium physics can be transferred to nonequilibrium systems. In this context, as in equilibrium physics, phase transitions are particularly interesting.

The hallmark of phase transitions in equilibrium statistical mechanics is the appearance of *nonanalyticities* in certain thermodynamic quantities. The sudden and discontinuous change in macroscopic variables at first-order (discontinuous) phase transitions can be related to discontinuities in the first derivative of the free energy. Nonanalyticities in higher derivatives give rise to continuous phase transitions. The specific heat, for instance, which is obtained from the free energy through double differentiation with respect to the temperature, diverges at a continuous phase transition. An important concept in equilibrium statistical mechanics which explains the emergence of nonanalytic behavior at phase transitions, originated more than half a century ago in the seminal work of *Yang* and *Lee* [97, 98]. Yang and Lee showed that the behavior of the *complex zeros of the partition function* can reveal how nonanalytic behavior emerges in the thermodynamic limit.

Since there is no partition function for nonequilibrium systems, it is in general not clear how the concept of Yang and Lee may be applied to systems far from equilibrium. Nevertheless, there has been recent progress in this direction, see Ref. [99] for a review. The main result of this chapter is that, despite the lack of a partition function for directed percolation, it is indeed possible to successfully apply the ideas of Yang-Lee theory to the phase transition of DP [100, 101]. This is in particular important since directed percolation is recognized as a paradigm for nonintegrable systems far from equilibrium. Moreover, I show that this new method does provide information about universal properties of the phase transition [101].

First, in Sec. 5.1, a brief sketch of the main ideas of Yang-Lee zeros in equilibrium statistical physics is presented. In Sec. 5.2 this concept is then transferred and applied to the absorbing-state phase transition of DP. Thereafter, in Sec. 5.3, analytical results for the survival probability for directed bond percolation in 1+1 dimensions are presented. A summary of recent applications of Yang-Lee theory to other nonequilibrium phase transitions is given in Sec. 5.4. The main results are summarized in Sec. 5.5 and an outlook is given for further activities in this field.

5.1 Yang-Lee zeros in equilibrium statistical mechanics

In their famous work, Yang and Lee [97, 98] studied the zeros of the partition function of the Ising model in the complex magnetic field plane, and showed how these zeros can be used to study phase transitions. Later Fisher [102] pointed out that a similar treatment is possible in the complex temperature plane. Therefore, partition function zeros for a field-driven phase transition are usually denoted as *Yang-Lee zeros* while in the case of a temperature-driven transition the term *Fisher zeros* is used. Since then, there have been numerous studies of partition function zeros in a large variety of different models.

In the following I shall briefly sketch the main ideas of complex zeros of the partition function in equilibrium statistical mechanics. For the sake of concreteness, I shall take the Ising model without external field as an example. For a more detailed discussion of this subject I refer the interested reader to Refs. [4, 102], to more rigorous presentations in Refs. [103, 104], as well as to the original work of Yang and Lee [97, 98].

Consider a system of N spins s_i (s_i=$\pm$1, i=1, ..., N) on a lattice. Each spin on site i interacts with its nearest neighbors, denoted by $<i,j>$. The energy $\mathcal{H}(\{s_i\})$ of a configuration $\{s_i\}$ of the spins is given by $\mathcal{H}(\{s_i\})= -J\sum_{<i,j>} s_i s_j$. $\sum_{<i,j>}$ has to be interpreted as $\sum_i \sum_j \theta_{ij}$ with θ_{ij}=1 if sites i and j are neighbors and θ_{ij}=0 otherwise. The system is said to be in thermal equilibrium at temperature T when the probability distribution $P(\{s_i\})$ to find the system in configuration $\{s_i\}$ is given by the stationary Gibbs ensemble $P(\{s_i\})\propto e^{-\beta\mathcal{H}(\{s_i\})}$, β=$1/k_{\mathrm{B}}T$, where k_{B} is Boltzmann's constant. In that case the statistical properties of the system are fully determined by the canonical partition function

$$Z_N(T) = \sum_{\{s_i\}} e^{-\beta\mathcal{H}(\{s_i\})} = \sum_{\{s_i\}} e^{\beta J \sum_{<i,j>} s_i s_j} \ . \tag{5.1}$$

Let q denote the number of nearest neighbors of a lattice site. One may write $Z_N(T)$ as

$$Z_N(T) = \sum_{\{s_i\}} e^{\beta J(\sum_{<i,j>} s_i s_j - qN + qN)} = e^{\beta J q N} \sum_{\{s_i\}} e^{-\beta J(qN - \sum_{<i,j>} s_i s_j)} \ . \tag{5.2}$$

Note that $\sum_{<i,j>} s_i s_j$ cannot be larger than qN. Hence, the canonical partition function is a *polynomial* in the variable x=$e^{-\beta J}$, leading to

$$Z_N(T) = Z_N(x) = \tilde{C} \sum_{k=0}^{M} C_k x^k \ , \ x=e^{-\beta J} \ , \tag{5.3}$$

with *positive integer coefficients* C_k and $\tilde{C}$=$e^{\beta J q N}$. The degree M of the polynomial is finite for a finite lattice. For a physical value of the temperature, the variable x is a real positive number. According to Eq. (5.3), one can express Z_N solely in terms of the M *zeros* x_n of the partition function. Apart from a constant, which from now on is safely ignored, this results in

$$Z_N(x) = \prod_{n=1}^{M} (x - x_n) \ . \tag{5.4}$$

Since the coefficients C_k in Eq. (5.3) are positive, there are no zeros of $Z_N(x)$ on the positive real axis, in particular, there are no zeros of Z_N in the physically accessible region of x. This means that the zeros are *complex* (which corresponds to a complex value of the temperature) and come in

complex conjugated pairs, or lie on the negative x-axis. The free energy per lattice site f_N in a *finite* system is obtained from Z_N for all values of $x \neq x_n$ through

$$f_N = -\frac{1}{\beta N} \ln Z_N = -\frac{1}{\beta N} \sum_{n=1}^{M} \ln(x - x_n) \ . \tag{5.5}$$

Let me assume that $x \neq x_n$ may even be a complex number (though the physical region is clearly given by real positive values of x), which results in a generalized complex free energy in Eq. (5.5). The hallmark of phase transitions is the appearance of nonanalyticities in the derivatives of the free energy. The natural question arises, how such discontinuities may emerge within the presented framework. In this context I note that a Taylor series expansion of f_N in Eq. (5.5) around a point $x \neq x_n$ has a finite radius of convergence, which is given by the distance to the nearest zero from x. This implies that f_N can be differentiated infinitely many times in any region of the complex plane that does *not* include zeros x_n of the partition function. Therefore, one may identify a phase of the system as a region of x which is devoid of zeros x_n. Singularities of f_N may only occur at zeros of the partition function Z_N, which makes them good candidates for indicating a phase transition. However, as was already pointed out, for physical values of x, Z_N cannot have zeros. Hence, one is led to the conclusion that there is *no phase transition for a finite system.*

If at all, the existence of a phase transition is only possible in the thermodynamic limit, which means $N \to \infty$, volume $V \to \infty$, and $N/V \to \text{const}$. In this case, the partition function Z and the free energy per lattice site are given by

$$Z = \lim_{N\to\infty} Z_N \quad , \quad f = \lim_{N\to\infty} f_N \ . \tag{5.6}$$

What may change when approaching the infinite system? Clearly, the number of zeros grows. Furthermore, the zeros may close up to form lines with a certain density of zeros ρ_z. Such a line may cut the positive real axis in the case of a phase transition. This would imply that in the thermodynamic limit an ever increasing number of complex zeros accumulates in the vicinity of a point on the positive real axis. In this case, the complex zeros may come arbitrarily close to the real axis, thereby inducing singularities at the accumulation point in the thermodynamic limit. Thus, one can identify the accumulation point of the complex zeros with the phase transition point. This scenario explains the crossover to nonanalyticity at the transition in the thermodynamic limit. A phase of the system is a region in the complex

plane which does not include zeros of Z. The lines of zeros mark phase boundaries. Such a behavior has indeed been observed for many equilibrium models. In the case of the $2d$ Ising model, for instance, without an external magnetic field the zeros are located on two circles in the complex x-plane ($x{=}e^{-\beta J}$) [102]. These circles cut the real axis in four points. Two of these points are unphysical while the other points locate the ferromagnetic (coupling $J{>}0$) and the antiferromagnetic ($J{<}0$) transition. It is even possible to relate several features of the distribution of zeros to the nature of the phase transition (first order or continuous) and to universal properties of the system under consideration (see, e.g., [102, 105, 106]). Moreover, though it was long thought that the density of zeros ρ_{z} is a purely theoretical quantity, Binek could show that ρ_{z} is in fact accessable by experiments [107], since he extracted ρ_{z} from isothermal magnetization data of Ising ferromagnets.

I conclude this summary of Yang-Lee zeros in equilibrium statistical mechanics with some further remarks. The concept of extending an intensive variable to the complex plane to study the behavior of the partition function is of course not restricted to the temperature. Similarly, one is not restricted to the canonical ensemble. In fact, in their seminal work Yang and Lee investigated the grand canonical partition function depending on the complex fugacity z. The 'Yang-Lee scenario' of complex partition function zeros accumulating at a phase transition point applies to a large variety of equilibrium models. However, proving this scenario in the general case is a difficult task (see Ref. [108] for recent progress in this direction), and therefore most results rely on specific models, such as the Ising model.

5.2 Yang-Lee zeros for directed percolation

Despite the lack of a partition function, in this section the ideas of Yang-Lee theory are transferred to describe the absorbing-state phase transition of directed percolation, which is recognized as a paradigm for phase transitions far from equilibrium. I will demonstrate below that for this purpose it is reasonable to study the order parameter in a *finite* system as a function of the percolation probability p in the *complex plane*. This will be done for *directed bond* and *site percolation* in 1+1 dimensions by studying the time-dependent survival probability $P_{\mathrm{s}}(t)$ (see Sec. 4.2), which is defined as the probability that a cluster generated in a single site at time $t{=}0$ survives up to time t (or even longer). For a finite system $P_{\mathrm{s}}(t)$ can be expressed as a *polynomial* in p (see below) with integer coefficients. Note that $\lim_{t\to\infty} P_{\mathrm{s}}(t)$ and the order parameter P^{∞} coincide, see Eq. (4.3).

The motivation to investigate $P_s(t)$ in the context of Yang-Lee theory is that the survival probability and the partition function EQ. (5.3) show a similar behavior in many respects. For finite systems, $P_s(t)$ and Z_N do not have relevant zeros in the physical region of the control parameter $0 \leq p \leq 1$ and $0 < T < \infty$, respectively, although the phase transition is marked by a vanishing $P_s(t)$ and Z_N at the critical points in the limit of infinite systems. At those points nonanalytic behavior emerges. The zeros of $P_s(t)$ and Z_N are generated by polynomials (see below) with real integer coefficients, thus the zeros come in complex-conjugate pairs. Moreover, it is even possible to express $P_s(t)$ in such a way that is has the structure of a transfer-matrix representation of an equilibrium partition function. This can be done by associating with each site a spin that is up if the site is connected to a site at time t and down otherwise [109]. Though these similarities between $P_s(t)$ and Z_N can be viewed as an indication that the survival probability might play a similar role as the partition function, it is by no means clear that necessarily a 'Yang-Lee scenario' is valid, as well. According to the Yang-Lee theory presented in SEC. 5.1, as the system size increases, some of the complex roots of Z_N approach an accumulation point within the physical region of the control parameter. The accumulation point marks the critical point. In fact, it turns out that analogous to the equilibrium case the complex zeros of $P_s(t)$ approach the critical value p_c [1] on 'trajectories' for increasing time t, and that the distance between the zeros and the critical point is related to the critical exponent for the temporal correlation length $\nu_\parallel$.

5.2.1 Exact determination of the survival probability $P_s(t)$

Simple realizations of DP in 1+1 dimensions are directed bond (in the following denoted as DPb) and directed site percolation (denoted as DPs) on a tilted square lattice. The critical exponents for DP in 1+1 dimensions are summarized in TAB. 4.2. Recall that in directed bond percolation the bonds are conducting with probability p and non-conducting with probability $1-p$. In this model, sites at time $t>0$ are activated by directed paths of conducting bonds, originating from active sites at time $t=0$. A cluster consists of all sites that are connected by such paths of conducting bonds to active sites

[1] Since $\lim_{t\to\infty} P_s(t)$ vanishes not only at p_c but for $0 \leq p \leq p_c$ one might expect that the whole interval is an accumulation set of the zeros. However, the observations indicate that $P_s(t)$ vanishes asymptotically on this interval due to the highly degenerated zero at $p=0$.

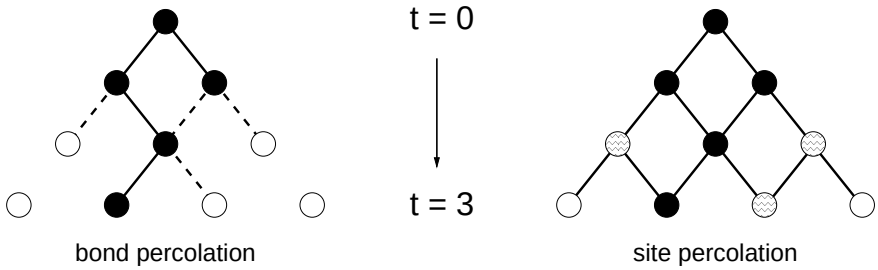

FIGURE 5.1: *Examples of DPb and DPs clusters which survive until time t=3. Active sites are shown as black circles, conducting bonds as solid lines. Left: Dashed lines denote the hull, irrelevant bonds are not shown. The corresponding weight to the survival probability $P(3)$ in* EQ. *(5.7) is $p^4(1-p)^4$. Right: White patterned circles belong to the hull. Simple white circles are irrelevant for the survival of the cluster. The corresponding weight to $P(3)$ in* EQ. *(5.7) is $p^4(1-p)^3$.*

in the initial state (see SEC. 4.2 and FIG. 5.1). The transition between the active phase, where a cluster may survive in the limit $t\to\infty$ (in an infinite system), and the absorbing phase, where it definitely dies out for long times, occurs for bond percolation on a tilted square lattice in 1+1 dimensions at the critical value p_c=0.644700185(5) [78]. In contrast to DPb, in directed site percolation all bonds are conducting while the sites themselves can be either permeable (p) or blocked ($1-p$). Activity can spread from permeable site to permeable site. A cluster is formed by permeable sites that are connected to active sites at time t=0 by a directed path of bonds that only connect permeable sites (see FIG. 5.1). In this case the transition point is given by p_c=0.70548522(4) [78].

The survival probability $P_s(t)$ is the probability that a cluster generated at a single site, called the origin, at time t=0 survives up to time t (or even longer). In directed bond (site) percolation the survival probability $P_s(t)$ is given by the sum over the weights of all possible configurations of bonds (sites) for which the process survives at least up to time t. Each conducting bond (permeable site) contributes to the weight with a factor p, while each non-conducting bond (blocked site) contributes with a factor $1-p$. However, the states of those bonds (sites) which do not touch the actual cluster are irrelevant, as they do not contribute to the survival of the cluster. Therefore, it is sufficient to consider the sum over all possible clusters $\mathcal{C}$ of bonds (sites) connected to the origin. Each cluster is weighted by the contributions of the

conducting bonds (permeable sites) belonging to the cluster, and the non-conducting bonds (blocked sites) belonging to its hull. Roughly speaking, the hull surrounds the cluster. More precisely the hull of a cluster is the set of non-conducting bonds (blocked sites) that would contribute to the cluster if they were conducting (permeable) (see Figure 5.1). Thus, the survival probability can be expressed as

$$P_{\mathrm{s}}(t) = \sum_{\mathcal{C}} p^n (1-p)^m \ , \tag{5.7}$$

where the sum runs over all clusters reaching the horizontal row at time t. For each cluster, n denotes the number of its active bonds (sites), while m is the number of inactive bonds (sites) belonging to its hull. Note that in this sense the hull does not include bonds connecting sites at time t and $t{+}1$ (DPb) or sites at time $t{+}1$ (DPs) since the cluster may survive even longer. Summing up all weights in Eq. (5.7) one obtains a polynomial in p with real integer coefficients. Exemplarily, Fig. 5.2 shows the configurations and the corresponding weights that contribute to $P_{\mathrm{s}}(2)$ for directed bond percolation. The first few polynomials for the survival probability in the directed bond percolation process are

$$\begin{aligned}
P_{\mathrm{s}}(0) &= 1 \ , \\
P_{\mathrm{s}}(1) &= 2p{-}p^2 \ , \\
P_{\mathrm{s}}(2) &= 4p^2{-}2p^3{-}4p^4{+}4p^5{-}p^6 \ , \\
P_{\mathrm{s}}(3) &= 8p^3{-}4p^4{-}10p^5{-}3p^6{+}18p^7{+}5p^8{-}30p^9{+}24p^{10}{-}8p^{11}{+}p^{12} \ , \\
P_{\mathrm{s}}(4) &= 16p^4{-}8p^5{-}24p^6{-}8p^7{+}6p^8{+}84p^9{-}29p^{10}{-}62p^{11}{-}120p^{12}{+} \\
&\quad 244p^{13}{+}75p^{14}{-}470p^{15}{+}495p^{16}{-}268p^{17}{+}83p^{18}{-}14p^{19}{+}p^{20} \ .
\end{aligned} \tag{5.8}$$

As t increases the number of cluster configurations grows rapidly, leading to complicated polynomials with very large coefficients (e.g., for $t{=}15$ the largest coefficient for bond percolation is of order 10^{44}). In order to determine the polynomials $P_{\mathrm{s}}(t)$, an explicit tour through all relevant configurations is necessary with a summation of the corresponding weights. This was done computationally for directed bond and directed site percolation up to $t{=}15$. Note that the expressions obtained for the polynomials $P_{\mathrm{s}}(t)$ are *exact*.

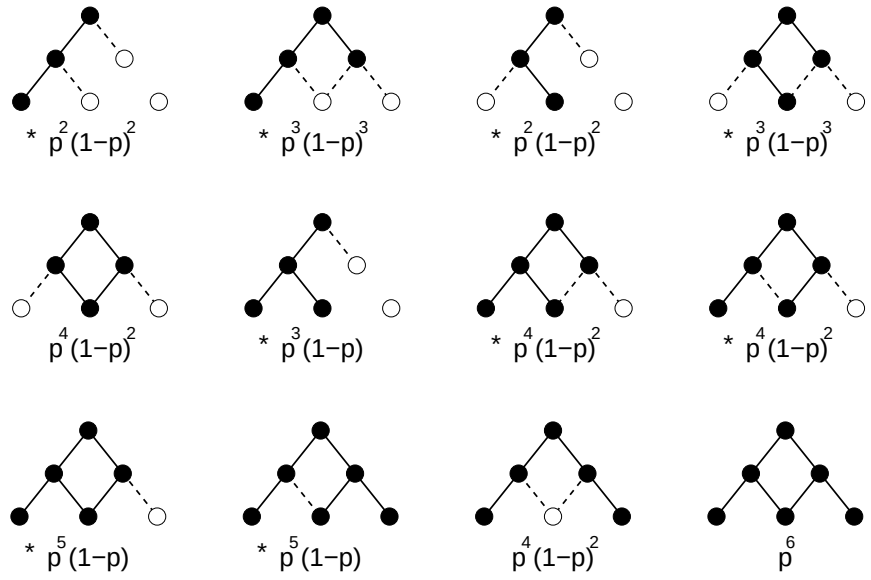

FIGURE 5.2: *All relevant configurations that contribute to* $P_{\mathrm{s}}(2)$ *in* EQ. *(5.7) for DPb with corresponding weights. Configurations that are marked with* $*$ *have to be counted twice as there is an additional mirrored configuration. Active sites are shown as black circles, conducting bonds as solid lines, dashed lines denote the hull and irrelevant bonds are not shown. Summation of the weights results in the polynomial* $P_{\mathrm{s}}(2)$ *in* EQ. *(5.8).*

5.2.2 Computational method

Here I briefly sketch how the polynomials $P_{\mathrm{s}}(t)$ were calculated numerically. For convenience I restrict myself to the case of directed *bond* percolation. Generalization to directed site percolation is straight forward.

Let c_t denote all configurations of *sites* at time t where the process survives until time t. There are $t{+}1$ sites that may be reached at time t when the process started with a single active site at time $t{=}0$. Hence, the number of configurations c_t is $2^{t+1}{-}1$. Each configuration c_t is associated with a probability $\pi(c_t)$. Clearly $\pi(c_t)$ is a polynomial in p which is given by a sum similar to EQ. (5.7), where now the sum includes all relevant configurations of the bonds that contribute to the configuration c_t of the sites at time t. Then, the survival probability may be written as

$$P_{\mathrm{s}}(t) = \sum_{c_t} \pi(c_t) \ . \tag{5.9}$$

To determine the polynomial $P_{\mathrm{s}}(t)$, I calculated all polynomials $\pi(c_t)$ given all polynomials $\pi(c_{t-1})$ from the previous time step.

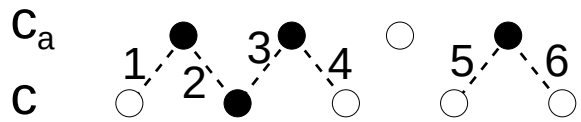

FIGURE 5.3: *c denotes a configuration of the sites at time t=4. c_a is one of its ancestor configurations. The numbers enumerate the bonds that are relevant for $\tilde{\pi}$ in* EQ. *(5.10). For this example on finds $\tilde{\pi}(c_a \to c)=P(10\to 0)^4 \cdot P(11\to 1)$, see text.*

Internally the polynomials $\pi(c_t)$ were stored in arrays $a[i]$, where $a[i]$ denotes the coefficient that belongs to p^i. Since the largest coefficients were of order $10^{44}\approx 2^{146}$, it was not possible to use standard integer numbers. Instead, a special library was used, which allowed to handle that large integers. A configuration c_t was represented by the bit sequence of an integer number. The computer algorithm went through all $2^{t+1}-1$ configurations $\pi(c_t)$. Let c_t^1 denote one of these configurations at time t. All possible ancestor configurations c_{t-1} of the previous time step were determined using bit operations. Ancestor configuration means that it is allowed by the dynamic rules to go from configuration c_{t-1} to configuration c_t within one time step. Let c_a^1 denote the ancestor configurations of c_t^1. The probability $\pi(c_t^1)$ may be obtained from

$$\pi(c_t^1) = \sum_{c_a^1} \pi(c_a^1)\tilde{\pi}(c_a^1 \to c_t^1) \ , \tag{5.10}$$

where $\tilde{\pi}(c_a^1 \to c_t^1)$ is a polynomial corresponding to the possible states of the bonds between row $t-1$ and t, that lead from configuration c_a^1 to c_t^1. This may be illustrated by FIG. 5.3. To go from the ancestor configuration c_a to the configuration c, the bonds $1, 4, 5, 6$ have to be nonconducting, leading to a weight $(1-p)^4 \equiv P(10\to 0)^4$, and simultaneously either bond 2 or bond 3 or both have to be conducting, leading to the weight $2(p-1)p+p^2 \equiv P(11\to 1)$. Therefore $\tilde{\pi}(c_a \to c)=P(10\to 0)^4 \cdot P(11\to 1)$, in the example of FIG. 5.3. Notations like $P(11\to 1)$ symbolize the fact that $P(11\to 1)$ corresponds to the situation that two neighboring active sites at time $t-1$ result in an active site at time t. Similar to this example it is always possible to write $\tilde{\pi}(c_a^1 \to c_t^1)$ in EQ. (5.10) as

$$\tilde{\pi}(c_a^1 \to c_t^1) = P(10\to 0)^{\kappa} P(10\to 1)^{\gamma} P(11\to 0)^{\mu} P(11\to 1)^{\nu} \tag{5.11}$$

where $P(10\to 1)=p$, $P(11\to 0)=(1-p)^2$ and the exponents are positive integer numbers that depend on the configurations c_a^1 and c_t^1. In the example of

Trajectory	$\mathrm{Re}\,(p^{\mathrm{zero}}_{t\to\infty})$	$\mathrm{Im}\,(p^{\mathrm{zero}}_{t\to\infty})$	Trajectory	$\mathrm{Re}\,(p^{\mathrm{zero}}_{t\to\infty})$	$\mathrm{Im}\,(p^{\mathrm{zero}}_{t\to\infty})$
Bond 1	0.64472(1)	0.0001(1)	Site 1	0.70547(3)	0.0001(3)
Bond 2	0.6445(2)	0.008(1)	Site 2	0.709(4)	0.006(1)
Bond 3	0.6470(4)	0.051(7)	Site 3	0.712(1)	0.01(1)

TABLE 5.1: *Bulirsch-Stoer extrapolants for the zeros of the 'trajectories' from* FIG. *5.5 for both bond and site percolation in 1+1 dimensions.*

FIG. 5.3 one has κ=4, ν=1 and γ=μ=0. The computer algorithm determined these exponents from the bit-sequence representation of configurations c^1_a and c^1_t by bit operations.

In conclusion, $P_{\mathrm{s}}(t)$ was determined by application of EQ. (5.9) where $\pi(c_t)$ was given by EQ. (5.10) with $\tilde{\pi}(c^1_a \to c^1_t)$ obeying EQ. (5.11).

5.2.3 Critical points and 'Yang-Lee scenario'

The distribution of the zeros of $P_{\mathrm{s}}(t)$ (from t=8 to t=15) in the neighborhood of the critical point is shown in FIG. 5.4. Away from the critical point, the appearance of the distributions for DPb and DPs is quite different. This implies that in this region the distribution of zeros depends strongly on microscopic details and hence is non-universal. However, there is also a general feature which can be observed in both cases. The innermost zeros approach the critical point on 'trajectories' as t increases (see FIG. 5.5). A behavior which is strongly reminiscent of the behavior of partition function zeros in equilibrium statistical physics. A more thorough investigation was carried out by application of a standard Bulirsch-Stoer (BST) acceleration algorithm [110] to the set of zeros of each enumerated 'trajectory' of FIG. 5.5, in order to determine $\lim_{t\to\infty} \mathrm{Re}\,(p^{\mathrm{zero}}(t))$ and $\lim_{t\to\infty} \mathrm{Im}\,(p^{\mathrm{zero}}(t))$. The results are listed in TAB. 5.1. Although the zeros were calculated only for small systems (until t=15) the extrapolants accord fairly well with the numerical values of the percolation threshold[2] p_{c}=0.644700185(5) (bond percolation) and p_{c}=0.70548522(4) (site percolation). This investigation

[2]The convergence for site percolation is slower than for bond percolation since the order of the polynomials $P_{\mathrm{s}}(t)$ for DPs is smaller than for DPb.

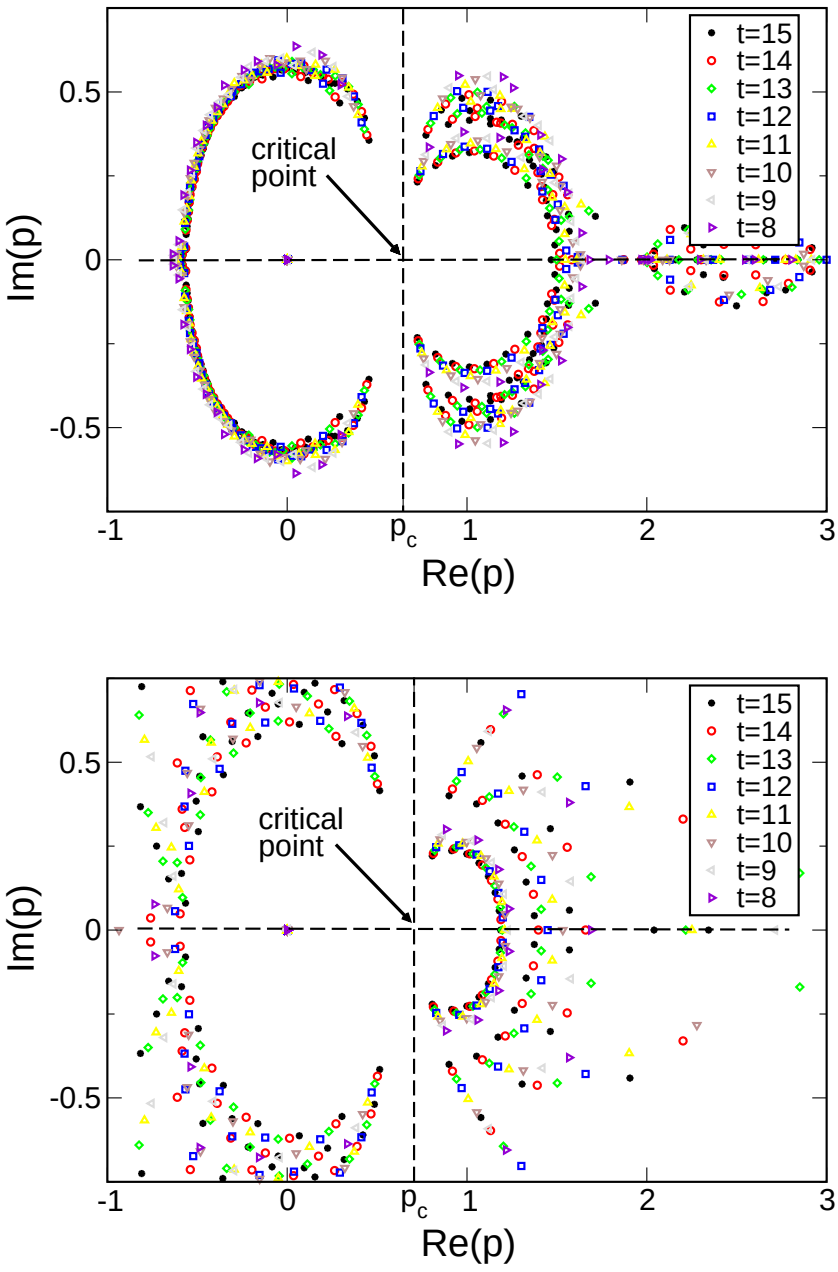

FIGURE 5.4: *Zeros of the survival probability $P_s(t)$ in the complex plane. Top: Directed bond percolation. Bottom: Directed site percolation.*

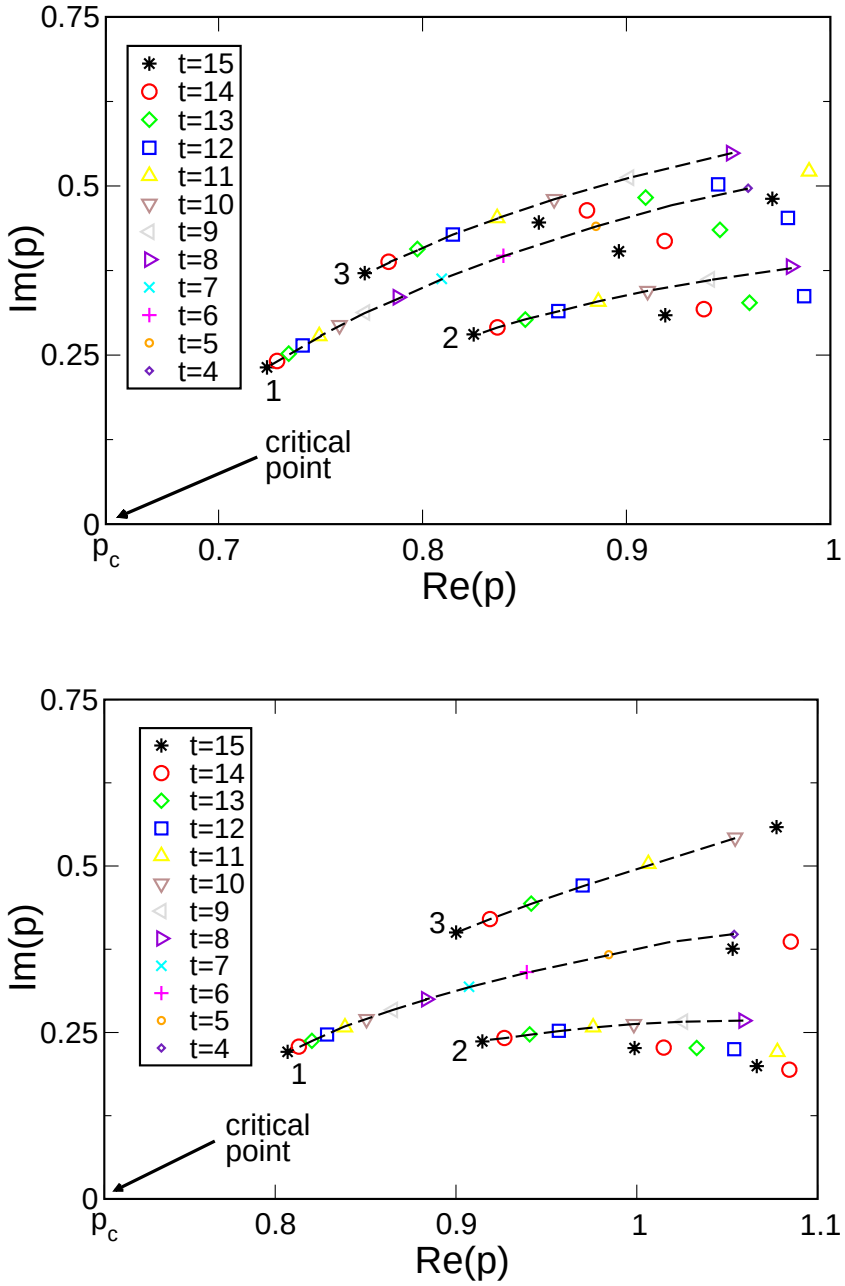

FIGURE 5.5: *Zeros approaching the critical point. Three 'trajectories' are enumerated and shown as dashed lines. Top: Directed bond percolation. Bottom: Directed site percolation.*

shows that a similar scenario as observed by Yang and Lee for equilibrium phase transitions proves to be suitable for the nonequilibrium phase transition of DP, as well. As time increases, the zeros of the survival probability $P_{\mathrm{s}}(t)$ approach the real axis between p=0 and p=1 and the accumulation point is the critical point.

Besides the clear analogy between the complex zeros of $P_{\mathrm{s}}(t)$ and partition function zeros, I want to turn the attention to a rather uncommon feature of the distribution of zeros in FIG. 5.4. The zeros are not located on well-defined lines but show a much more complicated distribution. In particular, there are *many* lines of zeros approaching the critical point, instead of a single line which is usually observed, as for instance in the 2d Ising model (or in *integrable* nonequilibrium models, see SEC. 5.4). This might be another indication of the nonintegrability of directed percolation, see SEC. 4.2.7.

5.2.4 Universal features

So far I have shown that the zeros of $P_{\mathrm{s}}(t)$ provide information about the existence of the phase transition and about the critical value p_{c}. Note that the value of p_{c} is non-universal and depends on the particular realization of DP. However, interest in DP mainly stems from the fact that its critical behavior is universal, i.e., it does *not* depend on the microscopic details of the underlying process. Hence, it is important to investigate whether the distribution of zeros in FIG. 5.4 reflects the universal character of the absorbing-state phase transition of DP.

For this purpose, I calculated the distance between the zeros and the critical point, $d(t)=|p^{\mathrm{zero}}(t)-p_{\mathrm{c}}|$ on each 'trajectory' of FIG. 5.5. I used the values of p_{c} which were given above (from REF. [78]). The distance d should exhibit the usual scaling behavior of $|p-p_{\mathrm{c}}|=|\Delta_p|$. Moreover, d is a function of time. According to EQ. (4.4) time scales as $|\Delta_p|^{-\nu_\parallel}$. Hence, led by simple scaling arguments one expects $d(t)$ to decrease as

$$d(t) \sim t^{-1/\nu_\parallel} \ . \tag{5.12}$$

For illustration, FIG. 5.6 shows the used data, which approach the asymptotic power law $d(t)\sim t^{-1/\nu_\parallel}$ with the numerical value of $\nu_\parallel\approx 1.7338$. Application of the BST algorithm yields results which support this claim, as shown in TAB. 5.2. The extrapolants are in fairly good agreement with the numerical value of $1/\nu_\parallel=0.576752$, even for small systems. This means that universal properties of the phase transition of directed percolation are indeed encoded in the complex zeros of the survival probability $P_{\mathrm{s}}(t)$.

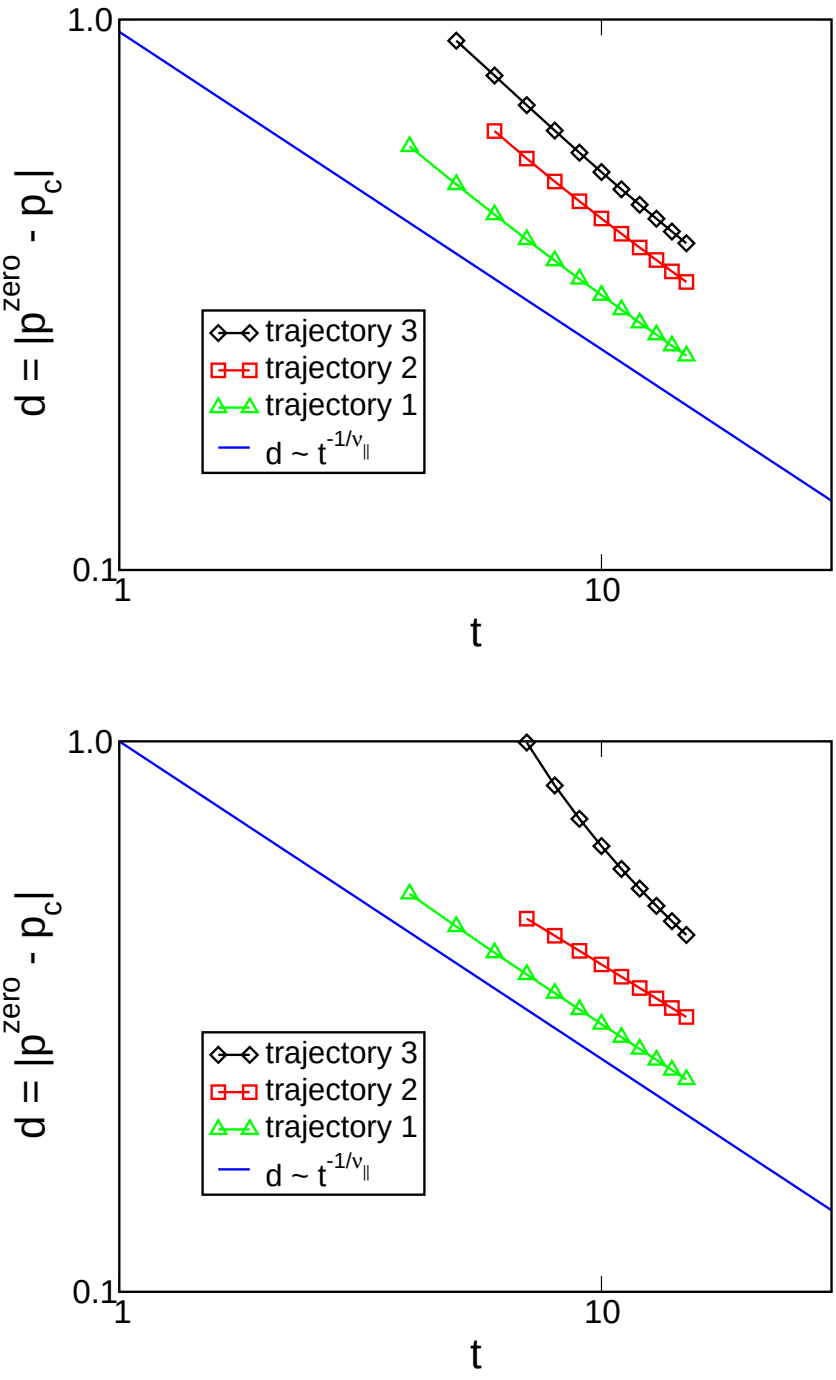

FIGURE 5.6: *The distance from the critical point* $d(t)=|p^{\mathrm{zero}}(t) - p_c|$ *versus time* t. *For comparison the power law* $d\sim t^{-1/\nu_\parallel}$ *is shown, with* $\nu_\parallel$=1.7338. *Top: Directed bond percolation. Bottom: Directed site percolation.*

Trajectory	$1/\nu_{\|\|}$	Trajectory	$1/\nu_{\|\|}$
Bond 1	0.57675(3)	Site 1	0.5765(7)
Bond 2	0.575(2)	Site 2	0.5771(2)
Bond 3	0.576(4)	Site 3	0.5731(2)

TABLE 5.2: *Bulirsch-Stoer extrapolants of the exponent* $1/\nu_{\|}$. *On each 'trajectory' in* FIG. *5.5 the distance* $d(t) = |p^{\mathrm{zero}}(t) - p_{\mathrm{c}}|$ *is assumed to decrease as* $d(t) \sim t^{-1/\nu_{\|}}$.

5.2.5 MC-Simulations

Here, I demonstrate that the value of the survival probability for a complex percolation probability p, as well as the polynomials $P_{\mathrm{s}}(t)$ are in principle accessible by computer simulations. This method is closely related to the procedure introduced in REF. [111].

Consider the definition of the survival probability as a sum over configurations of surviving clusters in EQ. (5.7). Formally this expression can be rewritten as

$$P_{\mathrm{s}}(t) = \sum_{\mathcal{C}} p^n (1-p)^m = \sum_{\mathcal{C}} q^n (1-q)^m \underbrace{\frac{p^n (1-p)^m}{q^n (1-q)^m}}_{f_{n,m}} \tag{5.13}$$

where n and m denote the number of bonds (sites) of the cluster and of its hull respectively. Therefore, instead of simulating the system at a given p, one can simulate it using a *different* percolation probability q reweighting each cluster by the factor $f_{n,m}$. While $q \in (0,1)$ still has to be a real number, p is no longer restricted to be real, it can be any complex number. Using this reweighting technique it is in principle possible to access the entire complex plane by numerical simulations. But even for small t the convergence time of such a simulation can be very long, limiting the range of applications. Especially when p and q are not very close together the applicability of this method is severely limited [111].

Using the reweighting technique it is also possible to approximate the coefficients of the polynomial $P_{\mathrm{s}}(t) = \sum_k a_k p^k$ by considering p as a free parameter and expanding the term $(1-p)^m$ in EQ. (5.13). The coefficients are then given by

$$a_k = \sum_{\mathcal{C}} q^n (1-q)^m \, \frac{C(m, k-n)(-1)^{k-n}}{q^n (1-q)^m} \,, \tag{5.14}$$

where $q\in(0,1)$ is again a free parameter and

$$C(m,k-n)=\begin{cases}\frac{m!}{(k-n)!(m-k-n)!} & \text{if } 0\leq k-n\leq m\\ 0 & \text{otherwise .}\end{cases} \tag{5.15}$$

However, in most cases the direct construction of the polynomials using symbolic algebra turns out to be more efficient.

5.3 Analytical results for $P_{\mathrm{s}}(t)$ for DPb

In this section I will first address a particularly surprising observation, namely, the existence of certain non-trivial points on the real axis, where the polynomials $P_{\mathrm{s}}(t)$ for bond percolation can be solved *exactly* for all values of t. Beside the trivial points p=0 (where $P_{\mathrm{s}}(t)$=$\delta_{t,0}$) and p=1 (where $P_{\mathrm{s}}(t)$=1), one finds a t-independent zero at p=2 and, even more surprisingly, a very simple solution if p is equal to one of the Golden Ratios $(1\pm\sqrt{5})/2$. The Golden Ratios are the roots of the quadratic equation p^2=p+1 and play an important role not only in number theory [112, 113] but also in other fields ranging from chaotic systems [114] to arts [115]. Although these special points are located outside the physically accessible region $0\leq p\leq 1$, their existence may be helpful for further investigations of the polynomials $P_{\mathrm{s}}(t)$.

Thereafter, I derive an analytical expression for the first non-vanishing coefficients of the survival probability $P_{\mathrm{s}}(t)$=$\sum_n a_n p^n$. This results in an analytical expression for $P_{\mathrm{s}}(t)$, which serves as an approximation close to p=0, which might prove to be useful for further studies, as well.

5.3.1 Time-independent zero at p=2

For p=2 and $t\geq 1$ all polynomials $P_{\mathrm{s}}(t)$ vanish identically. This can be shown as follows. Consider the probability $R(t)$ that a cluster dies out at time t, i.e., the row at time t is the last row reached by a cluster. Obviously $R(t)$ is related to the survival probability by

$$R(t)=P_{\mathrm{s}}(t)-P_{\mathrm{s}}(t+1)\ . \tag{5.16}$$

Clearly, $R(t)$ can be expressed as a weighted sum over the same set of clusters as in Eq. (5.7). However, in the present case the weights differ from those in Eq. (5.7) by the number of non-conducting bonds in the clusters hull

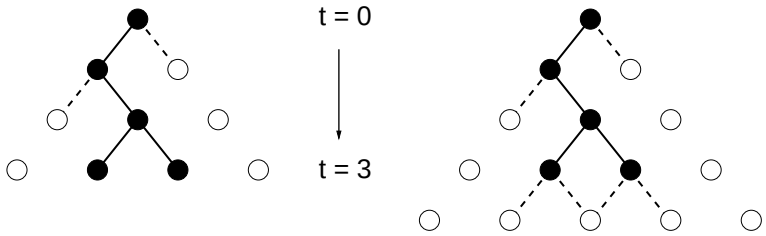

FIGURE 5.7: *Example of different weights for $P_s(t)$ and $R(t)$. Left: The contribution of the shown cluster to $P_s(3)$ in* EQ. *(5.7) is $p^4(1-p)^2$. Right: The contribution of the cluster to $R(3)$ in* EQ. *(5.17) is $p^4(1-p)^6$ since it is required that active sites at t=3 are not connected to sites at t=4 by active bonds.*

between t and t+1 since it is now required that all sites at time t+1 are inactive (see FIG. 5.7). This means that $R(t)$ can be expressed as

$$R(t) = \sum_{\mathcal{C}} p^n (1-p)^m (1-p)^{2k} \ , \tag{5.17}$$

where n, m and $\mathcal{C}$ have the same meaning as in EQ. (5.7) and k is the number of active sites in the horizontal row at time t. Obviously, for p=2 the additional factor $(1-p)^{2k}$ drops out so that $P_s(t) = R(t)$ for all values of t. Moreover, $R(0)$=$P(0)$=1 (for p=2). Combining these results with EQ. (5.16) one arrives at $P(t)$=0 for t>0, which completes the proof.

5.3.2 Exact solution for p at the Golden Ratio

For p=$(1\pm\sqrt{5})/2$ one finds that the survival probability 'oscillates' between two different values, namely

$$P_s(t) = \begin{cases} 1 & \text{if } t \text{ is even} \\ \frac{\pm\sqrt{5}-1}{2} & \text{if } t \text{ is odd.} \end{cases} \tag{5.18}$$

To prove this result, I first verify that EQ. (5.18) is indeed satisfied for t=0 and t=1. Then I show that

$$P_s(t) = P_s(t-2) \qquad \text{for } t \geq 2 \quad \text{and} \quad p = (1 \pm \sqrt{5})/2 \ . \tag{5.19}$$

However, instead of analyzing the survival probability directly, it turns out to be more convenient to consider the complementary probability $Q(t)$=1−$P_s(t)$ that a cluster does *not* survive until time t. Moreover, for

the calculation carried out in the following, it is also convenient to label the lattice sites slightly different than it was done in SEC. 4.2.2. Let $s_{0,t}$ denote the leftmost lattice site that may be reached at time t, starting from the origin. $s_{0,t}$ coincides with $s_{-t}(t)$, using the notation of SEC. 4.2.2. Starting from an active seed, in SEC. 4.2.2, the next possible active site to the right of $s_{-t}(t)$ is $s_{-t+2}(t)$, which in the new notation shall be labeled as $s_{1,t}$. Consequently, $s_{t,t}$ is the rightmost lattice site that may be reached at t starting from the origin, corresponding to $s_t(t)$ in SEC. 4.2.2. In conclusion, the notation used here, denotes the sites that may be reached at time t from the origin, beginning with the leftmost site, as $s_{0,t}, s_{1,t}, \ldots, s_{t,t}$.

Obviously, $Q(t)$ is the sum over the weights of all clusters which do not reach the horizontal row at time t, i.e., the boundary condition $s_{0,t}{=}s_{1,t}{=}\ldots{=}s_{t,t}{=}0$ are imposed. Depending on the states of the two sites $s_{0,t-1}$ and $s_{0,t-2}$ at the left edge of the clusters, this set of clusters may be separated into three different subsets, namely,

(a) a subset where $s_{0,t-1}{=}s_{0,t-2}{=}1$,
(b) a subset where $s_{0,t-1}{=}0$ and $s_{0,t-2}{=}1$, and
(c) a subset where $s_{0,t-1}{=}s_{0,t-2}{=}0$.

The weights of the clusters in the subsets (a) and (b) cancel each other. To this end I note that the weighted sum $\hat{Q}(t)$ over all clusters in subsets (a) and (b) may be decomposed into two independent factors $\hat{Q}(t){=}\hat{Q}_1\hat{Q}_2$. $\hat{Q}_1$ depends only on the state of the three bonds between the sites $s_{0,t-2}$, $s_{0,t-1}$, $s_{0,t}$, and $s_{1,t}$ (inside the box in FIG. 5.8), while $\hat{Q}_2$ accounts for all other relevant bonds. Obviously, the first factor is given by

$$\hat{Q}_1^{(a)} = p(1-p)^2 \ , \qquad \hat{Q}_1^{(b)} = 1-p \ , \tag{5.20}$$

while $\hat{Q}_2$ takes the same value in both subsets. Thus, if p is given by the Golden Ratio, one obtains $\hat{Q}_1^{(a)}{+}\hat{Q}_1^{(b)}{=}\hat{Q}_1(t){=}0$ and therefore the weights of subsets (a) and (b) cancel each other. Consequently, all remaining contributions to $Q(t)$ come from the clusters in subset (c) where the sites $s_{0,t-1}$ and $s_{0,t-2}$ are inactive. Now one can iterate this procedure by successively considering the sites $s_{j,t-1}$ and $s_{j,t-2}$ from the left to the right, where $j{=}1\ldots t{-}2$. In this way it can be shown that all these sites have to be inactive as well. Therefore, the only surviving contributions are those in which the entire row of sites at $t{-}2$ is inactive, implying that $Q(t){=}Q(t{-}2)$. The proof of EQ. (5.18) then follows by induction.

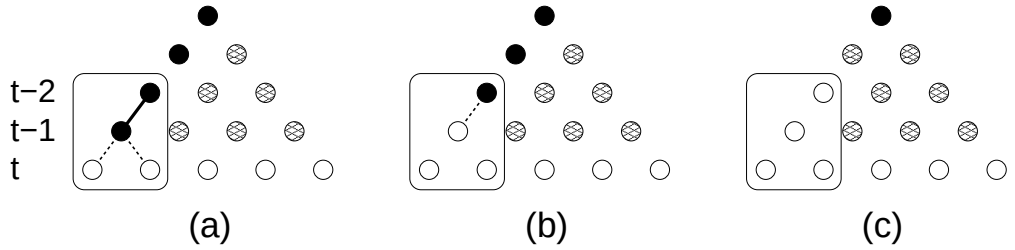

FIGURE 5.8: *Decomposition of the configurational sum of non-surviving clusters into three subsets. Open and closed bonds are denoted by solid (dashed) lines. Bonds which are not shown may be either open or closed. The box includes all bonds contributing to the factor $\hat{Q}_1$ while all other bonds contribute to the factor $\hat{Q}_2$. The proof shows that the configurations in (a) and (b) cancel each other so that only the configurations of (c) contribute to Q. Iterating the procedure by shifting the box to the right, it can be shown that all sites at $t-2$ and $t-1$ have to be zero.*

5.3.3 First coefficients of the polynomials $P_{\rm s}(t)$ in the limit $t\to\infty$

As can be seen in EQ. (5.8), the first non-vanishing coefficient of the polynomial for the survival probability $P_{\rm s}(t)=\sum_n a_n p^n$ for DPb is always a power of 2. This contribution corresponds to the configurational weight of surviving paths without branches. I point out that even the following coefficients obey a pattern, provided that t is large enough. More specifically, I conjecture that

$$\begin{aligned} &a_{t+k} = 2^{t-k-1}\, q_k(t) \quad , \quad \text{where} \\ &q_k(t) = \textstyle\sum_{m=0}^{M} b_m^{(k)} t^m \ , \quad M = \begin{cases} k/2 & \text{if } k \text{ even} \\ (k-1)/2 & \text{if } k \text{ odd} \end{cases} \end{aligned} \tag{5.21}$$

is a finite polynomial in t. Using the explicit expressions for $P_{\rm s}(t)$ up to t=15 one finds that the first eight polynomials read

$$\begin{aligned} q_0(t) &= 2 \\ q_1(t) &= -2 \\ q_2(t) &= -4-2t \\ q_3(t) &= -2t \\ q_4(t) &= -16+3t+t^2 \\ q_5(t) &= 32+t+3t^2 \\ q_6(t) &= -232+64/3\,t+3t^2-1/3\,t^3 \\ q_7(t) &= 808-34/3+5t^2-5/3\,t^3 \ . \end{aligned} \tag{5.22}$$

Led by these observations, I conjecture that the leading coefficient of the polynomials is given by

$$b_M^{(k)} = \begin{cases} 2(-1)^M/M! & \text{if } k \text{ even} \\ 2(k-1)(-1)^M/M! & \text{if } k \text{ odd} \, . \end{cases} \tag{5.23}$$

This implies that the first non-vanishing coefficients of the polynomial $P_{\rm s}(t)$ grow in such a way that their limit $\lim_{t\to\infty} \frac{a_{t+k}}{2^t t^M}$ for fixed k is well-defined. Summing up these contributions one obtains for the survival probability

$$\begin{aligned} P_{\rm s}(t) &\simeq (2p)^t \sum_{j=0}^{\infty} \frac{(-p^2t/4)^j}{j!} \Big(1 + p(j-1/2)\Big) \\ &= \tfrac{1}{4}(2p)^t e^{-p^2t/4}(4 - 2p - p^3 t) \, . \end{aligned} \tag{5.24}$$

Physically this expression corresponds to loop-free graphs and serves as an approximation close to p=0. The convergence radius of Eq. (5.24) determined from $2p{=}e^{p^2/4}$ is $|p|{<}0.53744$. Note that none of the non-trivial roots computed up to t=15 lies inside this radius. I conjecture that this might be true for any t.

5.4 Yang-Lee zeros in other nonequilibrium systems

Apart from directed percolation there has been recent progress in applying the ideas of Yang-Lee theory to other nonequilibrium phase transitions, see Ref. [99] for a review. Here I give a brief summary of the main results.

When applying Yang-Lee theory to nonequilibrium systems, the general strategy is to identify a suitable quantity that plays the role of the partition function in equilibrium. In Ref. [116] this quantity is denoted as effective partition function (EPF). The EPF is investigated depending on a complex control parameter and the zeros provide information about possible phase transitions. For directed percolation, which is a *nonintegrable* process without conservation of the particle number, it was shown above that the survival probability is an appropriate EPF. For *integrable* models it was shown [99, 116–120] that the normalization $\tilde{Z}$ plays the role of a partition function. $\tilde{Z}$ normalizes the steady state weights $f(\mathcal{C})$ of configurations $\mathcal{C}$ of the system. In the canonical equilibrium ensemble f is given by the

Boltzmann weight $e^{-\beta\mathcal{H}(\mathcal{C})}$ where $\mathcal{H}(\mathcal{C})$ is the energy of configuration $\mathcal{C}$. In this case $\tilde{Z}$ and the equilibrium partition function coincide. $\tilde{Z}$ is defined as

$$\tilde{Z} = \sum_{\mathcal{C}} f(\mathcal{C}) \tag{5.25}$$

such that

$$P(\mathcal{C}) = f(\mathcal{C})/\tilde{Z} \tag{5.26}$$

is the steady state probability distribution. To obtain $\tilde{Z}$ one has to calculate the steady state weights f, which can be written as polynomials of the elementary transition rates that define the dynamics of the system [117]. Generalizing the transition rates to the complex plane, one can identify the complex zeros of $\tilde{Z}$ as indicators for a phase transition. This method has proven to reveal important information about the existence and the nature of phase transitions [99, 116–120] (see below).

In nonequilibrium steady states, $\tilde{Z}$ normalizes the steady state probability distribution, Eq. (5.26), which is exactly what the partition function does in equilibrium systems. Moreover, there is also an additional argument why one can expect $\tilde{Z}$ to be an appropriate EPF [14, 99, 121]. One can show that it is possible to express $\tilde{Z}$ as

$$\tilde{Z} = \prod_{\lambda_i \neq 0} (-\lambda_i) \tag{5.27}$$

in terms of the λ_i eigenvalues of the transition matrix W (see Sec. 2.1). Each eigenvalue λ_i is associated with a 'mode' of the stochastic process that decays exponentially with a timescale $\tau_i{=}1/|\mathrm{Re}\lambda_i|$, with the real part $\mathrm{Re}\lambda_i$ of λ_i. Assume that there is a single steady state. Then there is one eigenvalue equal to zero, corresponding to an infinite decay time of the steady state. Note that this eigenvalue is not included in the product in Eq. (5.27). Approaching a phase transition, one expects diverging time scales: near first-order transitions one observes metastable, i.e., long-lived states, whereas the correlation time diverges at continuous phase transitions. According to Eq. (5.27) diverging time scales imply that $\tilde{Z}$ approaches zero. Hence, one expects that the zeros of $\tilde{Z}$ provide information about phase transitions of the underlying model.

In fact, this method has successfully been applied to integrable models where the normalization $\tilde{Z}$ is known. Examples include driven diffusive systems [117–119], as well as reaction diffusion models [120]. In Ref. [116] this approach was successfully used to describe the phase transition in an urn

model for the separation of sand. However, in contrast to previous studies (including the investigation presented in SEC. 5.2) in REF. [116] the EPF was investigated depending on a *size-dependent* control parameter. Note that the zeros for these integrable models are located on well-defined curves. Furthermore, the zeros approach the critical points on *single* 'trajectories' which differs significantly from the behavior reported in SEC. 5.2. This is another support for the conjecture that the irregular distribution of zeros and the fact that *many* trajectories approach the critical point may be viewed as a sign of the nonintegrability of DP (see SEC. 4.2.7).

5.5 Summary and outlook

In this chapter the applicability of Yang-Lee theory to nonequilibrium phase transitions was investigated with a focus on the absorbing-state phase transition of directed percolation.

In SEC. 5.1 I introduced the main concepts of Yang-Lee theory in equilibrium statistical mechanics. There, one studies the complex zeros of the partition function, depending on a generalized complex intensive variable, such as the temperature or an external magnetic field. For systems that exhibit a phase transition, in the thermodynamic limit the complex zeros accumulate at a point on the physically accessible real axis, by this generating nonanalyticities in thermodynamic quantities and inducing a phase transition. The accumulation point of the zeros marks the transition point.

In SEC. 5.2 the concepts of Yang-Lee theory were transferred to the absorbing-state phase transition of DP. This was done by studying the complex zeros of the survival probability $P_{\mathrm{s}}(t)$, depending on the generalized complex percolation probability p. It was argued that in the context of Yang-Lee theory $P_{\mathrm{s}}(t)$ might play a similar role as the partition function in equilibrium statistical mechanics. The zeros of $P_{\mathrm{s}}(t)$ have been studied for directed bond and directed site percolation on a tilted square lattice in 1+1 dimensions for times up to t=15. The main result of this chapter is that it is indeed possible to apply the ideas of Yang-Lee theory to the phase transition of DP. Similar to the behavior of partition function zeros, the zeros of $P_{\mathrm{s}}(t)$ approach the critical point with increasing time which corresponds to increasing system size. However, in contrast to what is usually observed for integrable models, the zeros exhibit a rather irregular distribution. In particular, they approach the critical point on *many* 'trajectories'. This might be a further indication of the nonintegrability of DP. Moreover,

applying scaling arguments, one finds a relation between the distance $d(t)$ (between the zeros and the critical point) and the critical exponent for the temporal correlation length $\nu_{\parallel}$. This relation was confirmed by the numerical data. It was possible to extract the value of $\nu_{\parallel}$ from the distribution of zeros. Hence, not only the existence of a phase transition is encoded in the distribution of zeros of $P_{\mathrm{s}}(t)$ but also *universal* properties of directed percolation.

Analytical results concerning the survival probability of directed bond percolation were derived in Sec. 5.3. More precisely, first it was shown that there are certain non-trivial points where $P_{\mathrm{s}}(t)$ can be calculated *exactly* for all times. Though these points are located outside the physically accessible region, their existence may be helpful for further investigations of the survival probability. Thereafter, an expression for the first coefficients of the polynomials $P_{\mathrm{s}}(t)$ in the limit $t\to\infty$ was given, which made it possible to derive an analytical expression for $P_{\mathrm{s}}(t)$ which serves as an approximation for p close to $p=0$.

A summary of applications of Yang-Lee theory to other nonequilibrium phase transitions was given in Sec. 5.4. It was reported that for integrable models the normalization $\tilde{Z}$ of the steady state weights plays the role of the partition function. Examples were given where this approach has been successfully applied.

In conclusion, the results of Sec. 5.2 and the summary in Sec. 5.4 show that the concepts of Yang-Lee theory are not restricted to thermodynamic equilibrium. The 'Yang-Lee scenario' of complex zeros approaching a phase transition point can be applied to nonequilibrium phase transitions, as well. Furthermore, as in equilibrium statistical mechanics, it is possible to relate the distribution of zeros to other important quantities such as the nature of the transition or critical exponents. These are important results since they provide the possibility to investigate nonequilibrium phase transitions from a new point of view, which may be helpful for models unyielding to treatment with other methods. Similar to the equilibrium case, the Yang-Lee theory in nonequilibrium systems relies mainly on specific properties of certain models. Therefore, the development of more general (and more rigorous) arguments is desirable. Moreover, compared to the equilibrium case, there are still few investigations on Yang-Lee zeros in nonequilibrium models. Hence, it would be interesting to investigate other nonequilibrium models with this method, in order to explore the features of complex zeros of the EPF (effective partition function, see Sec. 5.4) for different models more

systematically. In this context I want to stress the question if it is possible to interpret the distribution of zeros as a fingerprint for the integrability or nonintegrability of a model, as was conjectured in Sec. 5.2. Another important point is to investigate the role of the survival probability as an appropriate EPF for DP in more detail. Since the survival probability is rather the order parameter than a partition function, it is less clear why $P_{\mathrm{s}}(t)$ can be taken as the EPF for DP, compared to the case of taking $\tilde{Z}$ as EPF for integrable models.

Chapter 6

Spreading in media with long-time memory

A fascinating subject that is suitable to be studied by stochastic spreading processes, is the modeling of infectious diseases. Activity is interpreted as disease and lattice sites represent individuals that may be healthy (inactive) or infected (active). The probabilistic dynamics mimic the competition of infectious spreading and recovery. Depending on the rates for infection and recovery the disease may either spread over the entire population or disappear after some time. Apart from the relevance of stochastic spreading processes for statistical physics far from equilibrium, such models are therefore interesting from the point of view of theoretical biology [49, 50] as well. In fact, the contact process (CP), which is a popular realization of the directed percolation universality class, was originally introduced as a a model for *epidemic spreading* [92]. Since generally DP describes the spreading of some nonconserved agent in a medium *without* long-time memory, i.e., it is a Markov process (see Sec. 4.2.2), DP describes epidemic spreading without immunization. However, in epidemic spreading as well as in many other natural spreading phenomena memory effects are important. The spreading agent may change its environment in such a way that the dynamics of the process differ between regions that are invaded for the first time and those that have already been visited in the past. In epidemic spreading, for instance, immunization (or weakening) may cause that the susceptibility to infections decreases (increases) after the first infection. Another well-known example is a forest fire which cannot spread in regions that have already been burned. This chapter deals with stochastic spreading processes that are *non-Markovian* and model memory effects. In the following I will mainly adopt the terminology of epidemic processes.

If one changes the dynamics of DP to include *perfect* immunization, i.e., each individual can be infected only once, one obtains the so-called 'general epidemic process' (GEP) [49, 50, 53] which is discussed in SEC. 6.1. In this case, the absorbing-state phase transition between survival and extinction of an epidemic belongs no longer to the universality class of DP but to that of dynamical percolation (DyP) [77]. In SEC. 6.2, the main subject of the present chapter is addressed, which is the investigation of an epidemic process with *finite* immunization. This process is controled by two probabilities, namely, for first infections (p_0) and reinfections (p). When the two probabilities are equal, the model reduces to directed percolation (DP), while for perfect immunization one obtains the general epidemic process (GEP). First, known results for spatial dimensions d=1,2 are summarized before I turn to the main issue, the influence of immunization near the DP point in high dimensions $d\geq 2$. It is argued that the clusters of immune sites are compact for $d\leq 4$. This observation implies that a recently introduced scaling argument, suggesting a stretched exponential decay of the survival probability for $p=p_c$, $p_0 \ll p_c$ in one spatial dimension [122], should apply in any dimension $d\leq 3$ and maybe for $d=4$ as well. Here, p_c denotes the critical threshold for directed percolation. Moreover, it is shown that the phase transition line, connecting the critical points of directed percolation and of dynamical percolation, terminates in the critical point of DP with vanishing slope for $d<4$ and with finite slope for $d\geq 4$. Furthermore, an exponent is identified for the temporal correlation length for the case of $p=p_c$ and $p_0=p_c-\epsilon$, $\epsilon \ll 1$, which is different from the exponent $\nu_\parallel$ of directed percolation. Numerical estimates of several critical parameters and exponents are improved as well, especially for dynamical percolation in d=3,4,5.

Note also that more recently epidemic spreading with immunization appeared in a different context. Studying systems with infinitely many absorbing states, such as the non-diffusive pair contact process [123, 124], it was conjectured that these models are described by the same type of field theory as the model discussed in SEC. 6.2 [125, 126]. Roughly speaking, the frozen absorbing configurations generated by the process provide a local memory of activity in the past which effectively acts in the same way as immunization (or weakening). Meanwhile this conjecture is widely accepted, although some questions concerning the upper critical dimension are still debated [66, 127].

6.1 Dynamical percolation and the general epidemic process

Consider a model for epidemic spreading where individuals live on the sites of a d-dimensional simple cubic lattice while the bonds between sites represent contacts between individuals. At a given time, individuals are either infected or healthy. An infected individual may transmit the disease to each of its $2d$ nearest neighbors with probability p_0, provided the target site has never been infected before. Otherwise, an infection is not possible due to immunization of the individual, i.e, the reinfection probability is p=0. Infected sites recover after a single time step. This process is known as the 'general epidemic process' (GEP). Another possible interpretation is the growth of some population feeding from the environment, where additional food is not supplied once it has been exhausted. An example are mushrooms growing in 'fairy rings'. The mushrooms feed from the soil and leave exhausted regions behind, therefore typically growing in circular patterns.

Clearly, the GEP cannot create a stationary density since the disease can only spread in those parts of the system which have not been infected before. Nevertheless, in spatial dimensions $d\geq 2$, infinite spreading from a single infected site in a non-immune environment is still possible, provided that the susceptibility to primary infections is sufficiently large, i.e., $p_0 > p_0^{\mathrm{c}}$. In this case, activity propagates as a front, leaving a cluster of immune sites behind. At the threshold, $p_0 = p_0^{\mathrm{c}}$, the cluster of immune sites is fractal, as illustrated in Fig. 6.1. The transition between survival and extinction of the spreading agent is described by the critical behavior of *dynamical percolation* (DyP) [77]. In isotropic percolation (see Sec. 4.2.1) one assumes that the states of the bonds (permeable/blocked) are a mere lattice property, determined from the very beginning. Contrarily, in the GEP one assumes that the state of a bond between two sites is established only in the moment when the infection is to pass across it. However, since infections can pass only once through any bond, this is mathematically no difference to the case of isotropic percolation. Hence, the *static* properties of the GEP, i.e., the scaling properties of the distribution of immune individuals *after* an epidemic, are described by isotropic percolation. Therefore the GEP can be used as a dynamic procedure to grow isotropic percolation clusters. Note that the temporal evolution of the GEP cannot be described in terms of isotropic percolation. Tab. 6.1 summarizes critical thresholds p_0^{c} and critical exponents for the time dependent properties $P_{\mathrm{s}}(t)$, $N(t)$ and $R^2(t)$, see Eq. (4.10). The

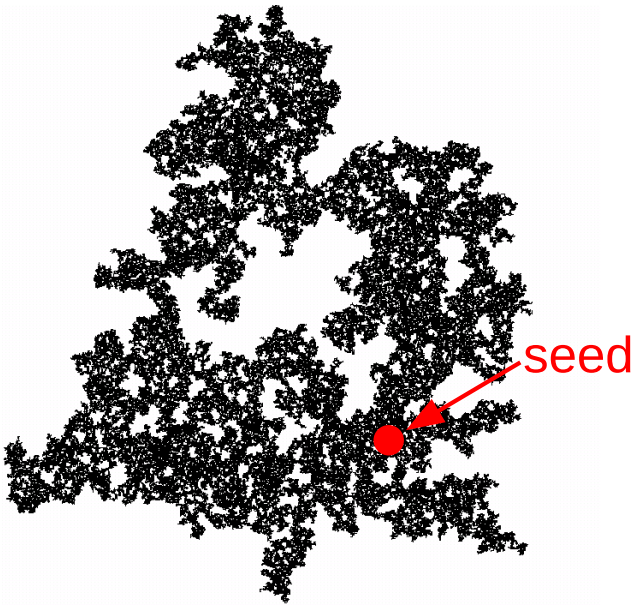

FIGURE 6.1: *Snapshot of a critical GEP-cluster grown from an active seed on a square lattice. The black region shows the immune domain after 1350 time steps. The red circle marks the location of the seed.*

values for $3 \leq d \leq 5$ were obtained during the studies presented in SEC. 6.2. To my knowledge, no numerical estimates for critical exponents for the GEP in d=4,5 have been published previously. Moreover, the values presented for d=3 are more precise than those published previously [128]. The estimate of $\theta = 0.488(7)$ is incompatible with the value of $\theta = 0.536$ reported in REF. [128]. However, in that case, θ was not directly measured but obtained via scaling relations, which presumably is the reason for the considerable difference between the two estimates. The upper critical dimension of DyP is d_c^{DyP}=6 [129]. As DyP does not create a stationary density of active sites in the steady state, it does not obey the generalized hyperscaling relation, EQ. (4.11). Instead, the hyperscaling relation for DyP reads [63]

$$\theta = d/z - 2\delta - 1 \ . \tag{6.1}$$

The estimates given in TAB. 6.1 are compatible with EQ. (6.1). For d=3,4,5 one obtains

$$\theta = d/z - 2\delta - 1 = \begin{cases} 0.49(2) & \text{for } d = 3 \ , \\ 0.30(3) & \text{for } d = 4 \ , \\ 0.14(4) & \text{for } d = 5 \ . \end{cases} \tag{6.2}$$

d	p_0^c	δ	θ	z	Ref.
2	$1/2$ †	0.092	0.586	1.1295	[128]‡
3	0.2488125(25)	0.346(6)	0.488(7)	1.375(5)	[81]
4	0.1601310(10)	0.595(8)	0.30(1)	1.605(9)	[81]
5	0.1181718(2)	0.806(12)	0.134(10)	1.815(10)	[81]
6	0.0942019(6)	1*	0*	2*	[130]

Table 6.1: *Numerical estimates for the GEP on a simple d-dimensional cubic lattice. For d=6, * denotes that the mean-field behavior is subjected to logarithmic corrections.* † *Exact result, taken from* Ref. *[77].* ‡ *Uncertainties are in the last digit. For d=1 the transition is shifted to p_c=1.*

For a general review of isotropic percolation I refer the interested reader to Ref. [77]. A numerical investigation of the GEP can be found in Ref. [53] and a field-theoretic treatment in Ref. [129].

6.2 Epidemic process with finite immunization (EPFI)

As an immediate generalization that interpolates between the GEP and DP, one may consider an epidemic process in which the strength of immunization can be varied [131]. For example, the initial susceptibility to infections p_0 may be locally set to a different value p, when the first infection is encountered. In the following, I shall denote this process as epidemic process with finite immunization, which for convenience is abbreviated as EPFI. The phase diagram of the EPFI in two spatial dimensions was studied in Ref. [51]. As shown in Fig. 6.2, it comprises three different phases, including the GEP (p=0) and DP (p=p_0) as special cases.

The horizontal phase transition line in Fig. 6.2 can be explained as follows. Obviously, when starting from a fully occupied lattice, all sites become immediately immune so that the infection rate is everywhere equal to p. Trivially, the dynamics is then precisely that of a DP process controled by p. This gives rise to a DP transition at p=p_c, independent of p_0, where p_c denotes the critical value of an ordinary DP process. However, starting

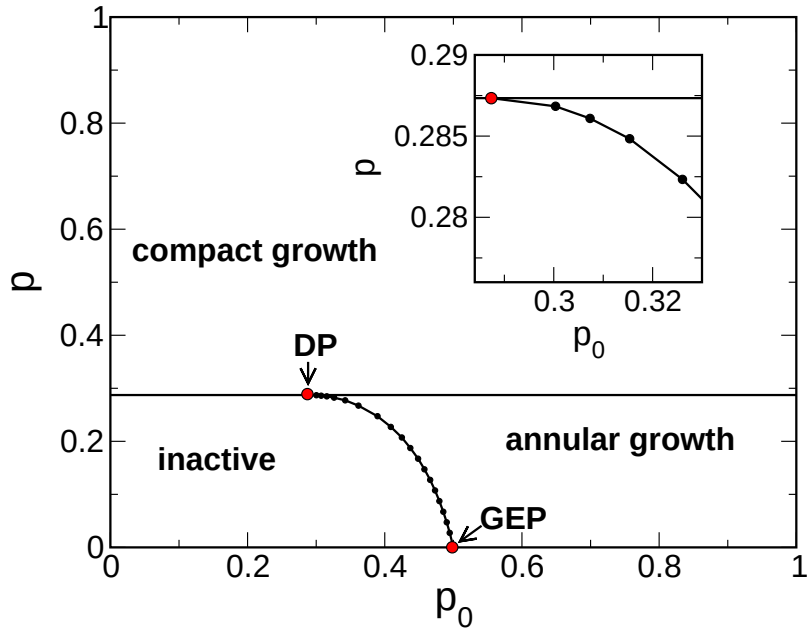

FIGURE 6.2: *Phase diagram of the epidemic process with finite immunization on a square lattice in 2+1 dimensions. p_0 denotes the primary infection probability and p the reinfection probability. The inset shows the vicinity of the DP point.*

with a localized infected seed in a non-immune environment, the situation is more subtle, though the horizontal line still exists. For example, slightly above the critical line, i.e. for $p{=}p_c{+}\epsilon$ with $\epsilon{\ll}1$, the interior of a surviving cluster is essentially dominated by an ordinary supercritical DP process. Since such a DP process is characterized on large scales by a finite density of active sites, there will be a finite chance for the process to survive in the limit $t{\to}\infty$ [51].

The situation below the horizontal line ($p{<}p_c$) is different. In at least two-dimensional systems this part of the phase diagram displays *two* distinct phases, namely, an absorbing phase, where the process stops after some time, and a phase of annular growth, where an expanding front of high activity survives with finite probability. Performing a field-theoretic renormalization group study close to the upper critical dimension of DyP, $d_c^{\mathrm{DyP}}{=}6$, and computing the corresponding critical exponents, it was shown that the critical behavior along the line connecting the GEP and the DP point in FIG. 6.2, is that of DyP [129]. In this sense immunization is

a relevant perturbation, driving the system away from the DP point in FIG. 6.2 towards the GEP. (I note that in the case of several competing infections with immunization, one observes a crossover back to DP [52] which will be discussed in CHAP. 7. Another four-state generalization leads to an interesting tricritical phenomenon belonging to a different universality class [22]).

While the mentioned field-theoretic results explain the transition line between the GEP and the DP point close to d_c^{DyP}=6, the critical properties along the horizontal line and in the vicinity of the DP point are less well understood. Simulating the Langevin equation of the EPFI at critical reinfection rate (corresponding to the horizontal line in Fig. 6.2) in 1+1 dimensions starting with a localized seed, López and Muñoz initially expected continuously varying exponents [132], but refined simulations and approximations suggest that there is no power-law scaling. Instead, the activity was found to decay as a stretched exponential in 1+1 dimensions [51, 122].

6.2.1 Monte Carlo simulations

Let me briefly describe the Monte Carlo (MC) simulations that are applied in the following to obtain numerical results. I perform MC simulations of the epidemic process with finite immunization on a simple d-dimensional cubic lattice using the model of REF. [51] generalized to arbitrary dimensions. The process is defined such that it reduces to directed *bond* percolation for p_0=p, and to dynamical *bond* percolation for p=0. In particular, an active lattice site i at time t may activate each of its d nearest neighbors, denoted as j, at the next discrete time step t+1. If neighbor j has never been active before, activity is transmitted from site i to site j with the primary infection probability p_0. Contrarily, if site j has been active at least once in the past the reinfection probability is given by p. Each site stays active only for one time step.

The process is initialized with an active seed at the origin at time t=0 in a non-immune environment. Each run is stopped either when the process dies out or when it reaches a preset maximum time. I average over many runs with different realizations of randomness. The lattice is always chosen large enough so that the process never reaches its boundary. Hence, finite size effects are eliminated. As usual in 'seed simulations' I measure the survival probability $P_{\mathrm{s}}(t)$ that the process survives at least up to time t, the number of active sites averaged over all runs $N(t)$, and the mean square spreading from the origin $R^2(t)$ averaged over surviving runs. According to EQ. (4.10)

at criticality these quantities obey power-laws. This behavior is observed for critical DP as well as for critical DyP. Of course, the exponents in EQ. (4.10) are generally different in both cases. In addition, I also measure the number of primary infections n_p (see below).

From a technical point of view, the simulations for $d \geq 3$ are based on the routine presented in REF. [130]. Lattice sites are labeled by 64-bit-long integers. I do not initialize storage for a whole L^d lattice since for high dimensions it is only possible to simulate small lateral lattice sizes L with this method. Instead I use lists to store the individual positions of active and immune sites. To perform an update from t to $t+1$ the algorithm goes through all active sites at time t and activates their neighbors at time $t+1$ with probability p_0 or p, respectively. The activated sites are stored in a list while the formerly active sites recover. In the case of a first infection, the site is added to the list of immune sites. In order to efficiently check whether a site is immune or not, and whether it has already been activated during the actual update step, a hashing algorithm is used as described in REF. [130]. Contrarily, the simulations for d=1,2 are carried out in the usual way where one initializes storage for a whole lattice. However, in this case I apply bit-coding, i.e., a single 64-bit-long integer stores the states of 64 lattice sites (active/inactive or immune/non-immune).

6.2.2 Phenomenological properties

Let me first consider the phenomenological properties of the process near the DP point, where the effect of immunization is small. Since the DP point itself is a critical DP process, the question arises how the upper critical dimension of DP influences the generated cluster of immune sites. As a conjecture, I propose that the generated cluster of immune sites at the DP point is *compact* in $d<4$ dimensions (in the sense that its fractal dimension is d), while in higher dimensions $d>4$ it is not. At the DP point $p=p_0=p_\mathrm{c}$ the influence of immunization vanishes so that the cluster of immune sites is merely the past activity of a critical DP process projected onto space. In other words, when looking through a critical DP cluster along the temporal axis I expect its appearance to be compact in $d<4$. Obviously, in d=1 the cluster of visited sites is compact by definition so that the conjecture is correct. In dimensions d=2,3 the statement is non-trivial. In fact, plotting the projection of a typical cluster in d=2 dimensions one obtains a compact object, as shown in FIG. 6.3. It is instructive to compare the compact cluster in FIG. 6.3 with the fractal region visited by the critical GEP in FIG. 6.1.

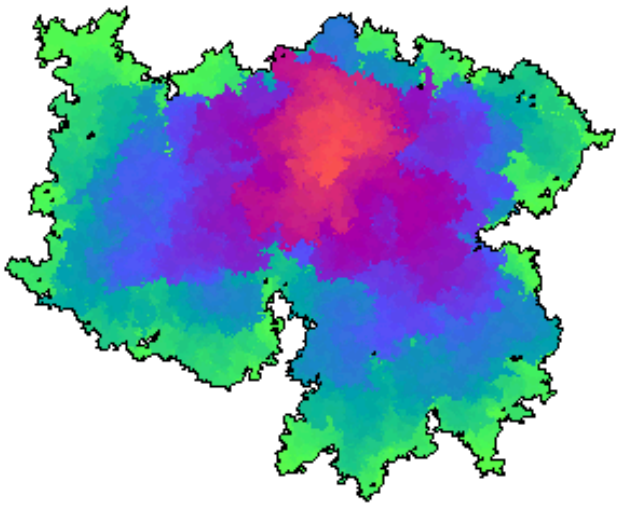

FIGURE 6.3: *Typical cluster of immune sites generated by the EPFI in 2+1 dimensions at the DP point after 2048 updates. The colors represent linearly the time at which the sites were visited for the first time. The black line marks the final boundary of the cluster.*

The above conjecture can be supported numerically as follows. Assuming compactness, the number of immune sites in a surviving run should grow linearly with the volume $\xi_\perp^d$, where $\xi_\perp \sim t^{1/z}$ is the spatial correlation length and $z=\nu_\parallel/\nu_\perp$ is the dynamical exponent of DP (see SEC. 4.1.1). Averaging over all runs, the volume has to be multiplied with the survival probability $P_\mathrm{s}(t) \sim t^{-\delta}$, where $\delta=\beta/\nu_\parallel$, and hence, the average number of immune sites $I(t)$ increases as

$$I(t) \sim t^{d/z-\delta} \ . \tag{6.3}$$

This implies that the number of *primary* infections n_p scales as the derivative of $I(t)$, i.e.,

$$n_\mathrm{p}(t) \sim t^{d/z-\delta-1} \ . \tag{6.4}$$

As shown in FIG. 6.4 by numerical simulations, in $d=1, 2$ and 3 dimensions this quantity scales indeed according to EQ. (6.4), supporting that the generated clusters of immune sites are compact.

For $d=4$ the data still exhibits a slight curvature which is presumably due to logarithmic corrections [67, 83] that affect the mean-field behavior

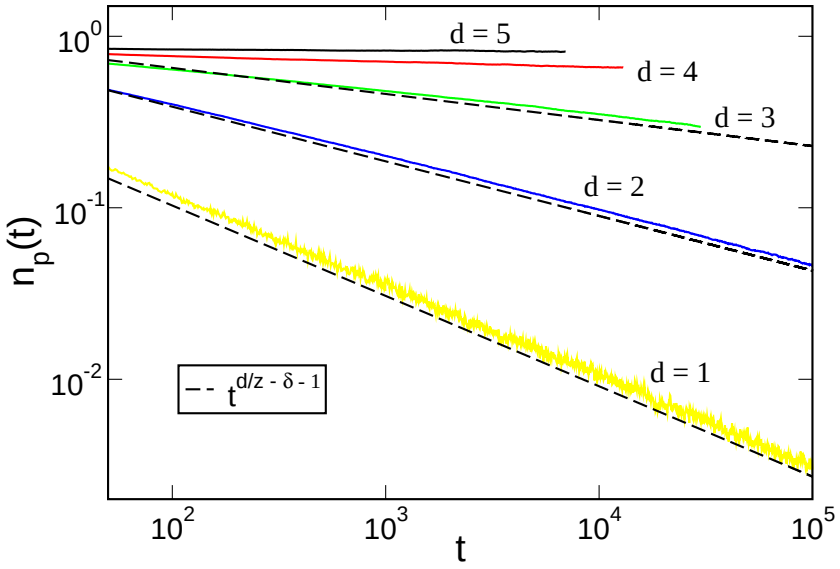

FIGURE 6.4: *Double logarithmic plot of the number of primary infections versus time, at the DP point for various dimensions. For comparison the power-law behavior predicted by* EQ. *(6.4) is shown by the dashed lines for* d=1,2,3. *For* d=4 *the mean-field prediction of* EQ. *(6.4) is* $n_{\rm p}(t)$=*const.*

($n_{\rm p}$=const) at the upper critical dimension of DP, $d_{\rm c}^{\rm DP}$=4. As usual, also for d>$d_{\rm c}^{\rm DP}$ one observes mean-field behavior and thus, I expect the resulting cluster of immune sites to be non-compact.

It is also possible to support the conjecture by a scaling argument. Obviously $I(t)$ cannot be larger than the integrated past activity $\int_0^t dt' N(t') \sim t^{1+\theta}$, see EQ. (4.10), leading to the inequality

$$d/z - \delta \leq \theta + 1 \ . \tag{6.5}$$

as a necessary condition for compactness. In d<4 dimensions, the initial-slip exponent θ is given by the hyperscaling relation, EQ. (4.15),

$$\theta = d/z - 2\delta$$

so that the inequality reduces to $\delta \leq 1$, which is indeed satisfied in d<4 (see TAB. 4.2). At the upper critical dimension of DP, $d_{\rm c}^{\rm DP}$=4, taking the mean-field exponents θ=0, z=2, and δ=1, the inequality EQ. (6.5) is sharply satisfied while it is violated above four dimensions. Hence, one can conclude that in d>4 dimensions the generated cluster is no longer compact.

To deal with the question whether clusters of immune sites in systems *at* the upper critical dimension of DP, $d_c^{DP}=4$, are still compact, it is worthwhile to compare the situation with a simple random walk whose upper critical dimension is $d_c^{RW}=2$. The random walk is *recurrent* in $d = 1, 2$ while it is *transient* for $d \geq 3$ [37]. This means that the probability $F(t)$ to visit a given site at least once until time t tends to 1 in the limit $t\to\infty$ for d=1,2 while it tends to a constant $c<1$ for $d\geq 3$. Therefore, the region visited by the random walker is compact in $d\leq 2$ whereas it is not in $d\geq 3$. However, for d=2 the probability $1-F(t)$ that the site has not yet been visited decreases asymptotically as $1-F(t)\sim(\ln t)^{-1}$ in contrast to algebraic behavior in d=1, where $1-F(t)\sim t^{-1/2}$. This implies that in d=2 compactness is reached only slowly and I refer to this as *asymptotically* compact. Therefore, in d=2 and finite time the cluster of visited sites is highly non-compact at its boundaries and differs significantly from the one shown in Fig. 6.3. Using this analogy, it is near at hand to speculate that the same happens in a critical DP process. Thus, I expect the cluster of visited sites to be compact at the upper critical dimension $d_c^{DP}=4$ as well. However, in this case compactness should be reached considerably slower than for $d<4$, i.e., I expect the clusters to be *asymptotically* compact.

The observed compactness in low dimensions leads to an important consequence regarding the critical behavior along the horizontal line in Fig. 6.2, as it allows the results of Ref. [122] obtained in d=1 to be generalized to 2 and 3 dimensions. In Ref. [122] the expansion of an immune region in one spatial dimension was studied in the limit of a very small probability of first infections $p_0\to 0$. Using a quasi-static approximation, it was shown that the survival probability does *not* obey a power law, instead it decays as a stretched exponential

$$P_s(t) \propto \exp\left(-Ap_0^{-\alpha}t^{1-\alpha}\right) \ , \tag{6.6}$$

giving rise to a *finite* survival time $T\sim p_0^{\alpha/(1-\alpha)}$. Here $\alpha=\nu_\parallel/(\nu_\perp+\beta_s)$ with β_s being the order parameter exponent next to a planar absorbing surface [133]. The main assumption made in this approximation is the compactness of the immune domain, wherefore the analysis had been restricted to d=1. Because of the observed compactness, the same arguments can be applied in two and three dimensions so that the formula Eq. (6.6) should be valid in these cases as well. Inserting the known values for β_s [133] one obtains $\alpha\simeq 0.947$ in $1d$ and $\alpha\simeq 0.72$ in $2d$ (so far there are no estimates of β_s in $3d$). Whether Eq. (6.6) is still valid at the upper critical dimension of DP where α would be 1/2, is not yet clear since in this case I expect the immune region to be only asymptotically compact.

Another important consequence concerns the ratio of first infections and reinfections. In $d<4$ dimensions the average number of first infections $n_p(t)$ (controled by the parameter p_0) decreases according to Eq. (6.4) while the average number of reinfections (controled by the parameter p) increases as t^θ with $\theta>0$. Thus, after sufficiently long time the parameter p controlling reinfections will have a much larger influence than the parameter p_0. As a consequence the curved phase transition line, which may be thought of as describing a situation where p and p_0 balance each other, terminates in the DP point horizontally, i.e., with zero slope. In $d\geq 4$ dimensions, primary infections and reinfections show the same scaling behavior (for $d=4$ probably affected by logarithmic corrections), and therefore one expects the transition line to terminate with a non-vanishing slope. I will later come back to this question.

6.2.3 Scaling properties

The previous phenomenological arguments suggested that the behavior of the model in $d<4$ dimensions differs significantly from the behavior above 4 dimensions. This difference becomes also obvious when studying the corresponding Langevin equations (see Secs. 2.2.2, 2.4 and 4.2.3).

According to Refs. [122, 129] the Langevin equation for the epidemic process with finite immunization reads

$$\begin{aligned} \frac{\partial}{\partial t}\rho(\mathbf{x},t) &= a\rho(\mathbf{x},t) - b\rho^2(\mathbf{x},t) + D\nabla\rho(\mathbf{x},t) + \xi(\mathbf{x},t) \\ &\quad +\lambda\,\rho(\mathbf{x},t)\,\exp\left(-w\int_0^t d\tau\,\rho(\mathbf{x},\tau)\right)\,, \end{aligned} \tag{6.7}$$

where $\xi(\mathbf{x},t)$ with $\langle\xi(\mathbf{x},t)\rangle=0$ represents a density-dependent Gaussian noise with the correlations

$$\langle\xi(\mathbf{x},t)\xi(\mathbf{x}',t')\rangle = \Gamma\,\rho(\mathbf{x},t)\,\delta^d(\mathbf{x}-\mathbf{x}')\,\delta(t-t')\,. \tag{6.8}$$

It consists of the usual Langevin equation for DP, Eq. (4.16), plus an exponential term describing the effect of immunization. Here the exponential function can be thought of as a switch: Initially, the integral is zero and hence the coefficient of the linear contributions in $\rho(\mathbf{x},t)$ is $a+\lambda$, representing as bare parameters the reduced rate for first infections p_0-p_c. However, when the integrated past activity exceeds $1/w$, the exponential function decreases rapidly so that the additional term is essentially switched

off. Roughly speaking, in a continuous description the parameter w is needed in order to specify a threshold telling us how much activity has to be accumulated at a given site in order to declare it as immune. Once the exponential term is switched off, the linear term is controled by the coefficient a which represents the reduced reinfection rate $p-p_c$. In most lattice models, sites become immune after a single infection, hence the parameter w is of the order 1 while $\lambda \sim p_0 - p$ controls the strength of immunization.

Rescaling the DP Langevin equation by

$$\mathbf{x} \to b\mathbf{x} \quad t \to b^z t \quad \rho \to b^{-\chi}\rho \tag{6.9}$$

with a scaling parameter b and the exponents $z=\nu_\parallel/\nu_\perp$ and $\chi=\beta/\nu_\perp$, one immediately recognizes that simple scaling invariance at the upper critical dimension $d_c^{\rm DP}=4$ can only be established if $z=\chi=2$ and $a=0$, the latter representing the critical point at the mean field level, see Eq. (4.18). Regarding the exponential term, scaling invariance requires the argument of the exponential function and the exponential function itself to be dimensionless, hence the coefficient λ and w have to be rescaled as

$$\begin{aligned} \lambda &\to b^{-y_\lambda}\lambda \\ w &\to b^{-y_w} w \ , \end{aligned} \tag{6.10}$$

where $y_\lambda=2$ and $y_w=0$. More generally, it can be shown by a field-theoretic calculation [122] that in $d\leq 4$ dimensions the two exponents are given by

$$y_\lambda = \frac{1}{\nu_\perp} \ , \qquad y_w = \frac{\nu_\parallel - \beta}{\nu_\perp} \ . \tag{6.11}$$

As y_w and y_λ are positive, the exponential term for immunization is relevant in $d\leq 4$ dimensions. Expanding the exponential function as a Taylor series, the resulting terms would be equally relevant in $d=4$ and *increasingly relevant* in $d<4$ dimensions. Therefore, in $d\leq 4$ dimensions a Taylor expansion of the exponential function in Eq. (6.7) is meaningless in the renormalization group sense, instead it has to be kept in as a whole. This circumstance is probably responsible for the observed non-universality along the horizontal line in Fig. 6.2.

In $d>4$ dimensions, however, the situation is different. Here, power counting at the upper critical dimension of DyP, $d_c^{\rm DyP}=6$, yields $y_w<0$, meaning that the relevancy of the terms in the Taylor expansion decreases. In this

case it is legitimate to carry out the Taylor expansion, keeping only the most relevant contribution. The zeroth order can always be absorbed in a redefinition of a. Thus, the most relevant contribution is the first-order term $-\lambda w\rho(\mathbf{x},t)\int_0^t d\tau\rho(\mathbf{x},\tau)$. In addition, one may drop the quadratic contribution $-b\rho^2(\mathbf{x},t)$, which is irrelevant at d_c^{DyP}=6, leading to the Langevin equation

$$\begin{aligned}\frac{\partial}{\partial t}\rho(\mathbf{x},t) &= (a+\lambda)\rho(\mathbf{x},t)+D\nabla\rho(\mathbf{x},t)+\xi(\mathbf{x},t) \\ &\quad -\lambda w\,\rho(\mathbf{x},t)\int_0^t d\tau\,\rho(\mathbf{x},\tau)\ ,\end{aligned} \tag{6.12}$$

corresponding to the field theory studied in Ref. [129]. In contrast to Eq. (6.7), the influence of immunization is effectively described by a single parameter, namely, by the product λw. Assuming y_w to be negative for any d>4, this scenario is expected to hold even in presence of fluctuation effects. Moreover, in contrast to Eq. (6.7) the parameter now appears in the prefactor of the linear term, shifting the parameter a. This suggests, in accordance with the discussion above, that at least in 4<d≤6 dimensions the reduced first infection and reinfection probability (here corresponding to λ and a) scale identically and that the phase transition line, along which the influence of a and λ is balanced, terminates with a nonzero slope in the DP point.

To summarize, one arrives at the following picture:

- In d≤4 dimensions the EPFI is described by Eq. (6.7), in which an expansion of the exponential function is not allowed. The exponential function is conjectured to produce non-universal features such as a stretched exponential decay of the survival probability, as observed in d=1 dimensions [122].
- In 4<d≤6 the process is described by Eq. (6.12). Fluctuation effects are still present and the corresponding field theory is well-defined and renormalizable [129].
- In d>6 the mean field approximation becomes valid. The system is driven to a trivial Gaussian fixed point, which is the same for the GEP and DP.

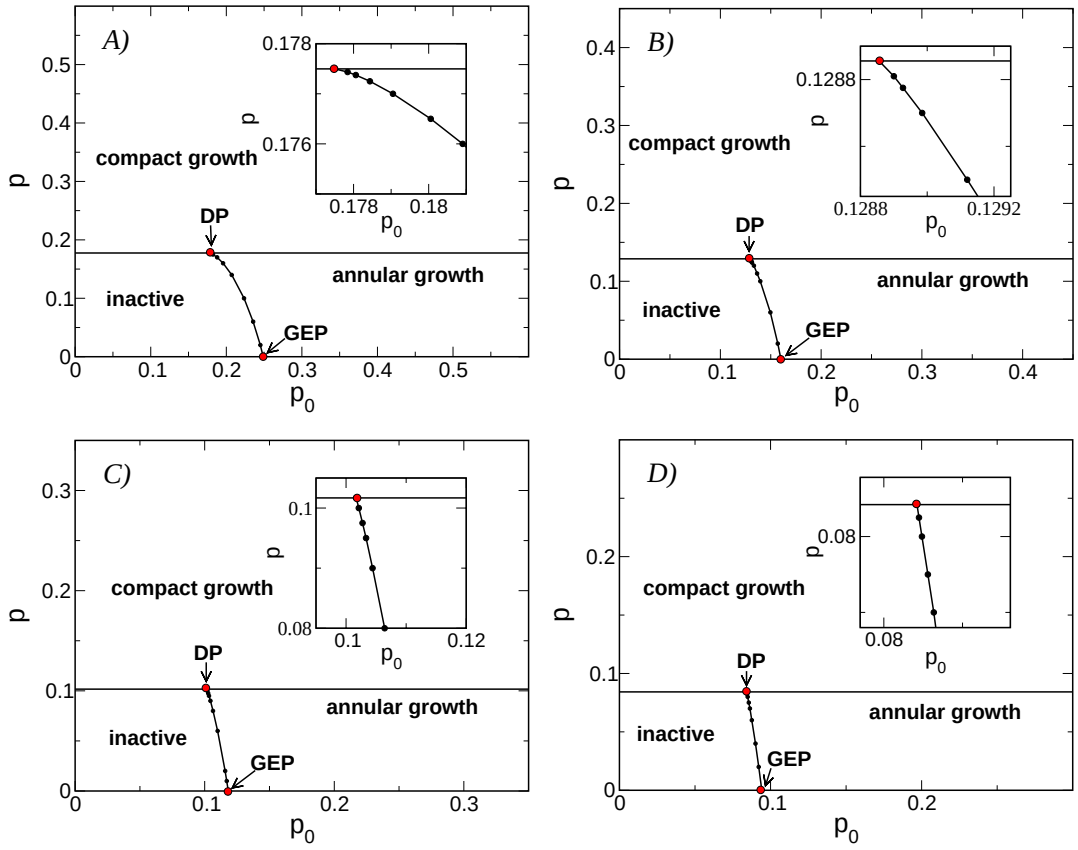

FIGURE 6.5: *Phase diagrams for the EPFI for $d = 3, 4, 5, 6$, A)–D), determined from MC simulations. The insets show the vicinity of the DP point. Circles mark the numerically determined critical points.*

6.2.4 Phase Diagrams

FIG. 6.5 presents phase diagrams of the epidemic process with finite immunization for spatial dimensions d=3,4,5,6, which were obtained from MC simulations. The horizontal lines obey p=p_c where the estimates of p_c have been determined by MC simulations as well and are given in TAB. 4.1. Additionally, this led to improved estimates for the critical spreading exponents z, δ and θ in d=3. The lines connecting the DP and the GEP point were determined as follows. First I performed spreading simulations at the critical point of the GEP, i.e., for p=0, using the critical values of bond percolation given in REF. [130]. Thereby, I estimated various critical exponents for DyP which are presented in TAB. 6.1. In order to locate the phase transition line, the fact was used that the critical behavior along this

line is that of dynamical percolation. I determined various critical points along the lines by keeping p fixed and varying p_0 until the quantities $P_s(t)$, $N(t)$ and $R^2(t)$, see Eq. (4.10), displayed the expected slope corresponding to DyP in a log-log plot.

In accordance with the predictions made above, the data indeed suggests that the curved phase transition line terminates at the DP point with vanishing slope for d=3 and with finite slope for $d\geq 4$. For d=4 this behavior is not so clear cut, which is presumably caused by logarithmic corrections at the DP point.

6.2.5 Temporal correlation length in the vicinity of the DP point

Off criticality but in the vicinity of the DP point, i.e., $p=p_c\pm\tilde{\epsilon}$, $p_0=p_c\pm\epsilon$, one initially observes the critical behavior of DP until the process eventually crosses over to a different type of behavior. This crossover takes place at a certain typical time scale $\xi_\parallel$. If $\tilde{\epsilon}\neq 0$ (moving vertically away from the DP point) one expects that asymptotically $\xi_\parallel \sim \tilde{\epsilon}^{-\nu_\parallel}$ with the critical DP exponent $\nu_\parallel$ for the temporal correlation length, see Eq. (4.4). The reason is the following. Near the DP point, for $d<4$, the process is dominated by reinfections that perform an ordinary DP process with parameter p on a compact region. It is only on the edge of the visited region where the first infection probability p_0 plays a role. Hence, the time scale associated with $\tilde{\epsilon}$ is expected to be smaller than that associated with a change ϵ of p_0. For $d\geq 4$, primary infections and reinfection show equal scaling behavior and therefore one expects both times to scale in the same way.

One is left with the question how the temporal correlation length behaves for $p=p_c$ and $p_0=p_c\pm\epsilon$ (moving horizontally away from the DP point) in $d<4$. Although I expect non-universal behavior on the horizontal line, it may nevertheless be possible to identify an exponent μ for the temporal correlation length

$$\xi_\parallel \sim \epsilon^{-\mu} \tag{6.13}$$

in the vicinity of the DP point, $\epsilon \ll 1$. In fact, as shown in Fig. 6.6, plotting $N(t)t^{-\theta}$ versus $t/\xi_\parallel$, one can produce a data collapse by tuning μ. With similar simulations in d=4,5 (not shown here) I get the estimates

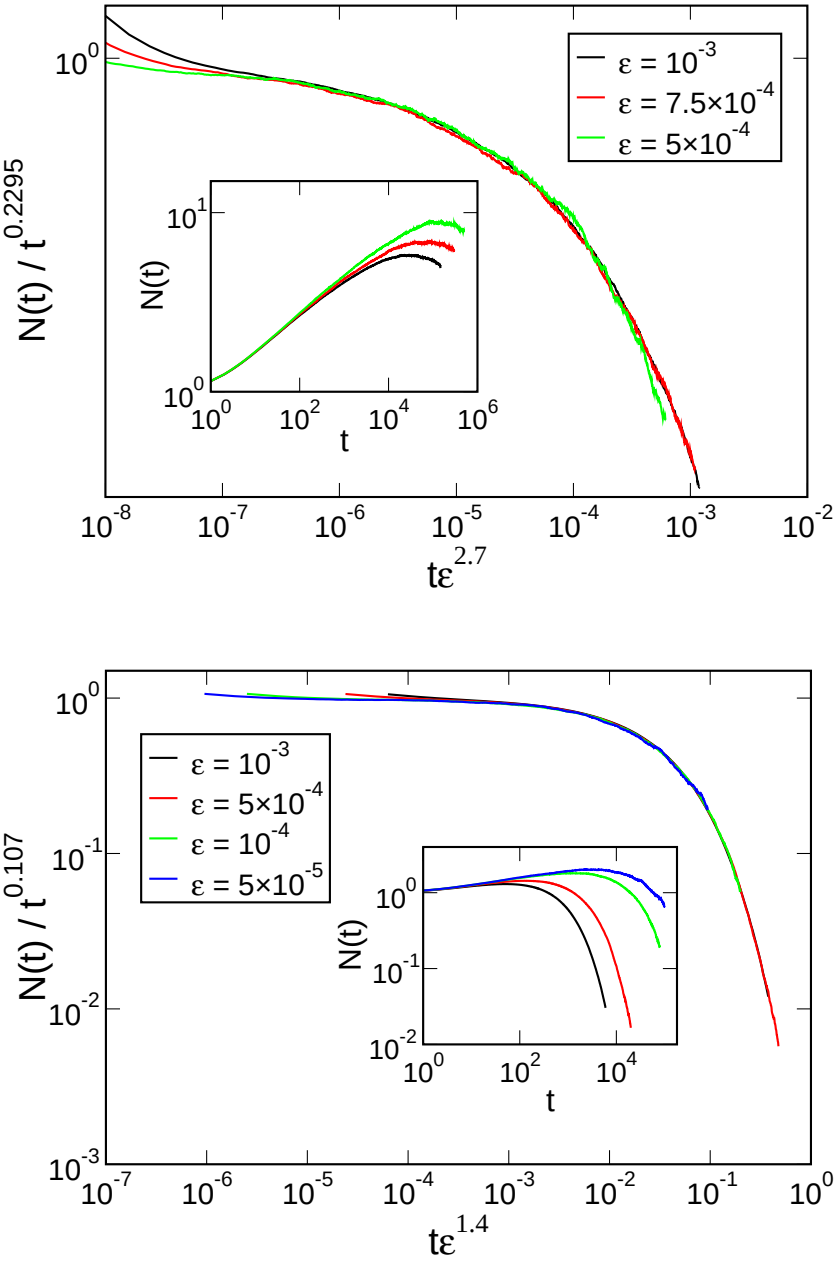

FIGURE 6.6: *Data collapses for p=p_c and p_0=p_c−ϵ for d=2 (top) and d=3 (bottom). $N(t)$ is scaled with t^θ with the values of θ from Tab. 4.2. The time is scaled with ϵ^μ such that the best data collapses were obtained. The insets show the original data.*

$$\mu = \begin{cases} 2.7(7) & \text{in } d=2 \\ 1.4(2) & \text{in } d=3 \\ 1.1(13) & \text{in } d=4 \\ 1.0(1) & \text{in } d=5\ . \end{cases} \tag{6.14}$$

Obviously, in $d<4$ the exponent μ differs from $\nu_\parallel$, see TAB. 4.2. Because of logarithmic corrections, it is likely that $\mu=1$ in $d=4$ as well. With decreasing dimension, the value of μ and therewith the simulation time increases rapidly. For this reason the estimate for $d=2$ is less precise, while simulations in $d=1$ turned out to be unreliable. However, for $d=3$ the data collapse is fairly good. In the following I present a heuristic argument for the value of μ in accordance with the numerical data.

Speculation about the value of μ : Consider first a subcritical DP process governed by the parameter $p=p_c-\epsilon$, $\epsilon\ll 1$. Initially the system behaves as if it was critical until the hostile conditions eventually lead to extinction. This happens on a time scale $\xi_\parallel\sim\epsilon^{-\nu_\parallel}$. During the active time the process produces active sites according to $N(t)\sim t^\theta$, see EQ. (4.10). Therefore, a subcritical DP process activates on the whole M sites before it dies out, where M scales as $M\sim\epsilon^{-\nu_\parallel(\theta+1)}$. Consider now the EPFI with $p=p_c$ and $p_0=p_c-\epsilon$ which dies out on a time scale $\xi_\parallel\sim\epsilon^{-\mu}$. In this case (for $d\leq 4$) one has basically a critical DP process in the compact interior region of the immune cluster and a subcritical process on the edge. According to EQ. (6.3), the integrated activity on the edge scales as $I(t)\sim t^{d/z-\delta}$. If one assumes that the critical reinfections do not introduce a time scale and that the process on the edge is subjected to the same bound as subcritical DP concerning the maximal activity, one arrives at $I\sim M$ leading to

$$\mu = \frac{z\nu_\parallel(\theta+1)}{d-\delta z}\ . \tag{6.15}$$

With the critical exponents of DP given in TAB. 4.2, EQ. (6.15) results in $\mu\approx 2.335$ for $d=2$, $\mu=1.437$ for $d=3$ and $\mu=1$ for $d=4$ which is compatible with the numerical results. For $d=1$ one obtains $\mu\approx 4.814$. However, this argument needs to be substantiated and therefore EQ. (6.15) has to be taken with care.

6.3 Summary and outlook

In SEC. 6, stochastic models for spreading in media with long-time memory have been discussed. It was argued that long-time memory plays a role in many spreading phenomena and may, e.g., mimic immunization or

weakening in models for epidemic spreading. Sec. 6.1 introduced the so-called 'general epidemic process' (GEP), which corresponds to perfect immunization and belongs to the universality class of dynamical percolation. The main subject, however, was the investigation of a model for spreading with finite immunization in Sec. 6.2. The model is controled by probabilities for first infections (p_0) and reinfections (p). It reduces to directed percolation (DP) for $p_0{=}p$, while for perfect immunization, $p{=}0$, one obtains the general epidemic process (GEP). I focused in particular on the critical behavior close to the directed percolation point, especially in high dimensions $d{>}2$. I argued that I expect the domains of immune sites to be compact for $d{\leq}4$, but with an approach to compactness that is (logarithmically) slow at the upper critical dimension of DP, $d_c^{\mathrm{DP}}{=}4$. Therefore I denoted the visited region as asymptotically compact in $d{=}4$. The compactness of the immune region was supported by MC-simulations. It was pointed out that this compactness implies that a recently introduced scaling argument, suggesting a stretched exponential decay of the survival probability for $p{=}p_c$, $p_0{\ll}p_c$ in one spatial dimension, should apply in any dimension $d{\leq}3$ and maybe in $d{=}4$ as well. Furthermore, I showed that for $d{<}4$ the number of first infections (averaged over all runs) decreases whereas the number of reinfections increases. Contrarily, for $d{\geq}4$ both quantities scale equally. From that I derived the result that the phase transition line connecting the GEP and the DP point terminates in the DP point with a finite slope for $d{\geq}4$ and with a vanishing slope for $d{<}4$, which was supported by numerically determined phase diagrams. I also discussed the Langevin equation for the process, in order to study how the properties of the process change depending on the spatial dimension. Investigating the behavior for $p{=}p_c$ and $p_0{=}p_c{-}\epsilon$, $\epsilon{\ll}1$ an exponent μ for the temporal correlation length was identified which is different from $\nu_\parallel$ for DP.

In the future, it would be interesting to investigate the topological structure of the immune clusters of the epidemic process with finite immunization at the DP point in further detail. One could for instance measure the time the process needs to visit a compact region of a certain size and whether one can observe the asymptotic compactness in $d{=}4$. Another interesting point is the behavior at the horizontal phase transition line of the EPFI, $p{=}p_c$, away from the DP point. Since the exponential term in the Langevin equation Eq. (6.7) may be expanded in a Taylor series for $d{>}4$ one would expect a significant change of the influence of immunization at $d{=}4$. Moreover, the scaling argument suggested by Eq. (6.15) that led to a speculation of the value of μ in accordance with the numerical data needs further substantiation.

Chapter 7

Epidemic spreading with immunization and mutations

In the last chapter it was pointed out that stochastic models may be utilized to study epidemic spreading processes. Certain probabilistic rules mimic the competition between infectious spreading and spontaneous recovery. To this end, directed percolation corresponds to an epidemic process without immunization of individuals, where the pathogen (e.g., a virus) is transmitted to nearest neighbors. The 'general epidemic process' (GEP) accounts for perfect immunization whereas the EPFI is a generalization that includes partial immunization. In nature, however, immunization is a much more complex phenomenon. For example, the protection by immunization may abate as time proceeds. Even more importantly, the strategy of immunization competes with the ability of the contagious pathogen to mutate so that it can no longer be recognized by the immune system of previously infected individuals, weakening the effect of immunization. The aim of the present chapter is to introduce and study a simple model which mimics epidemic spreading with immunization and mutations. The epidemic process with finite immunization discussed in the previous chapter is generalized by including mutations as well as a mechanism for the competition between different species of pathogens. The model is controled by three parameters, namely, a first infection probability p_0, a reinfection probability p (controlling the effect of immunization), and a probability for spontaneous mutations λ. The model is defined in such a way that it includes DP and GEP as special cases.

The analysis in this chapter will be restricted to perfect immunization (p=0) and two spatial dimensions. In this case the model exhibits a line of continuous phase transitions connecting the critical points of the GEP and of directed percolation. I study the scaling behavior along this phase transition line as well as in the vicinity of the GEP point. It is shown that mutations lead generically to a crossover from the GEP to DP. Using standard scaling arguments, I also predict quantitatively the form of the phase transition line close to the GEP point where the protection gained by immunization is drastically decreased by the occurrence of mutations.

7.1 Simulation model

The model is meant to describe the spreading of an infectious disease that evolves as follows. Individuals can be healthy or infected with a certain pathogen. During their illness, infected individuals may infect or reinfect neighboring individuals with certain probabilities. Moreover, there is a probability that a pathogen mutates during transmission. Because of the enormous number of possible mutations, one usually obtains an entirely new type of pathogen which has not been involved before. To simplify the model, it is also assumed that each individual can be infected at a given time by no more than a *single* type of pathogen. If the individual is exposed simultaneously to several competing pathogens, one of them is randomly selected.

In more technical terms it is assumed that individuals live on the sites of a d-dimensional simple cubic lattice. Pathogens are represented by positive integers and each site keeps track of all species of pathogens by which it has been infected in the past. Therefore, the state of a site is characterized by an integer n together with a dynamically generated list of all previous types of infections. n=0 denotes a healthy individual while for n>0 the individual is infected with pathogen n. The model evolves in time by synchronous updates, i.e., in each time step the whole lattice is updated in parallel as follows.

Each infected individual at time t transmits its pathogen n to its $2d$ nearest neighbors (target sites). The transmitted pathogen reaches the target site at time t+1 with probability p_0 (p) if it is a first infection (reinfection) with this species. If a target site is exposed to several transmitted pathogens, one of them is randomly selected with equal weight. Before infecting the target site, the selected pathogen mutates with probability λ, replacing n by a new integer number (drawn from a global counter), which has not been

used before. In case of a first infection, the type of pathogen is added to the list of species against which the site will be immune in the future. Time of illness is a single time step.

This model was simulated, using single-processor computers (for seed-simulations, see below) as well as a parallelized implementation (for full-lattice simulations, see below).

7.2 Phase diagram

In the following, I restrict the analysis to the special case of perfect immunization p=0. In this case the model is controled by only two parameters, namely, the probability of first infections p_0 and the probability of mutations λ. Moreover, I restrict myself to the case of d=2 spatial dimensions. The corresponding phase diagram is shown in FIG. 7.1. It comprises an active phase, where the epidemic spreads, and an inactive phase, where the disease dies out so that the system eventually enters the fully recovered absorbing state. Both phases are separated by a curved phase transition line.

I first note that the endpoints of the phase transition line correspond to well-known special cases. On the one hand, for λ=0 the model reduces to the GEP on a square lattice [53], provided that only one type of pathogen is involved. In this case the critical value of p_0 is exactly given by p_0^c=1/2, see TAB. 6.1. On the other hand, for λ=1, all transmitted pathogens mutate, i.e., the target sites are always infected with a new species so that immunization has no influence. It is easy to see that in this case the model reduces to directed bond percolation on a square lattice with $p_0^c \simeq 0.287338$, see TAB. 4.1. The other points on the phase transition line in FIG. 7.1 were determined numerically using seed-simulations (see SEC. 7.3.1).

As already discussed above, mutations generally weaken the effect of immunization. This explains why the critical value of p_0 decreases monotonically with increasing mutation probability λ. FIG. 7.1 clearly shows that introducing mutations in a GEP has a strong influence on p_0^c, especially if λ is very small. Since the phase transition line approaches the GEP point with infinite slope (see inset in FIG. 7.1) a tiny increase of λ reduces the corresponding critical value of p_0 dramatically. This indicates that mutations are a relevant perturbation and thus the spreading behavior of the model for λ>0 is expected to differ from that of the GEP. On the other hand, for larger values, $\lambda \gtrsim 0.1$, the critical value of p_0 decreases only moderately with

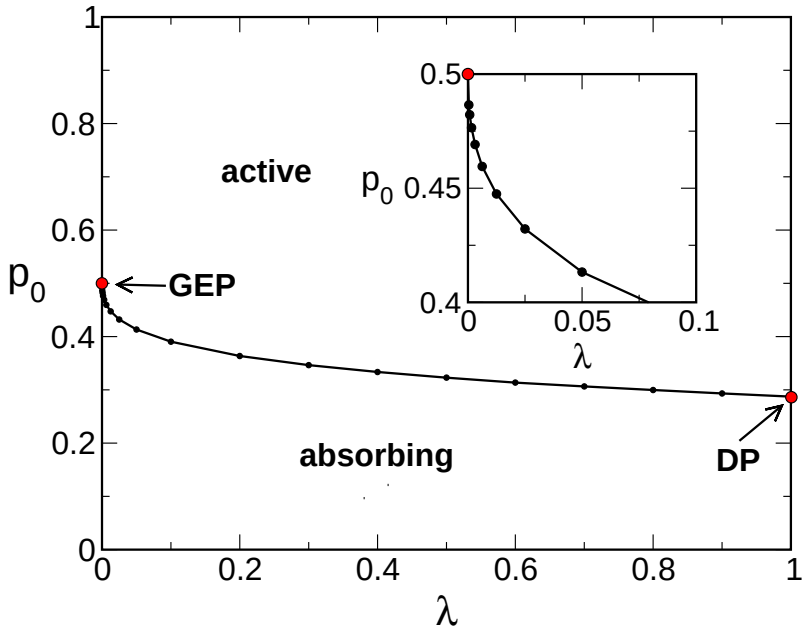

FIGURE 7.1: *Phase diagram of the model. The active and the inactive phases are separated by a curved line of continuous phase transitions, connecting the points of critical GEP and critical DP. Circles mark the numerically determined critical points. The inset shows the phase transition line for small* λ.

increasing λ, indicating that the behavior of the model in this region is essentially the same as for λ=1, where the transition is known to belong to DP.

FIG. 7.2 shows snapshots of simulations at the transition for different times and various values of λ. Infected individuals are represented by black dots. Healthy individuals which are immune against at least one active type of pathogen are marked by gray dots. The snapshots suggest the following qualitative behavior:

A) For λ=0 (GEP) the process creates a growing cluster of immune sites with infected individuals located at the edges. In the active phase this region is compact while it is fractal at the transition.

B) For small λ the disease first behaves as a GEP (for $t \leq 100$) while for larger times the spreading behavior changes and clearly differs from the GEP. There still is a region of immune individuals but it does no longer provide efficient protection since it is reinvaded by mutated pathogens.

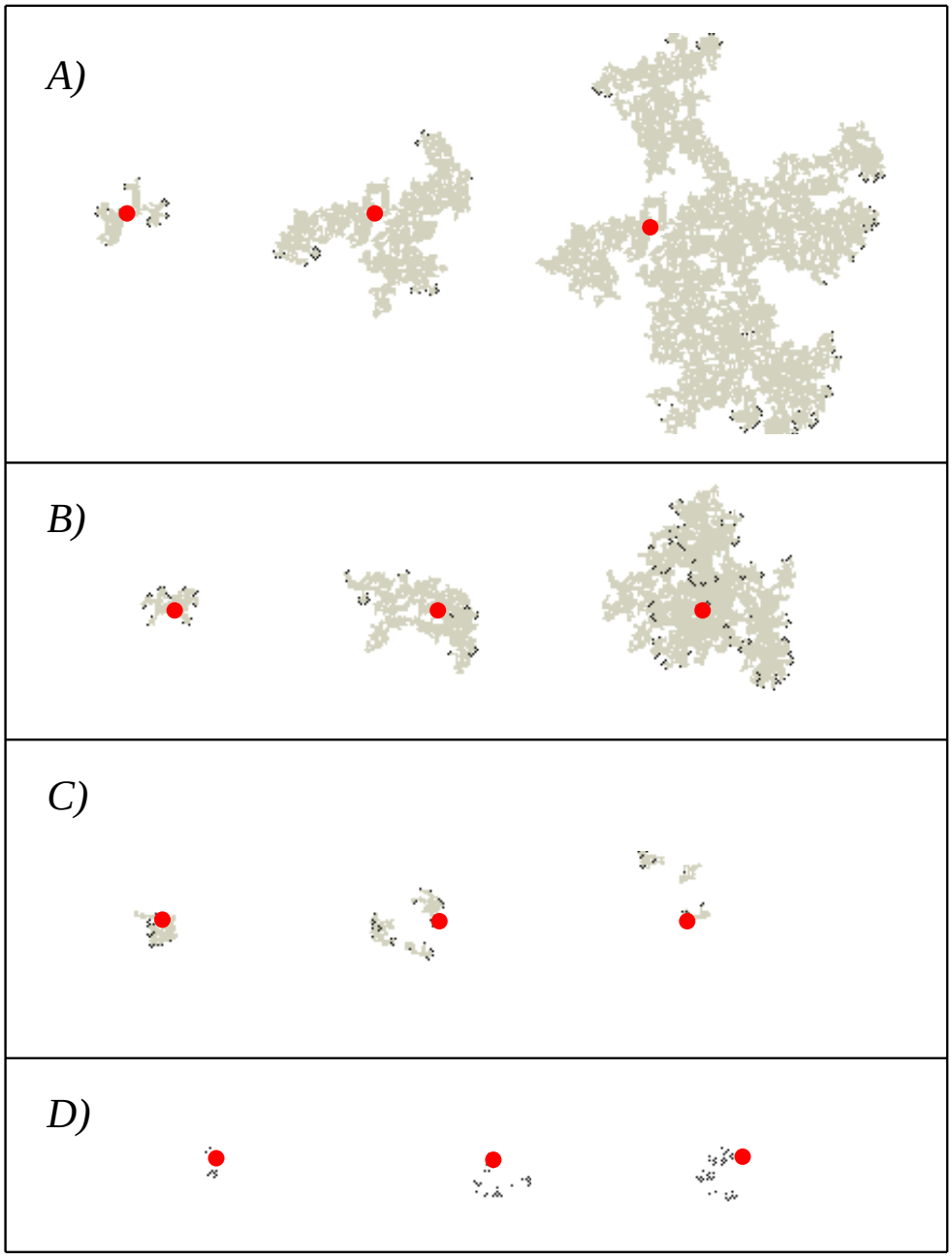

FIGURE 7.2: *Snapshots of seed-simulations at the phase transition. The red circles mark the positions of the seed. Each row shows a simulation for a fixed value of* λ *and times* t=30, t=100 *and* t=225 *(from left to right). From A) to D) values of* λ *are* 0 *(GEP),* 0.003125, 0.05 *and* 1 *(DP). Black (gray) dots denote active (immune) individuals (details in the text).*

C) Increasing λ further, the process changes its appearance already at an early stage. There are only small patches of immune sites and the process reminds more of DP than GEP.

D) Finally, for λ=1 every transmitted pathogen mutates into a new one. In this case immunization has no influence and the process reduces to DP.

Based on these phenomenological observations one expects the model to behave initially in the same way as a GEP. After a certain time mutations become relevant, allowing former immune areas to be reinvaded. Especially close to the transition the process survives long enough to reach this crossover time. The visual appearance of the process is then increasingly similar to that of a DP process. The time it takes to observe the crossover from GEP to DP grows with decreasing λ and eventually diverges in the limit $\lambda \to 0$.

7.3 Critical behavior along the phase transition line

I now analyze the critical behavior of the model, assuming that the scaling theory presented in Sec. 4.1.1 is valid everywhere in the vicinity of the phase transition line. Although the qualitative discussion in Sec. 7.2 suggests DP behavior for $0<\lambda\leq 1$, I note that this would be a non-trivial result since the 'DP-conjecture', see Sec. 4.2.6, does not apply in the present case. Recall that the 'DP-conjecture' states that phase transitions in two-state systems with a reachable absorbing state and short-range interactions belong to DP, provided that memory effects, non-conventional symmetries, and quenched disorder are absent. Contrarily the present model has many absorbing states and memorizes previous infections over a long time.

7.3.1 Seed simulations

As usual, seed simulations start with a single infected site at the origin in a non-immune environment. Each run is stopped when it dies out or reaches a preset maximum time. It is averaged over many runs with different realizations of randomness. In order to eliminate finite size effects, the lattice is always chosen large enough so that the epidemic never reaches its boundaries. The survival probability $P_{\mathrm{s}}(t)$, the number of active sites $N(t)$ averaged over all runs, and the mean square spreading from the origin $R^2(t)$ averaged over all active sites in surviving runs is measured. According to

Eq. (4.10) these quantities vary algebraically at criticality. Seed-simulations were performed on single-processor computers.

Figs. 7.3 and 7.4 show the results of seed-simulations along the phase transition line. Note that for each site one has to deal with the whole list of previous infections which is continuously updated. This makes these simulations numerically challenging.

In order to determine the critical threshold $p_0^c(\lambda)$, λ was kept fixed and p_0 was varied until $P_s(t)$ displayed the expected slope of DP in a log-log plot (dashed lines in Figs. 7.3) and 7.4). Although this procedure is in favor of DP scaling, the mere fact that it works consistently for all quantities in Eq. (4.10) confirms that the transition does belong to DP for any $0<\lambda\leq 1$ while GEP scaling can be ruled out. The data also shows the expected crossover. For small λ, the curves roughly display the slope expected for GEP (dotted lines) before they cross over to DP, confirming the crossover scenario discussed above. Thus the introduction of mutations in a GEP is a relevant perturbation in the sense that it changes the asymptotic critical behavior of the model. At the phase transition the interplay between immunization and mutations drives the system towards DP.

The involvement of different species of pathogens in a spreading process with mutations allows one to introduce the number of active species $N_{\rm sp}(t)$ as an additional order parameter. As shown in Fig. 7.4, the number of active species at criticality increases in the same way as the number of infected individuals. Thus their quotient tends to a λ-dependent constant $c(\lambda)=\lim_{t\to\infty} N/N_{\rm sp}$.

7.3.2 Full-lattice simulations

In this type of simulation, a finite system with periodic boundary conditions is used. The initial configuration is a fully occupied lattice where all individuals are infected by different types of pathogens. (If all sites were occupied with the same type of pathogen the process would immediately be trapped in the absorbing state.) I measure the density of active sites $\rho(t)$ and the density of active species $\rho_{\rm sp}(t)$. In the case of directed bond percolation, λ=1, the density of active sites decays as $\rho(t)\sim t^{-\delta}$, see Eq. (4.6). Exemplarily, I performed a full-lattice simulation for λ=0.5 at the critical point (not shown as a figure), confirming this type of decay with $\delta\approx 0.451$. Moreover, like in seed simulations, the density of active species also decays as $\rho_{\rm sp}(t)\sim t^{-\delta}$. Full-lattice simulations were carried out, using a parallelized implementation of the simulation model.

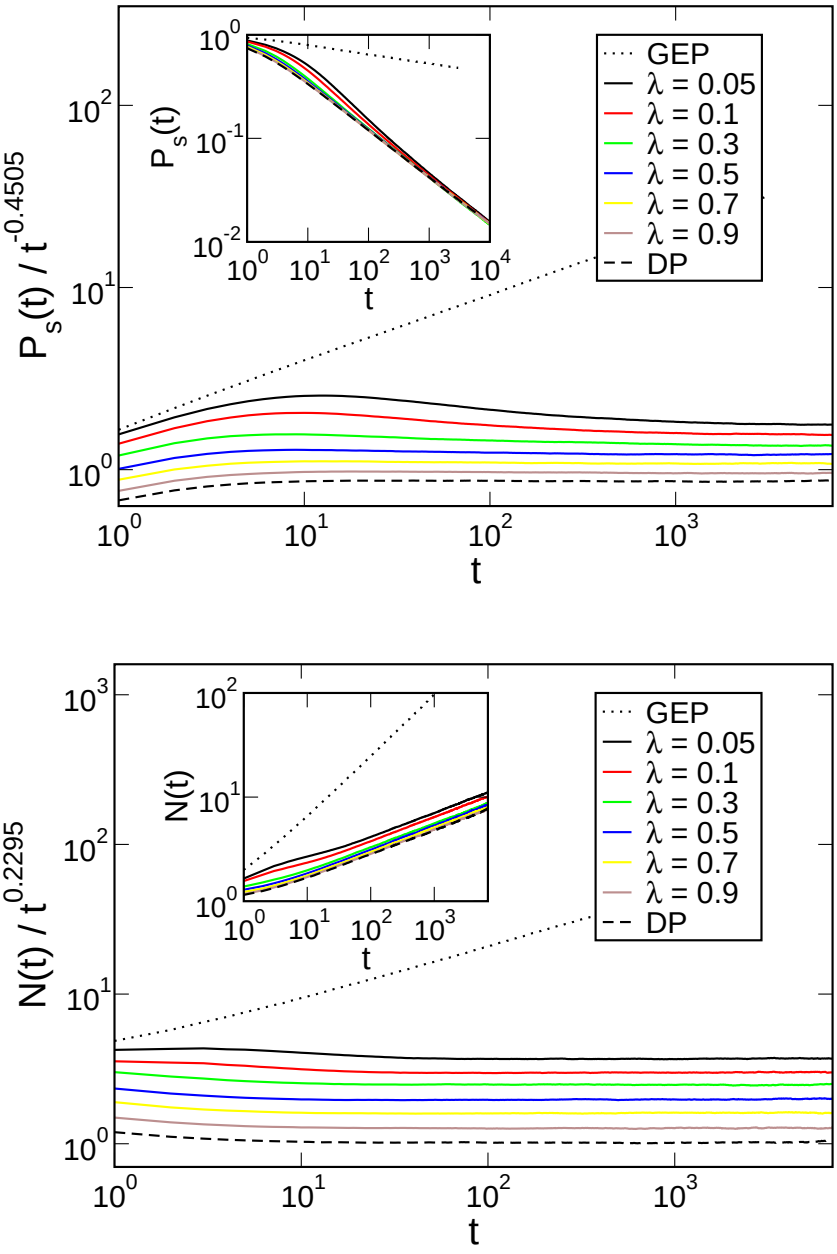

FIGURE 7.3: *Seed simulations:* $P_s(t)$ *and* $N(t)$ *at the phase transition for different values of* λ*. The data is multiplied by the expected asymptotic power-law and vertically shifted. The insets show the original data.*

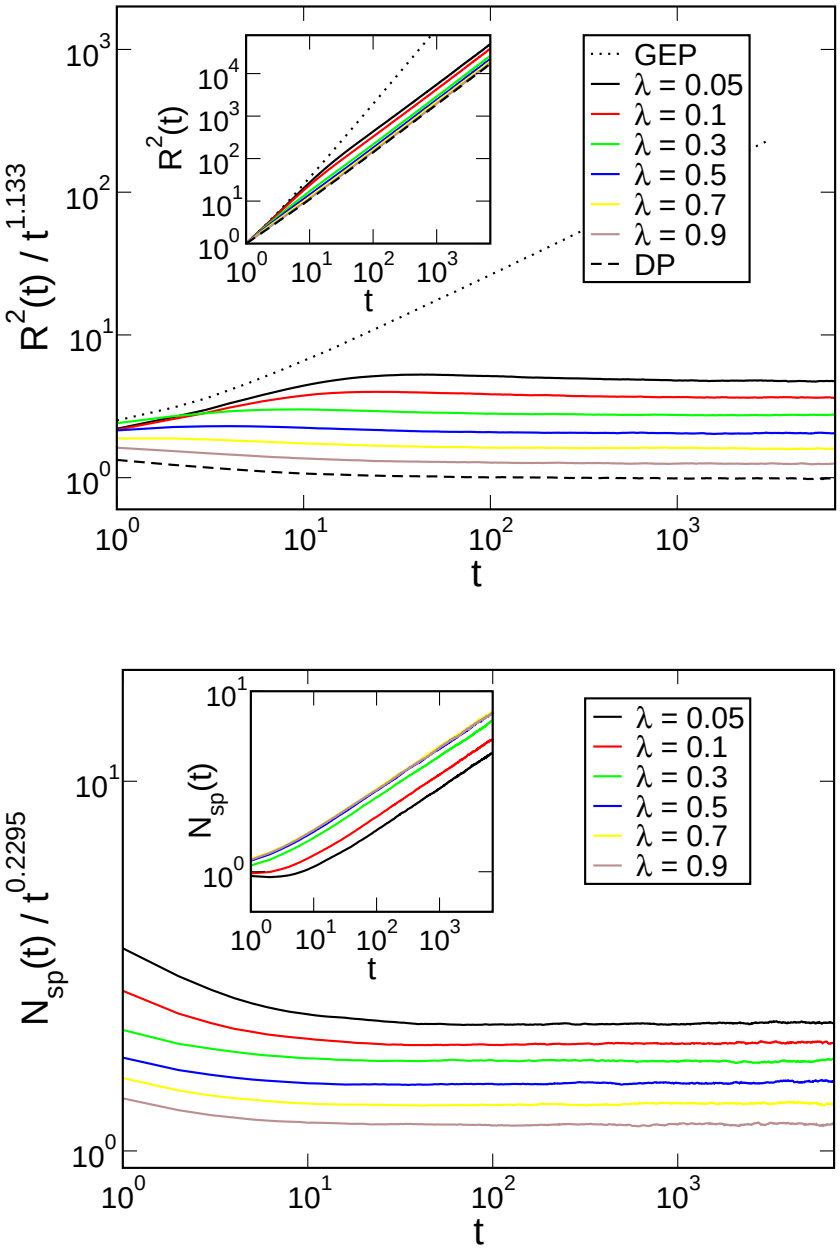

FIGURE 7.4: *Seed simulations:* $R^2(t)$ *and* $N_{\mathrm{sp}}(t)$ *at the phase transition for different values of* λ*. The data is multiplied by the expected asymptotic power-law and vertically shifted. The insets show the original data.*

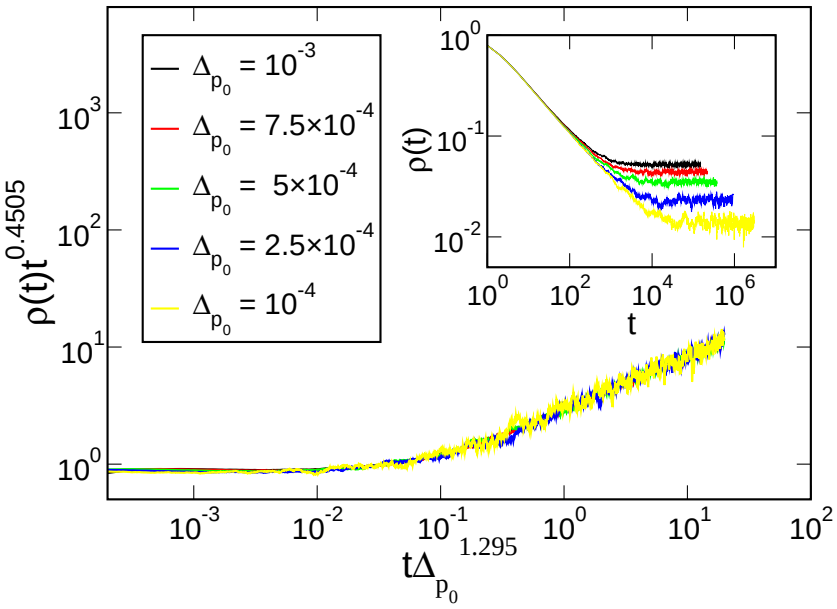

FIGURE 7.5: *Data collapse of $\rho(t)$ for λ=0.5 using the critical exponents of DP, i.e., δ=0.4505 and $\nu_{\|}$=1.295.*

The three exponents δ, θ, z in EQ. (4.10) that govern the spreading behavior at the transition, depend only on two of the three independent critical exponents that are needed to characterize the universality class of DP (see SEC. 4.1.1). To roughly check the value of the third independent exponent, I performed off-critical full-lattice simulations for λ=0.5 and different values of $0<\Delta_{p_0}\ll 1$. As is shown in FIG. 7.5 using the critical exponents δ and $\nu_{\|}$ of DP one obtains a reasonable data collapse of the density $\rho(t)$. Though the data in FIG. 7.5 can not be used for a precise analysis, it is strongly suggested that indeed all three exponents governing the scaling behavior of the spreading process for $\lambda>0$ are that of DP.

7.4 Critical behavior in the vicinity of the GEP point

In this section I investigate the influence of mutations in the vicinity of the GEP point in order to address two questions. How does the system cross over from critical GEP to a non-trivial fluctuating active state and why does the phase transition line terminate in the GEP point with an infinite slope?

7.4.1 Decay at the GEP point

Already at the GEP point the model exhibits a new feature, namely, the competition of different types of infections in full-lattice simulations, see above. One observes a coarsening process of competing species, leading to a slow decay of the density of active sites and active species. As shown in FIG. 7.6, the decay of these quantities suggests possibly asymptotic power-laws, although the data display a considerable curvature in both cases. *Assuming* asymptotic power laws

$$\rho(t) \sim t^{-\alpha} \qquad \rho_{\rm sp}(t) \sim t^{-\tilde{\alpha}} \tag{7.1}$$

at the GEP point, one extrapolates the effective exponents $\alpha(t), \tilde{\alpha}(t)$ visually for $t \to \infty$ (see insets of FIG. 7.6), obtaining the estimates

$$\alpha = 0.66(2)\,, \qquad \tilde{\alpha} = 1.33(4)\,, \tag{7.2}$$

suggesting that $\tilde{\alpha}=2\alpha$.

Regarding the limited accuracy of the numerical simulations the conjecture of an asymptotic algebraic decay has to be taken with care. However, indirect support comes from the one-dimensional case. Here the GEP transition is shifted to $p_0^c=1$ and the dynamics of competing species reduces to a ballistic coalescence process [134], for which asymptotic power laws could be derived exactly.

7.4.2 λ-controled transition at the GEP point

Let me now turn to the critical behavior in the vicinity of the GEP point. The GEP point in FIG. 7.1 can be approached either vertically by varying p_0 or horizontally by varying λ. The critical behavior in vertical direction has been studied in detail in REFS. [53, 129, 131] and can be described in terms of the scaling theory presented in SEC. 4.1.1. Contrarily, moving in horizontal direction by varying λ and keeping $p_0=1/2$ fixed one encounters mutations as a new feature, leading to a non-trivial fluctuating active state.

As usual in critical phenomena, the additional control parameter λ is associated with a novel critical exponent $\mu_\parallel$. Like $\nu_\parallel$ this exponent is defined in such a way that

$$\xi_\parallel \sim \lambda^{-\mu_\parallel} \tag{7.3}$$

is the correlation time in the stationary state for $p_0=1/2$ and $0<\lambda\ll 1$. Similarly, the corresponding spatial correlation length is expected to scale as

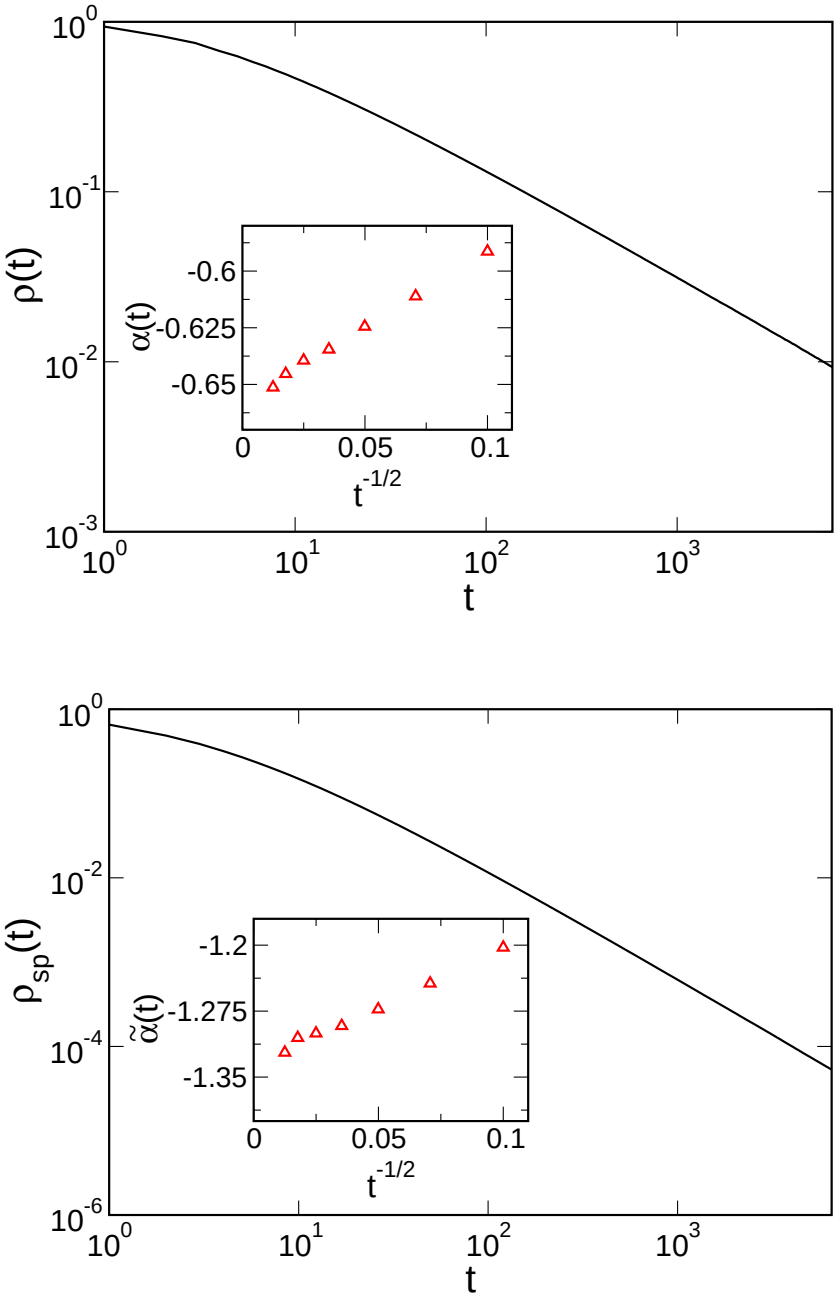

FIGURE 7.6: *Full-lattice simulations at the GEP point. The decay of ρ and $\rho_{\rm sp}$ may suggest a possible power-law behavior in the limit $t\to\infty$. The effective exponents can be extrapolated visually for $1/\sqrt{t}\to 0$ (see insets).*

$\xi_\perp \sim \lambda^{-\mu_\perp}$ where $\mu_\perp = \mu_\parallel / z$. According to standard scaling theory the survival probability $P_\mathrm{s}(t)$ should obey the scaling form

$$P_\mathrm{s}(t) = t^{-\delta}\, \Psi(\lambda t^{1/\mu_\parallel})\,, \tag{7.4}$$

where $\delta \simeq 0.092$ is the decay exponent of the GEP, see Tab. 6.1. With an appropriate scaling function Ψ Eq. (7.4) implies that the survival probability eventually saturates at a value $P_\mathrm{s}(\infty) \sim \lambda^{\delta\mu_\parallel}$. Using this scaling form I collapsed data sets for seed-simulations at $p=1/2$ for $\lambda = 5\times10^{-4}$ and $\lambda = 10^{-4}$ (not shown as a figure), obtaining the estimate

$$\mu_\parallel = 0.63(3)\ . \tag{7.5}$$

In the case of full-lattice simulations, provided that the power-law behavior in Eq. (7.1) is correct, one expects that $\rho(t)$ and $\rho_\mathrm{sp}(t)$ obey the scaling forms

$$\rho(t) = t^{-\alpha}\Omega(\lambda t^{1/\mu_\parallel})\ ,\ \rho_\mathrm{sp}(t) = t^{-\tilde{\alpha}}\tilde{\Omega}(\lambda t^{1/\mu_\parallel}) \tag{7.6}$$

where Ω and $\tilde{\Omega}$ are appropriate scaling functions such that eventually the densities reach stationary values $\rho(\infty) \sim \lambda^{\alpha\mu_\parallel}$ and $\rho_\mathrm{sp}(\infty) \sim \lambda^{\tilde{\alpha}\mu_\parallel}$. Using the value of $\mu_\parallel = 0.63$, Eq. (7.5), these scaling forms lead to reasonable data collapses, as shown in Fig. 7.7.

I now suggest an explanation for the numerically determined value of $\mu_\parallel = 0.63$. Initially the process behaves as a critical GEP until mutations become relevant at a typical time $\xi_\parallel$. The argument is based on the assumption that $\xi_\parallel$ scales in the same way as the typical time at which the first mutation occurs. With the mutation probability λ one needs on average λ^{-1} infections until the first mutation occurs. As the process initially behaves as a critical GEP the number of infections grows as $\int dt N(t) \sim t^{\theta+1}$. Hence one is led to $\xi_\parallel \sim \lambda^{-\frac{1}{\theta+1}}$ with $\theta = d/z - 2\delta - 1 = 0.587$, see Tab. 6.1. This implies the scaling relation

$$\mu_\parallel = \frac{1}{\theta+1} \simeq \frac{1}{1.587} = 0.630 \tag{7.7}$$

which is in perfect agreement with the numerical estimation in Eq. (7.5).

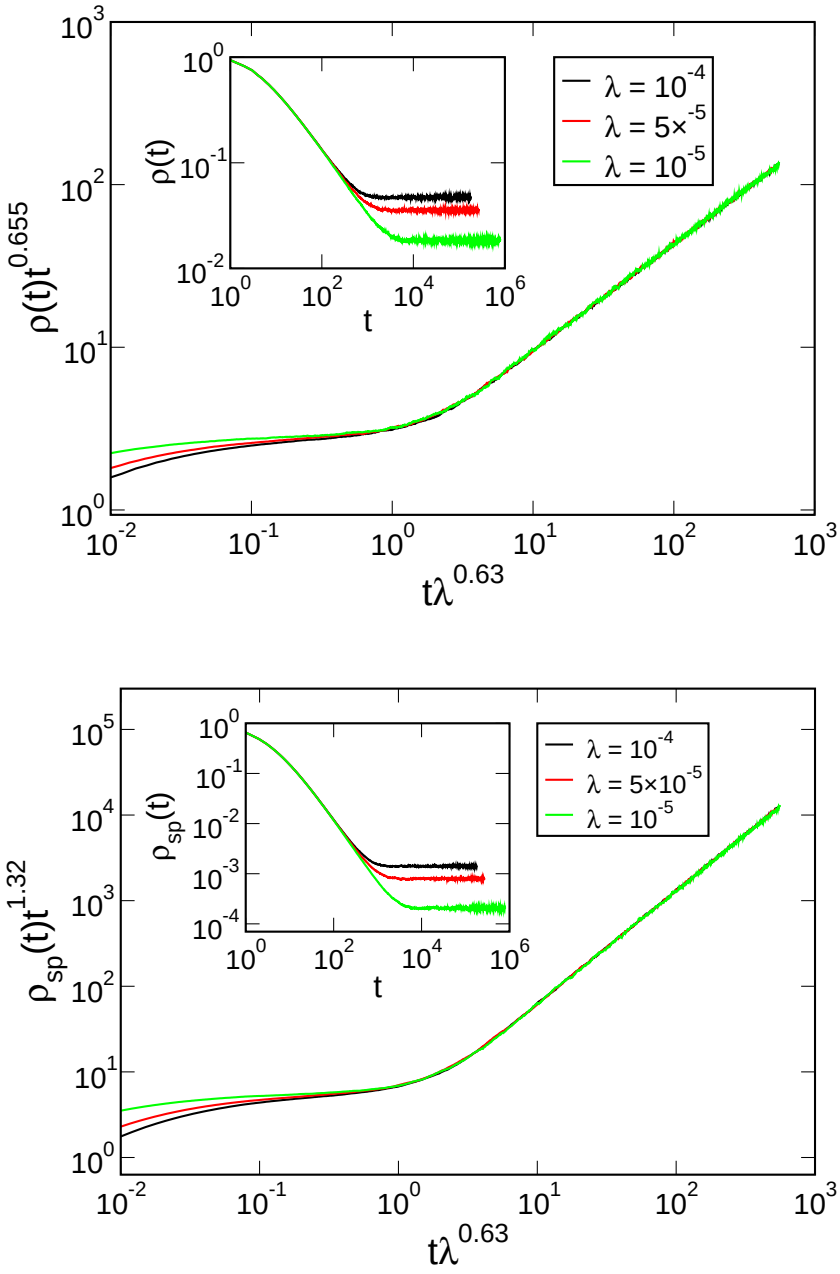

FIGURE 7.7: *Data collapse of ρ and ρ_{sp} based on the scaling forms* EQ. *(7.6) using the exponents of* EQS. *(7.2),(7.5).*

7.4.3 Curvature of transition line at the GEP point

So far the numerical analysis suggests that in the vicinity of the GEP point the epidemic process with mutations is invariant under scaling transformations of the form $x \to x' = b\,x$, $t \to t' = b^z\,t$, see also Eq. (4.5), and

$$\Delta_{\mathrm{p}_0} \;\to\; \Delta_{\mathrm{p}_0}{}' = b^{-1/\nu_\perp}\,\Delta_{\mathrm{p}_0} \;, \tag{7.8}$$

$$\lambda \;\to\; \lambda' = b^{-1/\mu_\perp}\,\lambda \;, \tag{7.9}$$

where b is a scaling factor, $\Delta_{\mathrm{p}_0}{=}p_0{-}1/2$, δ and z are the critical exponents of GEP, and $\mu_\perp{=}\mu_\parallel/z$. In addition, the order parameters have to be rescaled appropriately. In seed simulations this leads to the combined scaling form for the survival probability

$$P_{\mathrm{s}}(t, \Delta_{\mathrm{p}_0}, \lambda) = t^{-\delta}\tilde{\Phi}(\Delta_{\mathrm{p}_0} t^{1/\nu_\parallel}, \lambda t^{1/\mu_\parallel}) \tag{7.10}$$

in the vicinity of the GEP point. Similar relations should be valid for the densities $\rho(t)$ and $\rho_{\mathrm{sp}}(t)$ in full-lattice simulations, provided that the conjecture of asymptotic power-law behavior in Eq. (7.1) is correct.

As usual in the theory of critical phenomena, the phase transition line itself has to be invariant under scaling transformations. Comparing Eqs. (7.8) and (7.9) one is led to the conclusion that the form of the transition line for small values of λ is given by

$$\Delta_{\mathrm{p}_0} \;\sim\; \lambda^\gamma \;, \tag{7.11}$$

where

$$\gamma = \frac{\mu_\perp}{\nu_\perp} = \frac{\mu_\parallel}{\nu_\parallel} \simeq \frac{0.63}{1.506} = 0.42 \;. \tag{7.12}$$

Since $\frac{\partial \Delta_{\mathrm{p}_0}}{\partial \lambda} \sim \lambda^{-0.58}$ the phase transition line indeed terminates at the GEP point with an infinite slope.

In order to confirm the relations Eqs. (7.11),(7.12), $|\Delta_{\mathrm{p}_0}|$ is plotted versus $\lambda \ll 1$ in a double-logarithmic representation in Fig. 7.8. The local slope of this curve leads to the effective exponent (inset in Fig. 7.8) which can be extrapolated and leads to the estimation $\gamma \approx 0.41(3)$, in agreement with the prediction in Eq. (7.12).

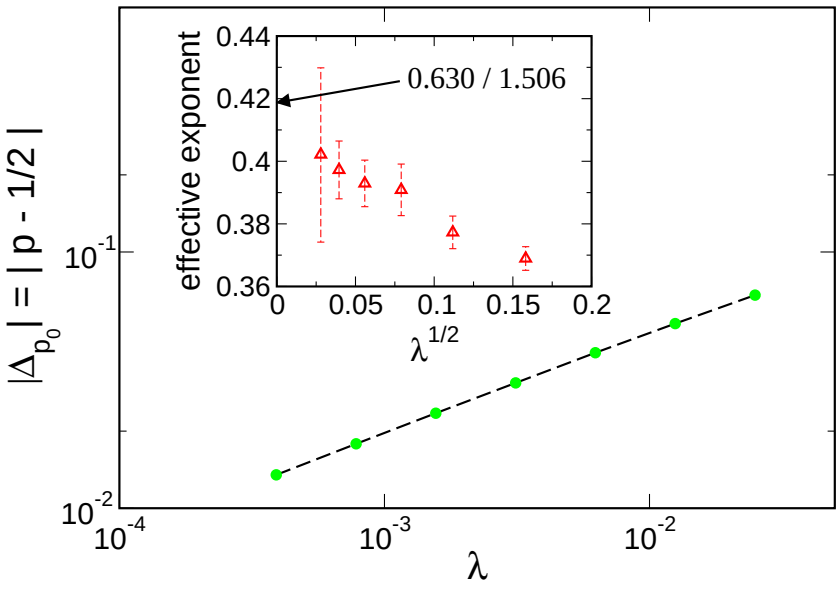

FIGURE 7.8: *Double-logarithmic plot of the phase transition line* $|\Delta_{p_0}(\lambda)|$ *for* $\lambda \ll 1$. *The effective exponent can be extrapolated for* $\sqrt{\lambda} \to 0$ *(see inset).*

7.5 Summary and outlook

In this chapter I have introduced a minimal model for epidemic spreading with immunization and mutations. Apart from the probabilities for first infections and reinfections, p_0 and p, the model is controled by a probability λ that a transmitted pathogen mutates, creating a new pathogen which was not involved before. The model includes the GEP (λ=0, p=0) and DP (λ=1 or p_0=p) as special cases.

Restricting the analysis to the case of perfect immunization and two spatial dimensions it was shown that at the transition between survival and extinction, the model shows DP scaling everywhere along the phase transition line except for the point where the model reduces to critical GEP. In the vicinity of the GEP point, even a small mutation probability drives the system away from criticality into a fluctuating active state. This crossover can be described in terms of a suitable scaling theory, which involves a new exponent $\mu_{\|}$. This exponent also determines the form of the phase transition line in the vicinity of the GEP point. I suggested an explanation for the value of $\mu_{\|}$ which turns out to be in perfect agreement with the numerical analysis.

Although the model presented here is highly idealized (individuals on a square lattice, homogeneous infection probabilities, nearest-neighbor infections etc.) there is an important conclusion to be drawn regarding realistic spreading of epidemics in nature. As in the model, realistic epidemic spreading starts at a certain threshold determined by various parameters such as the average susceptibility, the interaction frequency, and the degree of immunization and/or vaccination. Mutations weaken the effect of immunization, thereby decreasing this threshold. An important message of this chapter is that for a population which is mainly stabilized by immunization and/or vaccination this threshold varies *nonlinearly* with the mutation rate, in the present case roughly as the square root of λ. Thus even a small rate of mutations can significantly weaken the stability of a population at the onset of epidemic spreading.

As a possible extension of the present study it would be interesting to investigate similar spreading processes on a spatial network instead of a lattice. This is important since, e.g., contacts between individuals in a society are rather given by a network than by lattice. Another interesting point would be to include long-range infections [135, 136], which could be interpreted as pathogens transported over long distances, for instance, by insects.

Chapter 8

Conclusion

In this thesis, several stochastic models with irreversible underlying dynamics were studied. It was shown that these models, on the one hand, may be used to deepen the insight into particular natural or experimental systems under consideration. An example was the investigation of monopolarly charged suspensions in Chap. 3, which was motivated by the particle-coating process described in the appendix. On the other hand, the models discussed in this thesis are fundamentally interesting from the point of view of statistical mechanics, as they describe generically systems that are not at thermodynamic equilibrium. Compared to equilibrium statistical mechanics, nonequilibrium statistical physics is still at its beginning. Therefore, it is important to investigate different kinds of nonequilibrium models, in order to study what behavior may be observed and which theoretical concepts are appropriate for nonequilibrium systems. The thesis contributed to this issue by investigating different nonequilibrium systems. In Sec. 3.3, for example, a dynamical scaling regime was observed, where the asymptotic behavior was universal. Scaling concepts and universality were also decisive for the investigations of phase transitions into absorbing states carried out in Chaps. 5–7. Established models for spreading processes were generalized, in order to include additional features observed in natural spreading processes. The concepts of scaling and universality were shown to be appropriate for these models (though in Chap. 6 an example of nonuniversal behavior was given). Moreover, it was demonstrated in Chap. 5 that another concept, well-known from equilibrium statistical physics, applies to the nonequilibrium case as well. More precisely, the concept of Yang and Lee was transferred to the phase transition of directed percolation, by investigating the complex roots of the survival probability. For a detailed summary of the new results presented in this thesis, I refer to the summarizing sections in Chaps. 3, 5, 6 and 7.

Acknowledgments

In the first place I thank my wife Dana. For enduring live with someone who is writing a Ph.D. thesis, for disburden me whenever it was needed, and for much more. Furthermore, I want to thank my whole family, especially my parents, my brother and my sister, and my friends (also those making fun of me for still being some kind of student). Also thanks to Piet and Laika. On scientific grounds, I want to express my warmest thanks to my supervisor Prof. Dr. H. Hinrichsen, first of all simply for working with him and for having a joyful and very instructive scientific time during the last years. Among many other laudable things I want to emphasize that he always encouraged me to follow my own ideas and interests, which created a great working atmosphere. I am also grateful to Prof. Dr. D. E. Wolf. Working with him was very illuminating and inspiring, since he lively demonstrates that, besides all difficulties, working in science is an exciting, interesting and joyful enterprise. Special thanks to my long-time 'physics-mate' and 'computer-doctor' and 'X-BLAST-opponent' Guido Bartels. He was a great company during my time as a Ph.D. student and especially during my time as an undergraduate student (in particular in our laboratory courses). Moreover, I want to express my gratitude to the whole 'comphys'-group, which provided a very convenient working atmosphere. In particular, I thank Dr. L. Brendel, J. Werth, G. Bartels and H. Beyer for many help with the computers; Dr. L. Brendel and L. Sittler for many office-discussions about strange physical questions; J. Werth and Dr. H. Knudsen for instructive collaborations in the 'suspension-project'; Dr. D. Kadau, R. Zinetullin and F. Westerhoff for being good colleagues, as well as all the others in the 'comphys'-group. Thanks to H. Münstermann for help with bureaucratic questions. Thanks to Dr. Sven Lübeck, Guido Bartels and especially Dr. H. Knudsen for reading parts of the manuscript. Thanks to Prof. Dr. S. R. Dahmen for his hospitality and many fruitful discussions about scientific and non-scientific topics. Also thanks to Dr. Z. Farkas, I particularly enjoyed working with him. I am also grateful for the collaboration with Prof. Dr.-Ing. habil. K.-E. Wirth and M. Linsenbühler, which helped me to enrich my experimental perspective. I am rather sure that I forgot someone. Well, also thanks to this one. Finally, I thank my friend eddie for doing a good job, the DFG for support within the program 'Verhalten granularer Medien', and the DAAD for my stay in Porto Alegre.

Appendix – Electrostatically supported coating

The investigation of monopolarly charged suspensions that is presented in Sec. 3.3, plays an important role for the realization of an electrostatically supported coating process [40]. In the following I shall briefly sketch the basic motivation and ideas that led to the work of Ref. [40], and how it is related to aggregation dynamics in monopolarly charged suspensions.

The handling of powders is essential for all kinds of industrial processes. A major problem in this context is the tendency of fine powder particles to stick together due to attractive van der Waals forces between the grains. A particularly important example where such an agglomeration must be impeded is that of powders which are inhaled for medical purposes. In this case, large agglomerates cannot penetrate into the lungs. Note that in many cases it is reasonable to consider the van der Waals interaction as an irreversible short-ranged sticky force [41].

A promising technological approach to avoid lumping is to coat the particles by smaller nanoparticles which act as spacers, thereby decreasing the van der Waals force. A possible method to realize the coating experimentally was reported in [40] and is sketched in Fig. A.1. The two particle fractions are charged oppositely and kept in suspension. The carrying fluid is liquid nitrogen which does not screen the Coulomb interactions. The electrical charges support the coating process since the bigger particles attract the nanoparticles, while agglomeration of equally charged particles is hindered.

However, besides Coulomb and van der Waals forces the particles suspended in the fluid are subjected to various forces induced by the fluid molecules.

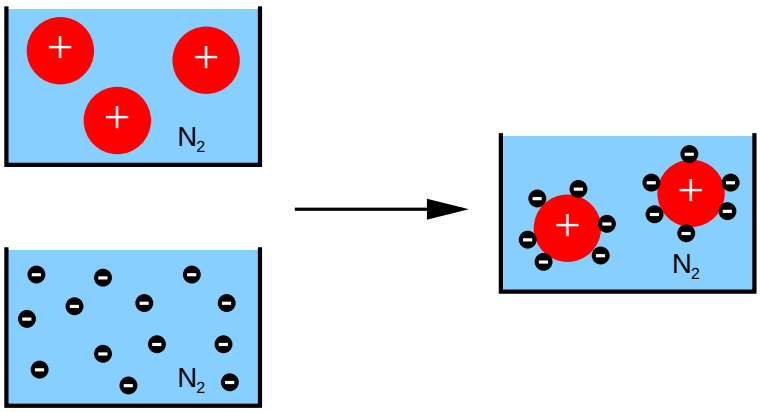

FIGURE A.1: *Sketch of an electrostatically supported coating process as reported in* REF. *[40].*

These lead to Stokes friction, long-range hydrodynamic interactions (which are neglected in SEC. 3.3) as well as Brownian motion. Due to Brownian motion, even equally charged particles may collide which, of course, should be avoided in the coating process, see FIG. A.2. Hence, important questions are, under which conditions a suspension of equally charged particles is stable against agglomeration and how does the suspension evolve in the case that it is unstable.

As was discussed in SEC. 3.3, a suspension is usually regarded as stable with respect to the agglomeration of equally charged particles, if the particle diameter d_p is small compared to the Bjerrum length l_B. In the experiments reported in REF. [40], the temperature of liquid nitrogen is 77K, and the dielectric constant is $\epsilon_\mathrm{r}{\approx}1.45$. Assuming that the charge q of the particles is z times the elementary charge, the Bjerrum length is

$$l_\mathrm{B} \approx 150 z^2 \mathrm{nm} \; . \tag{1}$$

Therefore it seems, aggregation is not an issue, if one uses nanoparticles for coating.

However, in practice the situation is often more complicated [40]. Usually one finds presintered aggregates of nanoparticles in the suspension, due to the production process. These clusters cannot be broken up into primary particles by common dispersion procedures. Typical cluster sizes are $d{\approx}500$nm,

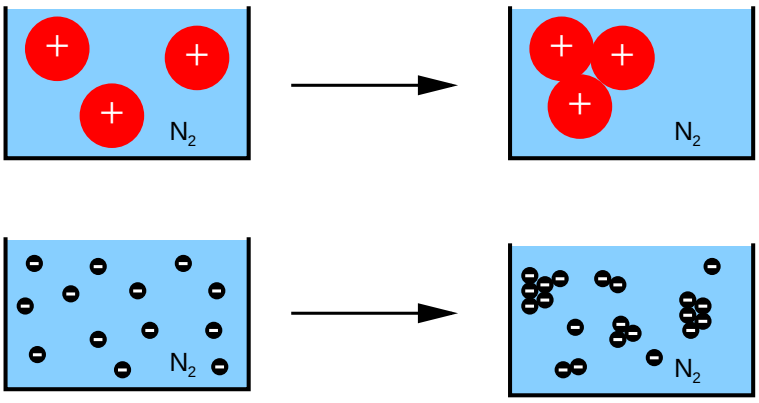

FIGURE A.2: *Aggregation of 'wrong' partners.*

and the charging process leads to about one elementary charge per cluster, z=1. In such a situation the Bjerrum length is smaller than the cluster diameter, so that Brownian motion should initially lead to further agglomeration of the clusters. This is exactly the case considered in SEC. 3.3.

Bibliography

[1] J. Marro and R. Dickman, *Nonequilibrium phase transitions in lattice models*, Cambridge University Press, Cambridge (1999).

[2] H. Hinrichsen, *Nonequilibrium critical phenomena and phase transitions into absorbing states*, Adv. Phys. **49**, 815 (2000).

[3] J.L. Cardy, *Scaling and Renormalization in Statistical Physics*, Cambridge University Press, Cambridge, (1996).

[4] L.E. Reichl, *A modern course in statistical physics*, University of Texas Press, Austin, (1980).

[5] W. Nolting, *Grundkurs Theoretische Physik 4, Spezielle Relativitätstheorie, Thermodynamik*, Vieweg-Verlag, third edition, (1997).

[6] A.J. Guttmann, *Asymptotic analysis of power-series expansions*, in *Phase Transitions and Critical Phenomena*, volume 13, ed. by C. Domb and J.L. Lebowitz, London, Academic Press, (1989).

[7] *The Monte Carlo Method in Condensed Matter Physics*, ed. K. Binder, volume 72 of Topics in Applied Physics, Springer-Verlag Berlin Heidelberg, (1992).

[8] B. Derrida, E. Domany, D. Mukamel, *An exact solution of of a one-dimensional asymmetric exclusion model with open boundaries*, J. Stat. Phys. **69**, 667 (1992).

[9] B. Derrida, M.R. Evans, V. Hakim, V. Pasquier, *Exact solution of a 1D asymmetric exclusion model using a matrix formulation*, J. Phys. A: Math. Gen. **26**, 1493 (1993).

[10] G. Schütz, E. Domany, *Phase transitions in an exact soluble one-dimensional exclusion process*, J. Stat. Phys. **72**, 277 (1993).

[11] C.W. Gardiner, *Handbook of Stochastic Methods for Physics, Chemistry and the Natural Science*, Springer-Verlag, Berlin, second edition, (1990).

[12] H. Risken, *The Fokker-Planck Equation*, Springer-Verlag, Berlin, second edition, (1989).

[13] N.G. van Kampen, *Stochastic processes in physics and chemistry*, North-Holland, Amsterdam, second edition, (1992).

[14] R.A. Blythe, *Nonequilibrium phase transitions and dynamical scaling regimes*, Ph.D. thesis, University of Edinburgh, http://www.ph.ed.ac.uk/cmatter/links/rab-thesis , (2001).

[15] G.R. Grimmet, D.R. Stirzaker, *Probability and random processes*, Oxford Science Publications, Oxford University Press, Oxford, second edition, (1992).

[16] B. Derrida, M. Evans, *The asymmetric exclusion model: exact results through a matrix approach*, in *Nonequilibrium statistical mechanics in one dimension*, ed. by V. Privman, Cambridge University Press, Cambridge (1997).

[17] D.E. Wolf, *Stochastic Differential Equations*, in *Advances in Computer Simulation*, ed. by J. Kertész, I. Kondor, Springer, Heidelberg, (1998).

[18] M. Doi, *Second quantization representation for classical many-particle systems*, J. Phys. A: Math. Gen. **9**, 1465 (1976)

[19] P. Grassberger, M. Scheunert, *Fock-space methods for identical classical objects*, Fortschr. Phys. **28**, 547 (1980).

[20] J.L. Cardy, *Renormalization group approach to reaction-diffusion problems*, in *The mathematical beauty of physics*, ed. by J.-M. Drouffe, J.-B. Zuber, volume 24 of *Advanced series in mathematical physics*, World Scientific, Singapore, (1997).

[21] M.J. Howard, U.C. Täuber, *'Real' versus 'imaginary' noise in diffusion-limited reactions*, J. Phys. A: Math. Gen. **30**, 7721 (1997).

[22] H.K. Janssen, M. Müller, O. Stenull, *A Generalized Epidemic Process and Tricritical Dynamic Percolation*, preprint, cond-mat/0404167 .

[23] H.K. Janssen, *On the renormalized field theory on nonlinear critical relaxation*, in *From Phase Transition to Chaos*, ed. by G. Györgyi, I. Kondor, L. Sasvári, T. Tél, World-Scientific, (1992).

[24] K. Binder, *Computersimulationen*, Physik Journal, 3, Nr. 5, (2004).

[25] S.K. Friedlander, *Smoke, Dust, and Haze*, Oxford University Press, second edition, (2000).

[26] M.H. Ernst, *Kinetics of clustering in irreversible aggregation*, in *Fractals in Physics*, ed. by L. Pietronero and E. Tosatti, North-Holland, Amsterdam (1986).

[27] N.A. Fuchs, *The mechanics of aerosols*, Elmsford, New York, Pergamon Press (1964).

[28] S.M. Dammer, D.E. Wolf, *Self-focussing dynamics of monopolarly charged suspensions*, preprint, cond-mat/0404546, submitted to Phys. Rev. Lett. .

[29] M.H. Lee, *N-body evolution of dense clusters of compact stars*, Astrophys. J. **418**, 147 (1993).

[30] D. ben-Avraham, *The coalescence process $A + A \to A$ and the method of interparticle distribution functions*, in *Nonequilibrium statistical mechanics in one dimension*, ed. by V. Privman, Cambridge University Press, Cambridge (1997).

[31] R. Kroon, H. Fleurent, R. Sprik, *Diffusion-limited exciton fusion reaction in one-dimensional tetramethylammonium manganese trichloride (TMMC)*, Phys. Rev. E **47**, 2462 (1993).

[32] R. Kroon, R. Sprik, *Diffusion-limited excitation kinetics in one dimensional systems*, in *Nonequilibrium statistical mechanics in one dimension*, ed. by V. Privman, Cambridge University Press, Cambridge (1997).

[33] K. Krebs, M.P. Pfannmüller, B. Wehefritz, H. Hinrichsen, *Finite-size-scaling studies of one-dimensional reaction-diffusion systems I: Analytical results*, J. Stat. Phys. **78**, 1429 (1995).

[34] G.M. Schütz, *Diffusion-limited annihilation in inhomogeneous environments*, Z. Phys. B **104**, 583 (1997).

[35] L. Peliti, *Renormalization of fluctuation effects in the $A + A \to A$ reaction*, J. Phys. A: Math. Gen. **19**, L365 (1986).

[36] D. Toussaint, F. Wilczek, *Particle-antiparticle annihilation in diffusive motion*, J. Chem. Phys. **78**, 2642, (1983).

[37] F. Spitzer, *Principles of Random Walks*, Springer, New York, (1976).

[38] M.H. Lee, *A survey of numerical solutions to the coagulation equation*, J. Phys. A: Math. Gen. **34**, 10219, (2002).

[39] P.G.J. van Dongen, M.H. Ernst, *Scaling solutions of Smoluchowski's coagulation equation*, J. Stat. Phys. **50**, 295, (1988).

[40] J.H. Werth, M. Linsenbühler, S.M. Dammer, Z. Farkas, H. Hinrichsen, K.-E. Wirth, D.E. Wolf, *Agglomeration of Charged Nanopowders in Suspensions*, Powder Technology **133**, 106, (2003).

[41] S.M. Dammer, J. Werth, H. Hinrichsen, *Electrostatically charged granular matter*, to appear in *The Physics of Granular Media*, ed. by H. Hinrichsen, D.E. Wolf, Wiley-VCH.

[42] M.P. Allen, D.J. Tildesley, *Computer Simulation of Liquids*, Oxford University Press, New York, (1987).

[43] A.V. Ivlev, G.E. Morfill, U. Konopka, *Coagulation of Charged Microparticles in Neutral Gas and Charged-Induced Gel Transitions*, Phys. Rev. Lett. **89**, 195502, (2002).

[44] T. Scheffler, D.E. Wolf, *Collision rates in charged granular gases*, Granular Matter **4**, 103, (2002).

[45] T. Pöschel, N.V. Brilliantov, T. Schwager, *Long-time behavior of granular gases with impact-velocity dependent coefficient of restitution*, Physica A **325**, 274, (2003).

[46] D. van der Meer, K. van der Weele, D. Lohse, *Coarsening dynamics in a vibrofluidized compartmentalized granular gas*, JSTAT P04004, (2004).

[47] W.H. Press, S.A. Teukolsky, W.T. Vetterling, B.P. Flannery, *Numerical Recipes in C*, Cambrigde University Press, second edition, (1992).

[48] J.E. Barnes, P. Hut, *A hierarchical O(N Log N) force calculation algorithm*, Nature **324**, 446, (1986).

[49] D. J. Daley, J. Gani, *Epidemic Modelling: An Introduction*, Cambridge University Press, Cambridge (1999).

[50] D. Mollison, *Spatial Contact Models for Ecological and Epidemic Spread*, J. Roy. Stat. Soc. B **39**, 283 (1977).

[51] P. Grassberger, H. Chaté and G. Rousseau, *Spreading in media with long-time memory*, Phys. Rev. E **55**, 2488 (1997).

[52] S.M. Dammer, H. Hinrichsen, *Epidemic spreading with immunization and mutations*, Phys. Rev. E **68**, 016114 (2003).

[53] P. Grassberger, *On the Critical Behavior of the General Epidemic Process and Dynamical Percolation*, Math. Biosci. **63**, 157 (1983)

[54] E.V. Albano, *Critical behaviour of a forest fire model with with immune trees*, J. Phys. A: Math. Gen. **27**, L881 (1994).

[55] S. Havlin, D. ben-Avraham, *Diffusion in disordered media*, Adv. Phys. **36**, 695 (1987).

[56] R.M. Ziff, E. Gulari, Y. Barshad, *Kinetic Phase Transitions in an Irreversible Surface-Reaction Model*, Phys. Rev. Lett. **56**, 2553 (1986).

[57] H. Hinrichsen, A. Jiménez-Dalmaroni, Y. Rozov, E. Domany, *Flowing Sand: A Physical Realization of Directed Percolation*, Phys. Rev. Lett. **83**, 4999, (1999).

[58] R.B. Griffiths, *Dependence of critical indices on a parameter*, Phys. Rev. Lett. **24**, 1479 1970.

[59] L.P. Kadanoff, in *Proceedings of 1970 Varenna Summer School on Critical Phenomena*, ed. by M.S. Green, Academic Press, New York (1971).

[60] K.G. Wilson, *Renormalization Group and Critical Phenomena. I. Renormalization group and the Kadanoff Scaling Picture*, Phys. Rev. B **4**, 3174 (1971).

[61] K.G. Wilson, *Renormalization Group and Critical Phenomena. II. Phase-Space Cell Analysis of Critical Behavior*, Phys. Rev. B **4**, 3184 (1971).

[62] P. Grassberger, A. de la Torre, *Reggeon field theory (Schlögels first model) on a lattice; Monte Carlo calculations of critical behaviour*, in Annals of Physics **122**, 373, ed. by H. Feshbach, Academic, New York, (1979).

[63] M.A. Mu noz, G. Grinstein and Y. Tu, *Survival probability and field theory in systems with absorbing states*, Phys. Rev. E **56**, 5101 (1997).

[64] H.K. Janssen, *Survival and Percolation Probabilities in the Field Theory of Growth Models*, preprint, cond-mat/0304631, submitted to Phys. Rev. E .

[65] J.F.F. Mendes, R. Dickman, H. Henkel, M.C. Marques, *Generalized scaling for models with multiple absorbing states*, J. Phys. A: Math. Gen. **27**, 3019 (1994).

[66] S. Lübeck, R.D. Willmann, *Universal scaling behavior of directed percolation and the pair contact process in an external field*, J. Phys. A: Math. Gen. **35**, 10205 (2002).

[67] S. Lübeck, R.D. Willmann, *Universal scaling behavior of directed percolation around the upper critical dimension*, J. Stat. Phys. **115**, 1231, (2004).

[68] S. Lübeck, *Scaling behavior of the order parameter and its conjugated field in an absorbing phase transition around the upper critical dimension*, Phys. Rev. E **65**, 046150, (2002).

[69] J.L. Cardy, U.C. Täuber, *Theory of Branching and Annihilating Random Walks*, Phys. Rev. Lett. **77**, 4780 (1996)

[70] M. Rossi, R. Pastor-Satorras, A. Vespignani, *Universality Class of Absorbing Phase Transitions with a Conserved Field*, Phys. Rev. Lett. **85**, 1803 (2000).

[71] S. Lübeck, P.C. Heger, *Universal Scaling Behavior at the Upper Critical Dimension of Nonequilibrium Continuous Phase Transitions*, Phys. Rev. Lett. **90**, 230601, (2003).

[72] T.M. Ligget *Interacting particle systems*, Springer-Verlag, Berlin, (1985).

[73] G. Ódor, *Universality classes in nonequilibrium lattice systems*, preprint, cond-mat/0205644 .

[74] M. Henkel, H. Hinrichsen, *The non-equilibrium phase transition of the pair-contact process with diffusion*, preprint, cond-mat/0402433, submitted to J. Phys. A: Math. Gen. .

[75] H. Hinrichsen, *On Possible Experimental Realizations of Directed Percolation*, Braz. J. Phys. **30**, 69, (2000).

[76] S.R. Broadbent, J.M. Hammersley, Proc. Camb. Phil. Soc. **53**, 629 (1957).

[77] D. Stauffer, A. Aharony, *Introduction to percolation theory*, Taylor and Francis, London, second edition, (1991).

[78] I. Jensen, *Low-density series expansions for directed percolation: I. A new efficient algorithm with applications to the square lattice*, J. Phys. A: Math. Gen. **32**, 5233 (1999).

[79] H. Hinrichsen, G. Ódor, *Correlated initial conditions in directed percolation*, Phys. Rev. E. **58**, 311 (1998).

[80] P. Grassberger, Y.-C. Zhang, *Self-organized formulation of standard percolation phenomena*, Physica A **224**, 169 (1996).

[81] S.M. Dammer, H. Hinrichsen, *Spreading with immunization in high dimensions*, preprint, cond-mat/0405577, submitted to JSTAT .

[82] H.K. Janssen, *On the Nonequilibrium Phase Transition in Reaction-Diffusion Systems with an Absorbing Stationary State*, Z. Phys. B **42**, 151 (1981).

[83] H.K. Janssen, O. Stenull, *Logarithmic corrections in directed percolation*, Phys. Rev. E **69**, 016125, (2004).

[84] M. Moshe, *Recent developments in Reggeon field theory*, Phys. Rep. C **37**, 255 (1978).

[85] P. Grassberger, K. Sundermeyer, *Reggeon field theory and Markov processes*, Phys. Rev. Lett. B **77**, 220 (1978).

[86] S.P. Obukhov, *The problem of directed percolation*, Physica A **101**, 145 (1980).

[87] J.L. Cardy, R.L. Sugar, *Directed percolation and Reggeon field theory*, J. Phys. A: Math. Gen. **13**, L423 (1980).

[88] J.B. Bronzan, J.W. Dash, *Higher order epsilon terms in the renormalization group approach to Reggeon field theory*, Phys. Rev. Lett. B **51**, 496 (1974).

[89] C.A. Voigt, R.M. Ziff, *Epidemic analysis of the second-order transition in the Ziff-Gulari-Barshad surface-reaction model*, Phys. Rev. E **56**, R6241, (1997).

[90] I. Jensen, *Critical behavior of the three-dimensional contact process*, Phys. Rev. A **45**, R563, (1992).

[91] W. Kinzel, *Annals of the Israel Physical Society* vol. 5, ed. by G. Deutscher, R. Zallen R, J. Adler, Bristol: Adam Hilger, (1983).

[92] T.E. Harris, *Contact interactions on a lattice*, Ann. Prob. **2**, 969 (1974).

[93] I. Jensen, A.J. Guttmann, *Series expansions of the percolation probability for directed square and honeycomb lattices*, J. Phys. A: Math. Gen. **28**, 4813 (1995).

[94] P. Grassberger, *On phase transitions in Schlögel's second model*, Z. Phys. B **47**, 365 (1982).

[95] P. Grassberger, *Directed percolation: results and open problems*, in *Nonlinearities in complex Systems*, Proceedings of the 1995 Shimla Conference on Complex Systems, ed. by S. Puri et al., Narosa Publishing, New Dehli, (1997).

[96] P. Rupp, R. Richter, I. Rehberg, *Critical exponents of directed percolation measured in spatiotemporal intermittency*, Phys. Rev. E. **67**, 036209, (2003).

[97] C.N. Yang, T.D. Lee, *Statistical theory of equations of state and phase transitions. I. Theory of condensation*, Phys. Rev. **87**, 404, (1952).

[98] T.D. Lee, C.N. Yang, *Statistical theory of equations of state and phase transitions. II. Lattice gas and Ising model*, Phys. Rev. **87**, 410, (1952).

[99] R.A. Blythe, M.R. Evans, *The Lee-Yang Theory of Equilibrium and Nonequilibrium Phase Transitions*, Braz. J. Phys. **33**, 464, (2003).

[100] P.F. Arndt, S.R. Dahmen, H. Hinrichsen, *Directed percolation, fractal roots and the Lee-Yang theorem*, Physica A **295**, 128, (2001).

[101] S.M. Dammer, S.R. Dahmen, H. Hinrichsen, *Yang-Lee zeros for a nonequilibrium phase transition*, J. Phys. A **35**, 4527, (2002).

[102] M.E. Fisher, *The nature of critical points*, in *Lectures in theoretical physics*, ed. by W.E. Brittin, volume 7C, University of Colorado Press, Boulder, (1965).

[103] R.B. Griffiths, *Rigorous Results and Theorems*, in *Phase Transitions and Critical Phenomena*, volume 1, ed. by C. Domb and M.S. Green, London, Academic Press, (1972).

[104] L.E. Ruelle, *Statistical mechanics: Rigorous results*, W.A. Benjamin, Inc., New York, (1969).

[105] S. Grossmann, W. Rosenhauer, *Phase Transitions and the Distribution of Temperature Zeros of the Partition Function. I. General Relations*, Z. Phys. **218**, 437 (1969).

[106] S. Grossmann, V. Lehmann, *Phase Tansitions and the Distribution of Temperature Zeros of the Partition Function. II. Applications and Examples*, Z. Phys. **218**, 449 (1969).

[107] Ch. Binek, *Density of Zeros on the Lee-Yang Circle Obtained from Magnetization Data of a Two-Dimensional Ising Ferromagnet*, Phys. Rev. Lett. **81**, 5644, (1998).

[108] M. Biskup, C. Borgs, J.T. Chayes, L.J. Kleinwaks, R. Kotecký, *General Theory of Lee-Yang Zeros in Models with First-Order Phase Transitons*, Phys. Rev. Lett. **84**, 4794, (2000).

[109] R.J. Baxter, A.J. Guttmann, *Series expansion of the percolation probability for the directed square lattice*, J. Phys. A: Math. Gen. **21**, 3193 (1988).

[110] M. Henkel, G. Schütz, *Finite-lattice extrapolation algorithms*, J. Phys. A: Math. Gen. **21**, 2617, (1988).

[111] R. Dickman, *Reweighting in nonequilibrium simulations*, Phys. Rev. E **60**, R2441, (1999).

[112] M. Schroeder, *Number Theory in Science and Communication*, Springer Series in Information Science, vol. 7, Springer Verla, (1999).

[113] S. Vajda, *Fibonacci and Lucas numbers, and the Golden Section*, Chichester: Horwood, (1989).

[114] A.M Ozorio de Almeida, *Hamiltonian Systems: Chaos and Quantization*, Cambridge: Cambridge University Press, (1988).

[115] M. Ghyka, *The Geometry of Art and Life*, New York: Dover Publications,(1977).

[116] I. Bena, F. Coppex, M. Droz, A. Lipowski, *Yang-Lee Zeros for an Urn model for the Separation of Sand*, Phys. Rev. Lett. **91**, 160602, (2003).

[117] R.A. Blythe, M.R. Evans, *Lee-Yang Zeros and Phase Transitions in Nonequilibrium Steady States*, Phys. Rev. Lett. **89**, 080601, (2002).

[118] P.F. Arndt, *Yang-Lee Theory for a Nonequilibrium Phase Transition*, Phys. Rev. Lett. **84**, 814, (2000).

[119] F.H. Jafarpour, *The Application of the Yang-Lee Theory to Study a Phase Transition in a Non-Equilibrium System*, J. Stat. Phys. **113**, 269, (2003).

[120] F.H. Jafarpour, *First Order Phase Transition in a Reaction-Diffusion Model With Open Boundary: The Yang-Lee Theory Approach* , J. Phys. A: Math. Gen. **36**, 7497, (2003).

[121] M.R. Evans, R.A. Blythe, *Nonequilibrium dynamics in low-dimensional systems*, Physica A **313**, 110, (2002).

[122] A. Jiménez-Dalmaroni, H. Hinrichsen, *Epidemic processes with immunization*, Phys. Rev. E **68**, 036103, (2003).

[123] I. Jensen, *Critical behavior of the pair contact process*, Phys. Rev. Lett. **70**, 1465, (1993).

[124] I. Jensen, R. Dickman, *Nonequilibrium phase transitions in systems with infinitely many absorbing states*, Phys. Rev. E **48**, 1710 (1993)

[125] M.A. Mu noz, G. Grinstein, R. Dickman, R. Livi, *Critical Behavior of Systems with Many Absorbing States*, Phys. Rev. Lett. **76**, 451, (1996).

[126] M.A. Mu noz, G. Grinstein, R. Dickman, *Phase Structure of Systems with Infinite Numbers of Absorbing States*, J. Stat. Phys. **91**, 541, (1998).

[127] F. van Wijland, *Universality Class of Nonequilibrium Phase Transitions with Infinitely Many Absorbing States*, Phys. Rev. Lett. **89**, 190602, (2002).

[128] M.A. Mu noz, R. Dickman, A. Vespignani, S. Zapperi, *Avalanche and spreading exponents in systems with absorbing states*, Phys. Rev. E **59**, 6175, (1999).

[129] H.K. Janssen, *Renormalized field theory of dynamical percolation*, Z. Phys. B **58**, 311, (1985).

[130] P. Grassberger, *Critical percolation in high dimensions*, Phys. Rev. E **67**, 036101, (2003).

[131] J.L. Cardy, P. Grassberger, *Epidemic models and percolation*, J. Phys. A: Math. Gen. **18**, L267 (1985).

[132] C. López, M.A. Mu noz, *Numerical analysis of a Langevin equation for systems with infinite absorbing states*, Phys. Rev. E **56**, 4864, (1997).

[133] P. Fröjdh, M. Howard, K.B. Lauritsen, *Directed percolation and other systems with absorbing states: Impact of boundaries*, Int. J. Mod. Phys. **15**, 1761, (2001), and references therein.

[134] R.A. Blythe, M.R. Evans, Y. Kafri, *Stochastic Ballistic Annihilation and Coalescence*, Phys. Rev. Lett. **85**, 3750, (2000).

[135] H.K. Janssen, K. Oerding, F. van Wijland, H. J. Hilhorst, *Lévy-flight spreading of epidemic processes leading to percolating clusters*, Euro. Phys. J. B **7**, 137, (1999).

[136] H. Hinrichsen, M. Howard, *A model for anomalous directed percolation*, Euro. Phys. J. B **7**, 635, (1999).

Curriculum vitae

Persönliche Daten

Name:	Stephan Markus Dammer
Geburtsdatum:	5. Mai 1975
Geburtsort:	Duisburg
Familienstand:	verheiratet, ein Kind (geboren im April 2003)

Hochschulausbildung

seit 2001:	Promotion an der Universität Duisburg Betreuer: Prof. Dr. H. Hinrichsen
1995-2000:	Studium der Physik an der Universität-Gesamthochschule Duisburg
2000:	Abschluß des Studiums als Diplom-Physiker
Diplomarbeit:	'Parametrisierung von Aktivierungsenergien für die Adatomdiffusion bei Eisen auf Fe(110)' Betreuer: Prof. Dr. D.E. Wolf
1997:	Erlangen des Vordiploms

Schulbildung und Ersatzdienst

1994-1995:	Zivildienst
1985-1994:	Gymnasium mit Abschluß (Abitur)
1981-1985:	Grundschule

Veröffentlichungen

Publikationen in Fachzeitschriften

Die folgenden Artikel sind im Zusammenhang mit dieser Dissertation entstanden.

- S.M. Dammer and D.E. Wolf, *Self-Focusing Dynamics in Monopolarly Charged Suspensions*, Phys. Rev. Lett. **93**, 150602, (2004).

- S. M. Dammer and H. Hinrichsen, *Spreading with immunization in high dimensions*, J. Stat. Mech.: Theor. Exp. **P07011**, (2004).

- S.M. Dammer and H. Hinrichsen, *Epidemic spreading with immunization and mutations*, Phys. Rev. E **68**, 016114, (2003).

- J.H. Werth, M. Linsenbühler, S.M. Dammer, Z. Farkas, H. Hinrichsen, K.-E. Wirth, D.E. Wolf, *Agglomeration of Charged Nanopowders in Suspensions*, Powder Technology **133**, 106, (2003).

- J.H. Werth, S.M. Dammer, Z. Farkas, H. Hinrichsen, D.E. Wolf, *Agglomeration in charged suspensions*, Computer Physics Communications **147**, 259, (2002).

- S.M. Dammer, S.R. Dahmen and H. Hinrichsen, *Yang-Lee zeros for a nonequilibrium phase transition*, J. Phys. A **35**, 4527, (2002).

Buchbeiträge

◇ S.M. Dammer, J. Werth and H. Hinrichsen, *Electrostatically charged granular matter*, to appear in *The Physics of Granular Media*, ed. by H. Hinrichsen, D.E. Wolf, Wiley-VCH.

In Bearbeitung

Folgende Artikel sind zur Zeit in Bearbeitung

◇ M. Linsenbühler, J.H. Werth, S.M. Dammer, H. Knudsen, H. Hinrichsen, K.-E. Wirth, and D.E. Wolf, *Cluster size distribution of charged Nanopowders in Suspensions*, in preparation, (2004).

Ausgewählte Vorträge und Poster Präsentationen

Im folgenden sind einige wissenschaftliche Veranstaltungen aufgeführt, bei denen Teile dieser Dissertation in Form eines Vortrags oder einer Poster-Präsentation vom Autor dieser Arbeit vorgestellt wurden.

◇ S.M. Dammer und D.E. Wolf, *Self-focussing dynamics of monopolarly charged suspensions*, Seminar des Lehrstuhls 'Physics of Fluids' an der Universität von Twente (Niederlande), März 2004, (Vortrag).

◇ S.M. Dammer und D.E. Wolf, *Aggregation dynamics of monopolarly charged particles*, Mitarbeiter-Treffen des DFG-Projektes *Verhalten granularer Medien*, Universität Duisburg, Februar 2004, (Vortrag).

◇ S.M. Dammer, Z. Farkas, H. Knudsen, J.H. Werth, H. Hinrichsen, D.E. Wolf, *Clustering in Charged Nanosuspensions*, International Symposium on Structure and Dynamics of Heterogeneous Systems-SDHS'03, Universität Duisburg, November 2003, (Poster).

◇ S.M. Dammer und H. Hinrichsen, *Epidemic spreading with immunization and mutations*, Seminar des Lehrstuhls 'Theoretische Physik III' an der Universität Würzburg, Oktober 2003, (Vortrag).

- S.M. Dammer und H. Hinrichsen, *Epidemic spreading with immunization and mutations*, Seminar am MPIPKS Dresden: 'Non-Equilibrium Statistical Physics in Low Dimensions and Reaction Diffusion Systems', September 2003, (Poster).

- S.M. Dammer und H. Hinrichsen, *Spreading with immunization and mutations*, Symposium am Forschungszentrum Jülich: 'Cooperativity in Biophysical Systems', Oktober 2002, (Poster).

- J.H. Werth, S.M. Dammer, Z. Farkas, H. Hinrichsen, D.E. Wolf, *Agglomeration in charged suspensions*, Europhysics Conference on Computational Physics, Aachen, September 2001, (Poster).

- S.M. Dammer, S.R. Dahmen, H. Hinrichsen, *Yang-Lee Zeros for Directed Percolation*, Wilhelm and Else Heraeus Summer School on: 'Dynamics of Complex Systems: Classical and Quantum Aspects', Lutherstadt Wittenberg, August 2001, (Poster).

- S.M. Dammer, S.R. Dahmen, H. Hinrichsen, *Yang-Lee Zeros for Directed Percolation*, Gruppenseminar bei Prof. Dr. S.R. Dahmen, Porto Alegre (Brasilien), Mai 2001, (Vortrag).